

Microfluidic-based 3D hepatic cell cultivation
as a new *in vitro* model for inflammation study

Dissertation

zur Erlangung des Grades

der Doktorin der Naturwissenschaften

der Naturwissenschaftlich-Technischen Fakultät

der Universität des Saarlandes

von

Mi Jang

Saarbrücken

2017

Tag des Kolloquiums: 21.11. 2017

Dekanin/Dekan: Univ. -Prof. Dr. rer. nat. Guido Kickelbick

Mitglieder des

Prüfungsausschusses

Vorsitzender: Univ. -Prof. Dr. -Ing. M. Nienhaus

Gutachter: Prof. Dr. A. Manz

Univ. -Prof. Dr. Ch. Wagner

Akad. Mitarbeiter: Dr. H. Gao

Eidesstattliche Versicherung

Hiermit versichere ich an Eides statt, dass ich die vorliegende Arbeit selbstständig und ohne Benutzung anderer als der angegebenen Hilfsmittel angefertigt habe. Die aus anderen Quellen oder indirekt übernommenen Daten und Konzepte sind unter Angabe der Quelle gekennzeichnet. Die Arbeit wurde bisher weder im In- noch im Ausland in gleicher oder ähnlicher Form in einem Verfahren zur Erlangung eines akademischen Grades vorgelegt.

Ort, Datum

Unterschrift

Table of Contents

Abstract.....	VI
Acknowledgments.....	VII
Abbreviation.....	IX
Chapter 1: Introduction	
1.1 Introduction of the liver organ.....	1
1.2 Role of liver in inflammation	8
1.3 Introduction of <i>in vitro</i> hepatocyte culture models	14
1.4 Aim and outline of this thesis.....	24
Chapter 2: On-chip three-dimensional cell culture in phaseguide improves hepatocyte functions <i>in vitro</i>	
2.1 Introduction.....	27
2.2 Materials and methods.....	29
2.3 Results.....	33
2.4 Discussion.....	41
2.5 Conclusion.....	44
Chapter 3: New HepG2-on-a-chip platform for study of melatonin effects on various hepatic inflammatory responses stimulated by IL-6	
3.1 Introduction.....	45
3.2 Materials and methods.....	48
3.3 Results.....	52
3.4 Discussion.....	61
3.5 Conclusion.....	64
Chapter 4: Differentiation of human liver progenitor cell line (HepaRG) directly on a biochip.	
4.1 Introduction.....	65
4.2 Materials and methods.....	68

4.3 Results.....	72
4.4 Discussion.....	83
4.5 Conclusion.....	87
Chapter 5: Conclusion	
5.1 Summary of the thesis.....	88
5.2 Conclusion and outlook.....	91
Reference.....	93
Appendix.....	106

Abstract

The liver is a vital organ which performs a variety of important functions, including protein synthesis, detoxification, carbohydrate metabolism and innate immunity, mainly by the hepatocytes.

In this thesis, a new perfused 3D culture model for human hepatocyte cells lines (HepG2 and HepaRG) using a commercial microfluidic device will be presented that combines different advantages for the *in vitro* cultivation of hepatocytes to apply for the study of hepatic inflammatory responses.

First, matrigel-embedded HepG2 cells cultured in the microfluidic device showed a high survival rate and improved hepatic functions compared to static two- and three-dimensional culture models. Next, we further investigated interplay between Interleukin-6 (IL-6) and melatonin in HepG2 cells-on-a-chip regarding acute phase response, detoxification, glucose metabolism, and mitochondrial functions. Additionally, HepaRG cells, the hepatic stem cell line, were successfully directly differentiated in the microfluidic device and produced C-reactive proteins by IL-6 stimulation.

Altogether, this new *in vitro* model is not only applicable to investigation of hepatic physiology and inflammatory responses, but can also be a tool for the differentiation of different types of stem cells.

Zusammenfassung

Die Leber ist ein lebenswichtiges Organ. Sie übt eine Vielzahl von wichtigen Funktionen aus, einschließlich Proteinsynthese, Entgiftungen, Kohlehydrat-Stoffwechsel und angeborene Immunabwehr, vor allem geleistet durch Hepatocyten.

In dieser Arbeit wird ein neues perfusionsbasiertes 3D Kulturmodell vorgestellt für humane Hepatocytenlinien (HepG2 und HepaRG), basierend auf einer kommerziellen, mikrofluidischen Plattform, welche die verschiedenen Vorteile verbindet wie die Kultivierbarkeit der Hepatocyten in vitro mit der Untersuchbarkeit von Leberentzündungsreaktionen.

Zuerst konnte für Matrigel-eingebettete HepG2-Zellen eine hohe Überlebensrate bei Kultivierung in mikrofluidischen Systemen gezeigt, sowie verbesserte Leberfunktionen nachgewiesen werden, im Vergleich zu den statischen 2D und 3D Kulturmodellen. Als nächsten Schritt wurde das Zusammenspiel von Interleukin-6 (IL-6) mit Melatonin bei HepG2-Zellen-on-a-chip untersucht hinsichtlich Akut-Phasenverlauf, Entgiftung, Glukosemetabolismus und Mitochondrien-Funktionen. Des Weiteren konnten HepaRG-Zellen, eine Leberstammzell-Linie, direkt in der mikrofluidischen Plattform differenziert werden und produzierten nach Stimulation durch IL-6 C-reaktives Protein.

Zusammenfassend kann dieses neue in vitro Modell nicht nur zur Untersuchung der Leberphysiologie und Entzündungsantwort verwendet werden, sondern ebenfalls als Werkzeug zur Differenzierung von verschiedenen Typen von Stammzellen.

Acknowledgements

When I first began my doctorate, it was a tremendous challenge for me to study completely new fields. First, I would like to express my deepest gratitude to my supervisor, Prof. Andreas Manz, for his encouragement, insightful comments, and scientific guidance. Without his courage and strength, I would have given up on my doctoral degree course. I am also deeply grateful to Dr. Astrid Kleber for the discussion of biological sides. Her guidance was helpful throughout my Ph.D. program. I was able to mitigate my fears of studying new fields. Furthermore, I would like to thank Prof. Leon Albelmann at Twente University for his wise advice and for teaching a scientific way of thinking: how to build logic for the scientific discussion and go back to one's first intention in order to focus on the purpose of the research.

For technical support, I appreciate my previous team leader, Prof. Pavel Neuzil, for the installation of a microscope, as well as Dr. Thomas Ruckelshausen, who worked at the INM for the support of the confocal microscope operation. I was also fortunate to be the first customer to use the microfluidic device developed by Mimetas company, and I am grateful for their kind support.

I am truly a lucky person, because I met amazing co-workers in this program: Dr. Matthias Altmeyer, Dr. Seungjae Lee, Dr. Ju Kyung Park, Dr. Christian Ahrberg, Tijmen Hageman, Marc Pichel, Dr. André-René Blaudszun, Vanessa Almeida, In-hyuk Baek, Gwang-hun Jeong, and Xianping Li. It was a wonderful experience of exciting scientific discussions between people from diverse research backgrounds and fields, helping and working together. I really appreciate all their support in sharing and helping to solve the difficulties that arise from studying and other types of external elements.

Finally, I would like to thank Dr. Ralf Betzholz, who supported and cheered me on at all times, both personally and scientifically. I am also so fortunate to have a wonderful family, including the strongest two women in the world, my mom and my younger sister, who have strengthened me spiritually through my life. Just before my father passed away on 27 May, 2014, I promised him that I would complete my Ph.D. I am glad to be able to keep this promise to my father, who always lives in my heart.

Abbreviation

List of abbreviations

2D	two-dimensional
3D	three-dimensional
Akt	Protein kinase B
APR	Acute phase response
ATP	Adenosine triphosphate
BMP	Bone Morphogenetic protein
BSA	Bovine serum albumin
CK	Cytokeratin
CREBH	cAMP responsive element binding protein 3-like protein 3 or H
CRP	C-reactive protein
CSPG	Chondroitin sulfate proteoglycans
CYP	Cytochrome P450
DDIT3	DNA damage-inducible transcript 3
DMSO	Dimethyl sulfoxide
ECM	Extracellular matrix
ELISA	Enzyme-linked immunosorbent assay
ER	Endoplasmic reticulum
FITC	Fluorescein isothiocyanate
FOXO1	Forkhead box protein O1
GSK	Glycogen synthase kinase 3
G6Pase	Glucose-6-Phosphatase
Gp130	Glycoprotein 130
IC 50	Half maximal inhibitory concentration
IL	Interleukin

IL-6R	Interleukin-6 receptor
JAK	Janus activated kinase
LC50	Lethal concentration 50
LD50	Median lethal dose
LDH	Lactatdehydrogenase
MRP	Multidrug resistance-associated protein
NPC	Nonparenchymal cell
NTCP	Sodium/Taurocholate Co-transporting Polypeptide
PEG	Polyethylenglycol
PERK	Protein kinase RNA-like endoplasmic reticulum kinase
PBS	Phosphate Buffered Saline
PI3K	Phosphatidylinositol-3-Kinase
RIP	Regulated intramembrane proteolysis
ROS	Reactive oxygen species
SMAD	SMA/MAD homology
STAT3	Signal transducer and activator of transcription 3
TNF- α	Tumor necrosis factor alpha
UPR	Unfolded protein response
ZO	Zonula Occludens

Chapter 1. Introduction

1.1 Introduction of the liver organ

The liver is the second largest and a very complex organ in the human body, and very complex. It performs various vital functions such as detoxification of drugs and xenobiotics; synthesis of proteins, secretion of bile; and control of the carbohydrate and lipid metabolism, as well as of the innate immune system. Furthermore, the liver has a remarkable capacity for regeneration after damage.

1.1.1 Structure and functional organization

The liver's structure is very complicated. Two types of cell populations are distributed in the organ: the majority of the liver is comprised of parenchymal cells (i.e. hepatocytes) that occupy 60% of the liver volume, whereas non-parenchymal cells account for 40% of the total volume of the liver [1].

The liver is divided into two lobes, each subdivided into several liver lobules defined by the histological unit. The classical lobule shows a hexagonal shape with a diameter of 1mm and a thickness of 2mm; the entire liver organ is contains approximately 1 million liver lobules [2]. At the vertex of the liver lobule, a portal triad containing a bile duct, a hepatic artery, and a portal vein is located. (Figure 1.1). Blood flow is generated from the portal triad and directed to the center of the lobule, while the direction of bile flow is opposite to that of the bloodstream [3].

The liver acinus is the liver's smallest functional unit, which is centered on the line connecting two portals and covers two adjacent lobule parts (Figure 1.1). It appears elliptical or diamond-shaped, and can be divided into Zone 1 (periportal), 2 (transition), and 3 (perivenous) based on blood composition, metabolic activity, and pathological processes. Zone 1 (periportal) is located close to the portal trial and receives oxygen-rich blood (O_2 pressure: 70-100mm Hg); therefore, hepatocytes in this location dominate the oxidative metabolism [4]. Conversely, Zone 3 (perivenous) is located near the central vein and far away from the portal trial, and is supplied by oxygen-poor blood (O_2 pressure: 35-45mm Hg). As a result, the hepatocytes in Zone 3 involve a reduction process. Therefore, those oxygen

gradients between Zone 1 and 3 cause different compositions of plasma produced by hepatocytes [5, 6]. This zone-specific structure is imperative to understanding functions of the liver and ECM distribution.

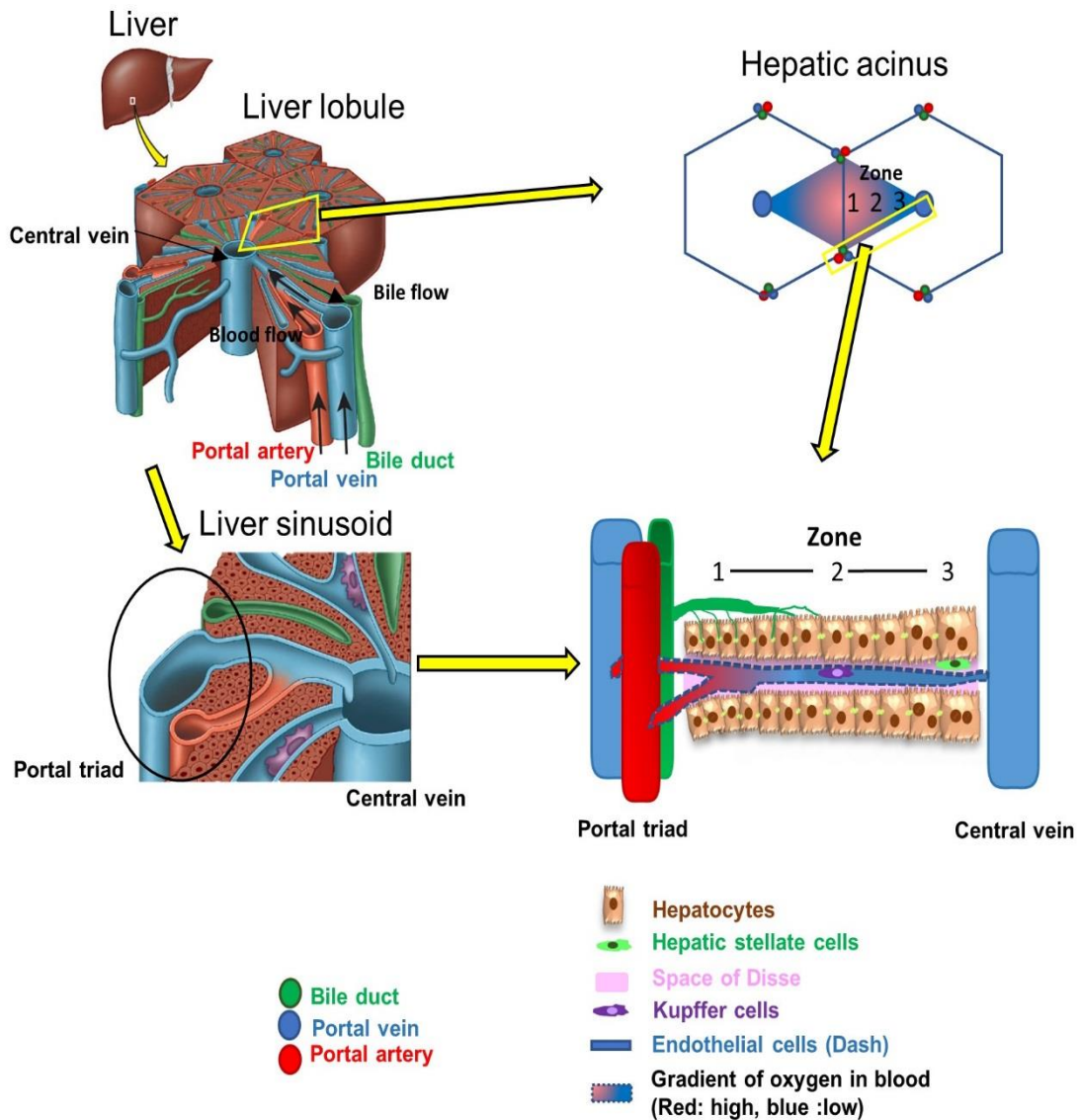


Figure 1.1 The structure of the liver from the whole organ to the liver sinusoid shows the population of the cells, portal triad, central vein, and oxygen gradient. The figure was modified from following website and manuscript. <http://medical-dictionary.thefreedictionary.com/liver+lobule> and Turner et al [7].

1.1.2 Introduction of various types of cells in the liver

The liver sinusoids are low-pressure vascular channels that receive oxygen and nutrient-rich blood from the hepatic artery and the portal vein, respectively. The fenestration of endothelial cells was observed at a diameters of 150-175nm and represented 6-8% of occupancy of the entire endothelial surface in the liver sinusoids [8].

Hepatocytes are plated at the space of Disse, which is a unique extracellular matrix (ECM) in the liver (Figure 1.1). Therefore, the hepatocytes exhibit microvilli that extend into the space of Disse, facilitating the efficient absorption and excretion of nutrition and metabolites from the sinusoid. Hepatic stellate cells (Ito cells) found within the space of Disse are responsible for the storage of fat and fat-soluble vitamins; they can also synthesize various ECM elements, including collagen, related to liver fibrosis [9]. Kupffer cells are involved in immune responses due to their ability to produce pro-inflammatory cytokines and phagocytosis in response to invading pathogens. They are located on the fenestrated liver sinusoidal endothelial cells at the wall of the sinusoid [10]. Liver sinusoid endothelial cells (LSECs) are specialized endothelial cells characterized by fenestrations—they act as a physical barrier to blood circulation [11]. LSECs can trigger inflammations, since they possess toll-like receptors (TLRs) that detect bacteria or debris from damaged cells [12]. Biliary cells (i.e. cholangiocytes) are found in a biliary tract, or a so-called bile duct, which are responsible for the production, storage, and secretion of bile. Most liver stem cells or progenitor cells are located in the canal of Hering, next to the bile duct. They produce daughter cells and can mature into parenchymal cells [7].

1.1.3 Introduction of hepatocyte's functions

As previously noted, hepatocytes are the major parenchymal cells in the liver. Mature hepatocytes are implicated in diverse biological processes, including the detoxification of xenobiotics, synthesis of plasma proteins, glucose and lipid metabolism, and bile secretion. Katz *et al.* have demonstrated that the functions of hepatocytes differ depending on their position along the periportal—central axis of liver lobule *in vivo* [13], and are specialized according to their position, determined as either “periportal” (PP) or “perivenous” (PV) [14]. Not all hepatic functions are limited in according this zonation classification; for example, albumin is synthesized in all hepatocytes. However, hepatocytes in the periportal area synthesize a higher concentration of albumin. The most studied hepatic functions, including glucose metabolism, ammonia detoxification, and metabolism of xenobiotics, are described in the following section (Figure 1. 2).

Chapter 1

Glucose metabolism: The liver controls glucose homeostasis and stores surplus carbohydrates via the formation of glycogen in overall hepatocytes. Gluconeogenesis occurs mostly in periportal hepatocytes, while glycolysis mostly occurs in perivenous hepatocytes [13]. In addition, it has been suggested that the glucose metabolism can be regulated depending on the status of nutrients and hormones [15].

Nitrogen metabolism: Ammonia is generated as a by-product during nitrogen metabolism. However, the accumulation of ammonia in the tissues or cells of the body has toxic effects, and must therefore be eliminated. The liver plays a vital role in ammonia detoxification after receiving the blood from the intestine through the portal vein to convert ammonia into urea and glutamine [16]. Ammonia is first metabolized by PP hepatocytes to generate urea; then, the remaining ammonia is converted to glutamine by PV hepatocytes [15, 17, 18].

Biotransformation: In one of its most important functions, the liver metabolizes xenobiotics, drugs, and endogenous substances in order to detoxify and excrete them from our body by the conversion of non-polar substrates to polar and hydrophilic metabolites. Drug metabolism can be divided into three phases. In phase I, the cytochrome P450 enzymes (CYP) are mainly involved in the oxidation of the substances. The CYP 1,2, and 3 families are responsible for the biotransformation of 70-80% of all drugs, and are classified as the most abundant enzymes in humans [19]. In phase II, modified compounds from phase I are conjugated with either glucuronic acid (in PV hepatocytes) or sulfuric acid (in PP hepatocytes) [20]. In phase III, the final metabolized xenobiotics are excreted via efflux transporters [21].

Various nuclear receptors regulate the expression of genes and proteins that coordinate the metabolism of xenobiotics. The pregnane-X-receptor (PXR) is highly expressed in the human liver and shares its targeted promoters with the constitutive androstane receptor (CAR) to regulate the expression of transport proteins and enzymes that regulate bile acid homeostasis and phase I-III metabolism, including the CYP3A, CYP2B family, and MRP2 transporter [22]. The aryl hydrocarbon receptor (AhR) is also classified as a xenosensor, and the CYP1A and CYP1B families are regulated by the AhR [23].

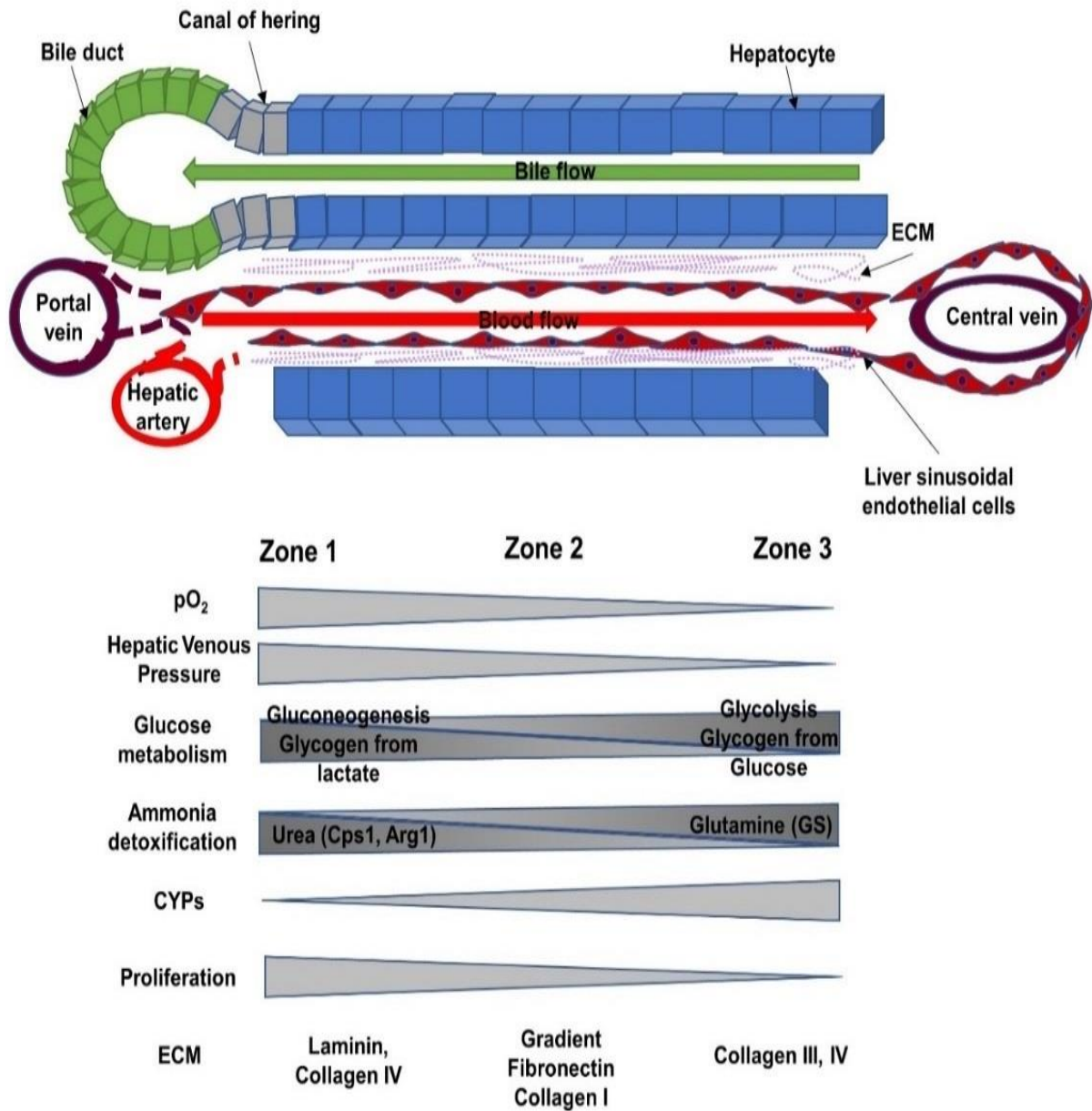


Figure 1. 2 Schematic diagram of the basic liver structure: functions and zonation of hepatocytes.

1.1.4 Introduction of extracellular matrix (ECM) in the liver

The liver includes a minor portion of the ECM. However, it plays a vital role in the control of the structural framework and function of the liver cells, such as cell-cell contact, cell migration, differentiation, and regeneration [24]. The complex ECM compositions can be divided into two major parts: the periportal region (PP) and the pericentral region (PV). The PP region contains basement membrane proteins including laminin, collagen IV, entactin,

and perlecan, whereas the PV region has abundant collagen I, III, and IV. A different composition of ECM in the liver was found in the region between PP and PV, showing gradient-like matrix molecules that is known as the space of Disse located between hepatocytes and sinusoid [25]. Interestingly, the space of Disse lacks the typical basement membrane proteins such as laminin and entactin, while containing an abundance of fibronectin, discontinuous deposits of collagen III, and a continuous network of collagen I [26]. This organization of the ECM supports and maintains different functions, sizes, and expression of enzymes of hepatocytes according to different zonation [27]. Interestingly, the liver progenitor cells can be found only in the canals of Hering, which belong to Zone 1. The microenvironment of this place consists of soluble paracrine signals and ECM proteins including laminin, collagen type III, and—minimally—chondroitin sulfate proteoglycans (CSPGs). During the differentiation of stem cells to continuous maturational lineage stages, an alteration of the soluble paracrine signals and matrix composition has been observed [28].

1.1.5 Hepatocyte morphology and polarization

Hepatocytes are large polyhedral cells, with a diameter of around 20-30 μ m, that possess abundant endoplasmic reticulum (rough and soft), numerous mitochondria, lysosomes, peroxisomes, and glycogen deposits. Most hepatocytes contain one round central nucleus, while approximately 25% are binucleated.

Hepatocytes are highly polarized, exhibiting different localized membrane proteins on different membrane domains for the uptake, processing, and excretion of blood components and bile. This distinct polarization acts as a barrier between the bloodstream and the bile. Moreover, the trafficking of substances taking place between the liver sinusoid and the bile canaliculi is dependent on the polarity of hepatocytes. The formation of this polarity requires cell-cell and cell-matrix interaction; the organization of actin filament; and the adhesive machinery, which facilitates downstream signaling for the formation of local cues of polarity [29].

Hepatocytes possess three distinct domains, each consisting of different functional proteins including adhesion proteins, receptors, and transporters (Figure 1.3). (1) The basal or sinusoidal domain, which faces the bloodstream or sinusoids, facilitates mass exchange. (2) The lateral domain is specialized for cell-cell contact and cell-cell communication, allowing cell-cell adhesion [30]. The lateral domain faces the adjacent hepatocytes and functions as a structural barrier to separate the basal from the apical domains. Tight, adherent, and gap junctions belong to the lateral domain. (3) The apical domain faces the bile canaliculi, or adjacent point, for bile secretion. These domains form one or more

capillary-like structures, so-called bile canaliculi, which comprise the smallest branch of the bile ductal structure [31]. In hepatocytes, sealed tight junctions are observed surrounding functional bile canaliculi structures [32].

Regarding transport polarity, both sodium-dependent and sodium-independent uptake of bile salts are mediated by Na^+ taurocholate co-transporting (NTCP) and organic anion-transporting polypeptide (OATP1B) at the basal domain, respectively. Bile salts are exported via ATP-binding cassette11 (ABCC11 or BSEP) at the canaliculi domain. Xenobiotics are imported by the organic anion-transporting polypeptide (OATPs) and exported by the multidrug resistance protein 1 (MDR1) and multidrug resistance-associated protein 2 (MRP2 or ABCC2) at the apical domain. Some xenobiotics are transported into the bloodstream by multidrug resistance-associated protein 3 and 4 (MRP3 and MRP4) for renal elimination [2].

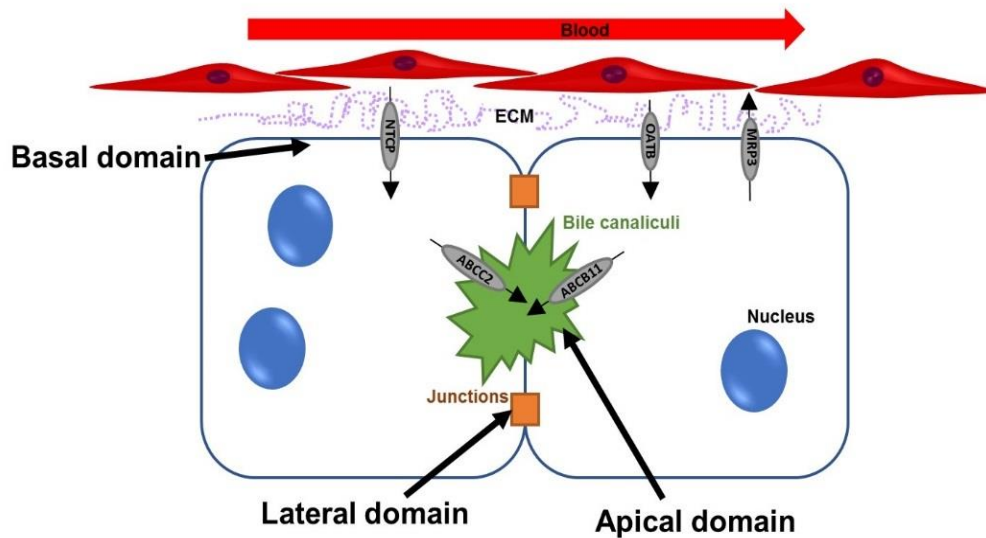


Figure 1.3 The unique polarity of hepatocytes with the expression of transport proteins located at each domain.

1. 2 Role of the liver in inflammation

The liver is usually regarded as a non-immunological organ, since its primary functions are related to metabolic activities, nutrient storage, and detoxification. However, the liver is also involved in an immunologically complex process including the production of acute phase response proteins, complement components, cytokines, and chemokines, and possesses diverse populations of immune cells [33, 34]. The liver is continuously influenced by foreign substances or infections, which can potentially induce inflammatory responses. Also, certain molecules derived from the gut should be tolerated in the liver, since the portal vein receives 80% of the hepatic blood from the gut [35]. The inflammation reactions are tightly controlled, stimulated only when the liver must remove pathogens or toxic products produced during metabolic processes. Failure to remove such dangerous stimuli often leads to chronic inflammation; in the worst-case scenario, severe inflammation—such as sepsis—can disrupt tissue homeostasis and induce liver failure. The inflammatory process in the liver controls haemodynamics, capillary permeability, leukocyte migration into tissue, and secretion of inflammatory mediators [35]. Therefore, the liver plays a central role in the response to systemic inflammation.

1.2.1 Hepatocytes in inflammation

Hepatocytes modify their metabolic pathways in inflammation status, and are responsible for the acute phase response (APR), which is a complex early defense system or innate immune system responding to inflammation, injury, infection, stress, and trauma (Figure 1.4).

Hepatocytes also regulate increases or decreases in the synthesis of acute-phase response proteins (APPs). APPs are defined as a group of proteins whose plasma concentration levels increase (positive APPs) or decrease (negative APPs) by more than 25% in response to inflammation [36]. Interestingly, APP patterns differ between species. For examples, in humans, the primary positive APPs include the C-reactive protein (CRP), serum amyloid A (SAA), and haptoglobin (Hp). In contrast, in rats, the main positive APPs are α_2 -Macroglobulin and α_1 -Acid glycoprotein. The major negative APPs are albumin and transferrin in humans and rats, but differ in chickens [37]. Therefore, rather than using animal models, human hepatic cells should be applied in inflammation studies.

Glucose metabolism is also modified by hepatocytes due to glycogenolysis and gluconeogenesis during the inflammation. Additionally, metabolism of xenobiotics is affected by inflammation, resulting in a reduced biotransformation including cytochrome P450 activity. These metabolic changes lead to impaired elimination of xenobiotic compounds [38].

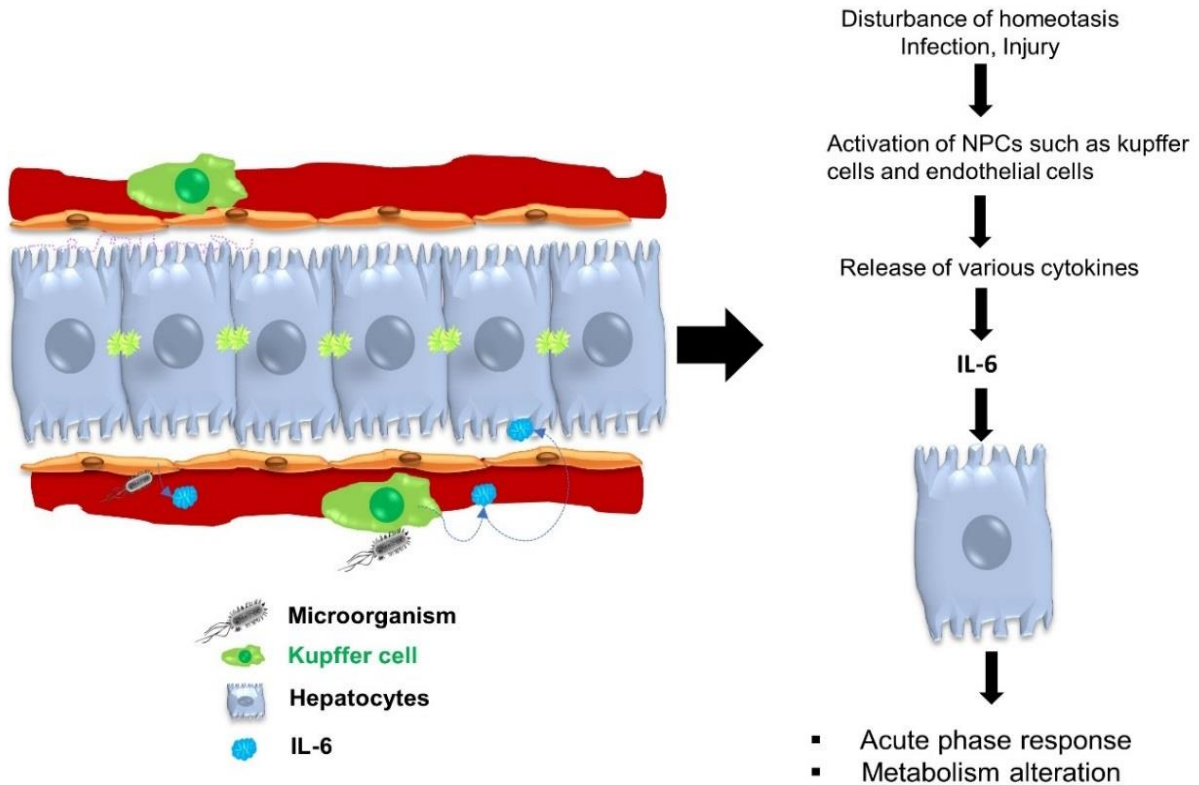


Figure 1.4 A schematic image of the inflammation process in the liver organ *in vivo*. Kupffer cells and liver endothelial cells can be activated via toll-like receptors by binding with microorganisms, and initiate the innate immune system. IL-6, one of the cytokines released from NPCs in the liver, stimulates the hepatocytes to modify the metabolic functions and to produce positive APPs.

1.2.2 Relation of Interleukin-6 with human hepatocytes

During the APR or innate immune process in the liver, immune cells, such as macrophages and Kupffer cells, first recognize bacteria via their membrane-bounded toll-like receptor (TLR), which binds components of microorganisms. They then begin to produce cytokines and chemokines that directly influence various functions of the hepatocytes (Figure 1.4).

Mainly, pro-inflammatory cytokines including IL-6, IL-1, and TNF- α —induce various reactions, including APR, which is a core part of the innate immune response [39]. It is not clear whether exogenous mediators such as lipopolysaccharide (LPS), a component of the cell wall in gram-negative bacteria, modulate hepatocyte functions directly. Among various cytokines, IL-6 is believed to be the main cytokine implicated in the liver inflammatory response [38].

In vivo, the liver seems to be the primary target organ for IL-6. 80% of injected ^{125}I -labeled recombinant human IL-6 disappeared in the circulation and was found in the liver after 20 minutes. Moreover, ^{125}I -labeled recombinant human IL-6 was remarkably observed on the surface of parenchymal cells [40]. Those observations suggest that hepatocytes in the liver might be the main target location for IL-6 *in vivo*.

As previously noted, hepatocytes synthesize or change their level of APPs during the inflammation process. Among pro-inflammatory cytokines including IL-1, TNF- α , and IL-6, only IL-6 can induce a full spectrum of both positive and negative APPs in humans. In contrast, IL-1, and TNF- α showed a limited or moderate stimulation on positive APPs [41]. Therefore, IL-6 is regarded as a key mediator, particularly in inducing APR in the liver.

1.2.3. The introduction of Interleukin-6 and its signaling pathway system.

Interleukin-6 (IL-6) was discovered in 1986 as a B-cell differentiation factor [42]. It is a multifunctional cytokine that regulates the immune response, hematopoiesis, the acute phase response, and inflammation [43, 44]. IL-6 is produced by various types of cells, including Kupffer cells, endothelial cells, and stellate cells in the liver. It has numerous biological activities through its receptor-combined system to recruit signaling. There are two distinct IL-6 signaling systems.

The first process is the so-called 'IL-6 classic signalling'. IL-6 binds to the membrane-bounded IL-6 receptor (IL-6R) to form the IL-6/IL-6R complex and associates with a second receptor, glycoprotein (GP)130. Gp130 dimerization activates Janus kinases (JAKs), leading to the activation of the signaling pathways, including signal transducer and activator of transcription 3 (STAT3) pathway. After phosphorylation at the tyrosine and serine residue of STAT3, phosphorylated STAT3 translocates into the nucleus and binds directly to targeted genes [45, 46].

Interestingly, the expression levels of IL-6R and gp130 in the liver vary depending on cell type. All cells of the body express gp130, while only a few cell types—such as hepatocytes,

some leukocytes, biliary epithelial cells, and hepatic stellate cells—express the membrane-bound IL-6 receptor (mIL-6R) [46]. IL-6 trans signaling is found in cells that do not express IL-6R, such as endothelial cells in the liver. In this case, IL-6 complexes with the soluble form of the IL-6R (sIL-6R) [47, 48].

In conclusion, hepatocytes, Kupffer cells, and stellate cells in the liver fulfil a classic IL-6 signaling by direct binding of IL-6/mIL-6 complex formation, whereas the IL-6 trans signaling process occurs only in endothelial cells [46]

1.2.4 APPs and their function

The C-reactive protein (CRP) was first discovered as a positive APR in 1930 [49]. Nowadays, it is considered a significant marker for infection or inflammation. It can act as opsonin by binding directly to polysaccharides, a component of the bacterial wall, as well as to residue of several microorganisms. Therefore, it can activate complement molecules and phagocytosis. In addition, the CRP gene transcription is induced by the IL-6/STAT3 pathway [39].

Hepcidin is a small, 25-amino acid peptide, and a central regulator of the iron metabolism [50]. It is classified as a positive APP, is synthesized by hepatocytes, and controls iron homeostasis. When iron is overloaded, hepcidin synthesis is induced. In contrast, when iron is deficient, its production is suppressed [50]. The ferroportin transporter at the membrane of hepatocyte regulates the excretion of the hepcidin [51]. It has been reported that administration of IL-6 induces an increased hepcidin production and results in a low-serum iron through STAT3 activation to bind the hepcidin promoter [45].

Albumin is one of the major negative APR proteins. It is the most abundant protein in the blood of animals and humans, and accounts for 35–50% of total protein content. Approximately 75% of the total produced albumin is utilized to maintain osmotic pressure of the plasma, which is one of the main functions of albumin. Additionally, albumin may be a major alternative source of amino acids for the synthesis of positive APPs during APR, thus reducing their production under an inflammation situation [52, 53].

1.2.5 Introduction and functions of melatonin

The isolation and identification of the structure of the hormone melatonin were first reported in 1958 [54]. Melatonin is secreted by the pineal gland during the dark phase, and also plays a significant role in the regulation of sleep and wake cycles, i.e. circadian rhythm.

One of the major functions of melatonin is reported its anti-oxidant effect [55, 56]. Acute inflammation typically results in an oxidative stress condition, such as excessive secretion of reactive oxygen species (ROS), and a relative lack of endogenous antioxidants [57]. Melatonin's actions depend in part on receptor-dependent processes and on independent pathways. Generally, the independent receptor pathways are associated with direct radical scavenging functions [58].

Mitochondria are cell organelles that produce energy in the form of ATP via electron-transport chain reactions, which generates reactive oxidative species (ROS) as a by-product. Interestingly, mitochondria are regarded as the main target organelles of melatonin due to their hydrophilicity and lipophilicity [59]. Melatonin can accumulate in mitochondria at a high concentration (presumably adjacent to the polar head of phospholipids at the mitochondrial membrane) and protects against mitochondrial oxidative stress and apoptosis [60]. Furthermore, diverse previous studies have demonstrated that melatonin shows a potent antioxidant activity by direct scavenging of radicals and the regulation of pro-oxidant and antioxidant enzymes. In general, it is agreed that melatonin stimulates antioxidant-related enzymes from a nanomolar range *in vitro* cell culture model [61].

1.2.6 Protective effects of melatonin in inflammation and liver

The positive effects of melatonin in the liver during severe inflammation, such as sepsis, have been demonstrated by the inhibition of elevated production of nitric oxide and lipid peroxidase, and by an increase in glutathione levels [62, 63]. In addition, melatonin administration reduces the plasma levels of alanine aminotransferase and aspartate aminotransferase—typical markers for liver damage—which provides additional evidence for the beneficial effects of melatonin in the liver [64]. In particular, our collaboration group has been investigating the liver protective functions of melatonin in severe inflammation disease models for several years. They demonstrated melatonin's hepatoprotective actions by confirming the improvement of liver functions, hepatic perfusion, and hepatocellular integrity [65], as well as its role in modifying cellular stress, including reactive oxygen species and the unfolded protein response [66]. Mainly, they discovered a cAMP-responsive element binding

protein 3 like 3 (CREBH) transcription factor that was entirely suppressed in severe inflammation disease, which was normalized by administration of melatonin. This fact is very intriguing to investigate the interaction of inflammation and melatonin since CREBH is associated with APR in the liver [67].

The CREBH protein belongs to the regulated intramembrane proteolysis (RIP) that is the process by which transmembrane proteins are cleaved and then the cytosolic domain are translocated into the nucleus to regulate the gene transcription [68]. CREBH is also one of transmembrane proteins at the endoplasmic reticulum (ER) and is activated by the regulated intramembrane proteolysis (RIP) process. Interestingly, the expression of CREBH (Creb3l3) is strictly restricted to the liver tissue, and pro-inflammatory cytokines can act as inducers for the CREBH mRNA expression in hepatocytes [67]. It has been reported that activated CREBH induced by ER stress or IL-6 directly regulates the production of CRP and hepcidin by binding their promoter in hepatocytes [67]. Therefore, the investigation of the interplay of melatonin and hepatic inflammation reactions is fascinating.

1.3 Introduction of *in vitro* hepatocyte culture models

1.3.1 Various cells types for *in vitro* hepatocytes

There are various hepatic cell lines that can replace primary human hepatocytes for *in vitro* culture models. The limitations of using human hepatocytes are addressed, and two hepatic cell lines, HepG2 and HepaRG, are introduced in this thesis.

Limitations of human primary hepatocyte

Primary human hepatocytes are considered a gold standard for *in vitro* liver cell culture models. They can be collected after complicated isolation steps of the entire liver organ from the patients. However, the functions of isolated human primary hepatocytes can be maintained only for several days in an *in vitro* cultivation and they rapidly lose their polarity. Furthermore, there are huge variations between the donors, and it is difficult to have accessibility [2, 69].

HepG2 cell line

The HepG2 cells line was developed in 1979 from a 15 years old American adolescent. Due to easy handling and unlimited availability, this cell line became a promising alternative to primary hepatocytes as a liver cell line. However, HepG2 expresses a low level of detoxification-related genes and proteins and shows epithelial cell-like morphology. Nevertheless, HepG2 cells can synthesize and produce major plasma proteins such as albumin, transferrin, and the acute phase proteins, thereby it can still be a promising cell line instead of human hepatocytes [70].

HepaRG cell line

HepaRG cells were isolated in 2002 from the liver tumour of a female patient suffering from hepatocarcinoma and a hepatitis C infection and have been applied for a primary *in vitro* model for the infection of hepatitis B [71]. HepaRG cells show liver progenitor cells properties before they reach a confluent state and can differentiate into both hepatocyte-like cells and biliary-like cells, approximately showing a 1:1 ratio by the addition of 2% of DMSO [72–74]. HepaRG cells well retain many liver-specific functions which are related to detoxification processes such as cytochrome P450s, phase II enzymes, and membrane transporters and show the most similar gene expression and transcriptomic patterns as compared to human hepatocytes [70, 75]. Therefore, the utilization of HepaRG is encouraging as a surrogate for hepatocytes as well as liver stem cells *in vitro*.

1.3.2 Culture models for liver cells *in vitro*

Limitation of *in vitro* and *in vivo* animal models.

In cell biology, including hepatocytes cultivation, a traditional method is the monolayer cultivation in a flask or multi-well plate. However, the abnormal morphology and dramatically decreased viability and functionalities of hepatocytes were observed in 2D culture model, thereby responses to external stimuli or diseased conditions in monolayer culture often showed huge gaps compared to clinical or *in vivo* data. Also, most standard methods for *in vivo* tests are animal experiments using rat or mouse model. However, due to genetic and metabolic differences between species, the results from *in vivo* animal experiments were inconsistent with human clinical data. Furthermore, a sacrifice of animals causes always ethical issues. Therefore, researchers endeavoured to develop various new *in vitro* liver models which can overcome the limitations mentioned above.

Hepatocyte cultivation in *in vitro* 3D model

First of all, a 3D culture model was proposed to maintain the hepatocyte's viability and improve their metabolic functions *in vitro*. In various previous studies, hepatocytes and hepatic cell lines cultured in the 3D model showed improved hepatic functions and well-organized cell structures, compared to 2D models, and indicated phenomena similar to *in vivo* data [2].

Representative methodologies for creating a three-dimensional structure of liver tissues can be divided according to whether the scaffolds are present or not. Scaffold-free methods such as hanging drop and spinner cultivation are the most common techniques. However, the spinner culture method can cause intercellular collision due to it's a constant high stirring rate, thereby reducing the cell viability and destroying the cell structure [76, 77].

The hanging drop method is widely used for forming cell spheroids in the lab, and there were various commercially available devices manufactured by 3D Biomatrix Perfecta3D® hanging drop plates [78] and InSphero [79]. Although this method is convenient and popular, a limited mass transfer can occurred [80].

Scaffold techniques using hydrogels, such as naturally-derived or synthetic materials, also can generate 3D cultures by their gelation under particular conditions. Matrigel and collagen I are mammalian-derived ECM and the most widely used materials, as they are identified as the most abundant ECM *in vivo*. Alginate extracted from brown algae is also a standard material particularly for the encapsulation of cells, since it showed low toxicity and the cost is

low [81]. PEG is a widely used synthetic material and is often employed for encapsulation [82].

Microtechnology is often used for the encapsulation and cell aggregation. Previously, a hepatic cord-like structure model was introduced with co-culture of nonparenchymal cells (NPC) using a microencapsulation technique [83]. Using the micromolds is also a common platform to generate scaffold-free liver spheroids [84].

However, still, there is one critical parameter for hepatocyte cultivation is missing, and which is mechanical fluidic force. The supply of a constant flow can lead to a sufficient mass transfer to 3D cell aggregates. Although the hepatocytes in the liver do not even directly contact the flow *in vivo*, blood flow exists as a unidirectional, supporting the nutrient supply and the removal of waste products.

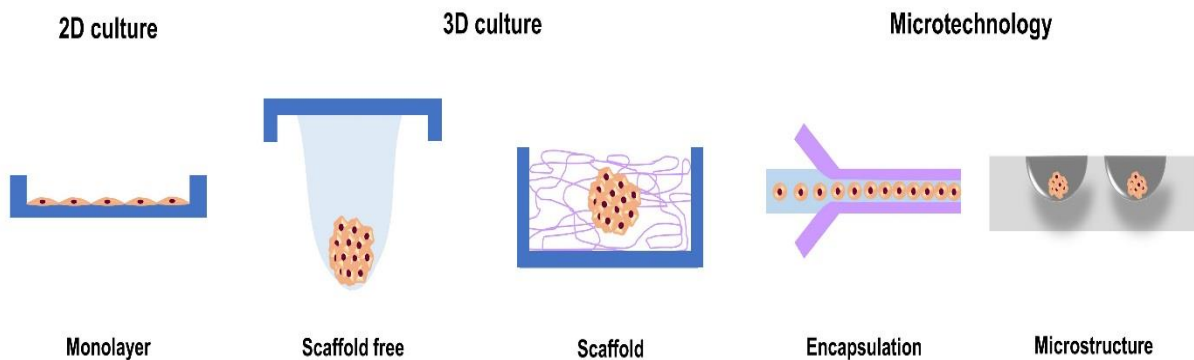


Figure 1.5 Various *In vitro* models for hepatocyte cultivation including monolayer, 3D culture with scaffold or scaffold-free, and combination with microtechnology for encapsulation of cells with matrix and matrix free spheroid formation.

1.3.3 Introduction of microfluidics in cell biology

The area known as microfluidic technology or the ‘micro total analysis systems’ is growing rapidly in the field of developing *in vitro* models in cell biology. The first concept of miniaturized total chemical analysis system was proposed by Manz in 1990 [85]. The initial researches related with μ TAS were dominated in analytical chemistry and physics field.

Over the last decade, the integration of cell biology with microfluidic technologies has emerged and has provided sophisticated *in vivo* mimicking microenvironments that have greatly influence *in vitro* cell biology research. *In vivo*, cells and their surrounding environments have microscale physical dimensions, thereby microfluidic technologies can be manipulated to answer and to observe complicated biological phenomenon [86].

The number of publications using the keywords “microfluidics cell culture” and “microfluidics and liver” has increased excessively over the last decade, according to the PubMed website (<https://www.ncbi.nlm.nih.gov/pubmed>). This indicates that the number of new *in vitro* models integrating microfluidics technologies is still growing extensively, including new *in vitro* models for liver cell cultivation. (Figure 1.6)

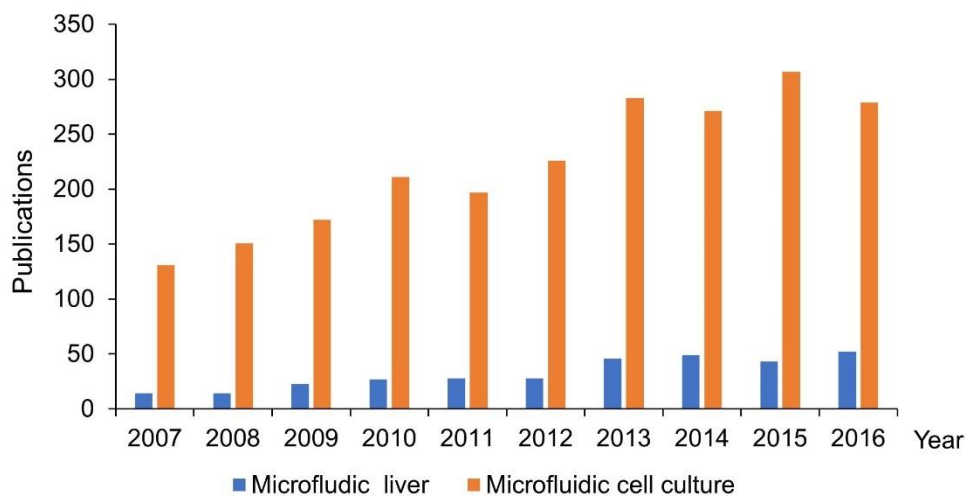


Figure 1. 6 The number of publications found per year using the keywords ‘microfluidics and liver’ (blue) and ‘microfluidics and cell culture’ (orange) in PubMed website.

1.3.4 Introduction of liver-on-a-chip devices

Over the last decade, diverse liver-derived *in vitro* microfluidic chip platforms have been developed by mimicking microenvironment of the liver *in vivo*, resulting in an improved maintenance of liver functionalities compared to conventional culture models. Therefore, they allowed investigating toxicological studies and various hepatic responses upon treating substrates or drugs. Here we introduce selected platforms that are considered from the perspective of the history of the development of microfluidic liver models and their applications.

Griffith and co-workers developed a microfluidic device for the cultivation of primary hepatocytes under flow supply in a three-dimensional platform integrated by fabricated scaffold compartments in 2001 [87]. They proved that hepatocytes were highly viable for two weeks and organized in tissue-like structure. They further estimated the hepatic functions in comparison of different cultivation models including 2D, collagen sandwich culture, 3D matrigel, and microfluidic 3D culture devices. Interestingly, cells cultured in a 3D perfused microreactor (microfluidic device) showed the most similar tendency toward a native liver compared to the other *in vitro* culture models, providing that three-dimensional cultures with flow supply can maintain hepatocyte functions at nearby physiological levels [88]. They further improved their device which contains the compartment for a higher throughput capability in the perfused multi-well plate with an integrated pneumatic micropump for hepatocyte culture [89].

Sin *et al.* reported the concept of an organ-on-a-chip platform in 2004. The device consists of three culture chambers, and each culture chamber was connected with supply of a continuous flow [90]. After that, Chao *et al.* developed a H μ REL $\text{\textcircled{R}}$ biochip for multi-organ cells cultivation including primary hepatocytes by a modification of Sin's device. Briefly, each biochip is enclosed and connected to another biochip (up to 4 biochips) by tubing lines [91], allowing independent experiments to be performed simultaneously. After the evaluation of the hepatocyte functionalities, the device was applied to the study of substrates clearance [92]. The device showed a better prediction level than monolayer cultivation compared to *in vivo* data for one of the tested substrates.

In 2007, a new microfluidic device which resembles the hepatocytes *in vivo* microenvironment was introduced for hepatocytes cultivation. The culture chamber in this device has unique physical barriers that can act as the endothelial barrier layers between the fluid and the cell culture area, allowing the cells to exchange nutrients and waste without direct contact to the flow [93]. After slight modifications, the next generation of device was

introduced for the alignment of hepatocytes to help a better organization of bile canaliculi by adding separated cell injection compartments and by reducing the width of the cell culture chamber to make a compact cell culture area [94]. Very recently, *in vitro* a so-called nonalcoholic fatty liver disease model has been proposed using the same device [95].

Yu and co-workers presented a microfluidic 3D hepatocyte chip, so-called 3D HepaTox chip [96]. The 3D HepaTOX chip was designed for 3D cell cultures of hepatocytes and for the generation of linear concentration gradients for dose-dependent responses to the drugs *in vitro*. The device consists of 8 cell culture chambers in parallel. Positively charged methylated collagen and negatively charged HEMA-MMA-MMA terpolymer were used for a 3D matrix, and micropillars helped the retention of the cells from the laminar flow in the device. This device was used for the assessment of IC 50 value of 5 different drugs, and the IC 50 correlated with LD 50 *in vivo* data. The results were comparable to the freshly isolated rat hepatocytes cultured in collagen-coated multi-well plates.

Marx and co-workers reported a dynamic multi-organ-chip for long-term cultivation of a 3D human liver and skin tissue co-culture. This device is commercially available at TissUse GmbH [97]. The system of the device offers two different culture models: i) direct exposure to flow of the cells, ii) no direct contact of the flow to the cells grown on the membrane surface in the Transwell®. This device also allows to study crosstalk between two organ models due to the multi-culture chambers. Furthermore, the device is operated by an on-chip micropump and contains independent culture chamber. Instead of using primary hepatocytes, they chose HepaRG cells. For the creation of 3D liver microtissues, differentiated HepaRG cells and human hepatic stellate cells were co-cultured in hanging drop plates and cell aggregates were transported into the microfluidic device for the evaluation of long-term cultivation (28 days) and drug-induced toxicity tests. Interestingly, cell aggregates cultured on the membrane in Transwell® survived longer than cells that were exposed to flow directly [98]. They further used the same device for three different organ cultivations (liver-intestine and liver-skin) to qualify a repeated dose substance test [99].

The Multi-organ-tissue-flow (MOTif) biochip was developed in 2015 by Mosig's group for endothelial cell cultivation by applying a hemodynamic force generated by the microfluidic flow. The culture chamber consists of a single membrane plate on which cells can adhere and grow on both sides of the membrane [100]. Later, this device was used to make an artificial liver sinusoid *in vitro* model. It consists of two layers on both sides of the membrane. The endothelial cell layer contained endothelial cells and macrophages, and the hepatic layer included co-cultured differentiated HepaRG cells and stellate cells. The endothelial layer was only exposed to perfusion flow [101]. Later, sepsis (severe inflammation disease) associated

hepatocellular dysfunction was investigated for the first time in a microfluidic *in vitro* model. They observed the release of pro- and anti-inflammatory cytokines and a decreased expression of the hepatic transporter (MRP2) as well as a disruption of the endothelial barrier. However, the intensive investigation regarding the alteration of hepatic metabolisms by inflammation is still lacking. Their results were comparable with *in vivo* data, suggesting that this new liver *in vitro* model is a valuable tool to study inflammation processes. This fact is of particular importance to inflammation research because many inflammation disease models rely on murine *in vivo* animal experiments for studying human inflammatory responses even though they show a poor correlation with human conditions [102]. Therefore, the development and validation of new *in vitro* liver models is urgently needed to investigate inflammation.

More detailed information of the various *in vitro* microfluidic liver platforms that were not introduced in this chapter is presented in Table 1. Each device was classified according to the dimension of the cell culture, the type of cells, the *in vivo* mimetic factor, whether a physical barrier between the cell culture area and the flow region exists or not, and according to their application field. Through an investigation of various microfluidic *in vitro* liver models, we have found that the paradigm shifts from the development and the characterization of new *in vitro* models to the integration with various application fields including not only for drug-induced toxicity but also for various disease models.

Chapter 1

Table. 1 Summary of various *in vitro* liver models based on microfluidics technology.

Cell type	Culture model (2D or 3D)	Model (Name of device)	Physical separation to flow from culture area	Applications	[Ref] Year
Primary hepatocytes	3D:	Perfusion 3D culture	No: directly exposed to the flow	No tested applications	[87] 2002
	Fabricated scaffold (3D)				[88] 2005
					[89] 2010
Primary hepatocytes	2D	Multi-tissues model H μ REL \circledR biochips	No: directly exposed to the flow)	Drug metabolism	[90] 2004
					[91] 2009
					[92] 2010
Primary hepatocyte	2D	Mimicking liver sinusoid	Physical artificial barrier	Drug-induced hepatotoxicity Nonalcoholic fatty liver disease	[93] 2007
					[94] 2011
					[95] 2016
Primary hepatocyte	3D: With ECM	Perfusion 3D culture	Micropillar	Drug-induced hepatotoxicity	[96] 2009
Primary hepatocyte	3D: Scaffold-free	Cord-like structure	Micropillar	No tested applications	[103] 2010
HepG2/C3A	2D	Perfusion 2D culture	No: directly exposed to the flow	Genomic, metabolomic, proteomic and transcriptomic investigation of drug-induced hepatotoxicity	[104] 2011
					[105] 2011
					[106] 2013
Primary hepatocyte	3D: Scaffold-free	Perfusion 3D culture	No: directly exposed to the flow	Interaction of paracrine parameters	[82] 2013
HepaRG	3D : Scaffold-free	Multi-organ platform	No: directly exposed to the flow	Drug-induced hepatotoxicity	[97] 2013
					[98] 2015
					[99] 2015
HepaRG	3D: multi-layered with other cell types	Liver sinusoid MOTiF biochips	Membrane	Interaction of Monocyte and Hepatocytes under Inflammation model	[101] 2015
					[100] 2015
					[107] 2016
Primary hepatocytes	3D: With ECM	Liver sinusoid	ECM	Drug induced hepatotoxicity	[108] 2016
Primary hepatocyte	2D	Zonation of liver by gradient of chemical	No: directly exposed to the flow	Drug-induced hepatotoxicity	[109] 2016

1.3.5 Introduction of a newly developed biochip

The newly developed biochip used in the thesis is introduced in this section. Originally, this microfluidic-based biochip was invented by the Mimetas company (The Netherlands) [110]. The most important component of this device is the so-called phaseguide, which was invented by Vulto et al. [111, 112]. This technology controls filling and emptying of liquid independently in any type of microfluidic structure, such as the chamber or complicated channel-based geometries. The phaseguide is a physical barrier of low height, made by dry film resist. It induces a liquid meniscus pinning effect in which the liquid aligns itself along the phaseguide before overflowing. Phaseguides can be patterned in accordance with various structures to control the alignment of liquid in microenvironments (Figure 1.7).

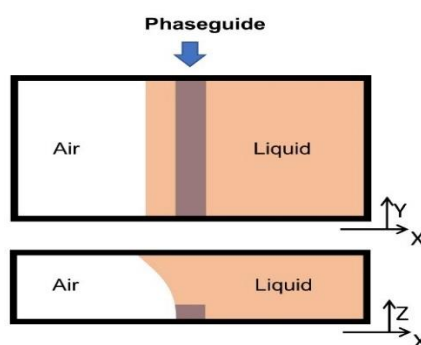


Figure 1.7. The principle of the phaseguide for liquid alignment in microenvironments.

The organoplate™ biochip used in the thesis is a modified 384-well plate consisting of integrating microfluidic structures made by glass substrates on the bottom side (Figure 1.8A). Details about the fabrication process were reported by Trietsch et al [113]. Two different designs—2-lanes and 3-lanes platforms—are available, and a phaseguide is positioned between the lanes. Each culture chamber is juxtaposed to 9 or 4 wells of a 384-well plate, resulting in 40 or 96 arrays of culture chambers in the 3-lanes (Figure 1.8.A+B) or 2-lanes platform (Figure 6.1 in appendix), respectively. The size of each lane (or channel) and phaseguide is presented as 200µm and 50µm of the width and 120 µm and 30µm of the height, respectively.

Our final choice of device was the 3-lanes platform. Each lane possesses an inlet and outlet that face each well in the plate, allowing liquid to fill the well by pipetting without any additional connection of pumping setups and to be injected by capillary force into the lane (Figure 1.8.B). Furthermore, spontaneous perfusion can occur by a difference between of liquid volume between the inlet and outlet, in order to equilibrate their volume (Figure 1.8.D). Average fluid flow was measured as 1.5 µl/h. This indicates that a continuous perfusion is supplied for approximately 24 hours in the case of 25µl of outlet and 100µl of inlet volume.

Trietsch *et al.* proposed a 3-D cultivation model of the various types of cells in this microfluidic device. Cells suspended in hydrogels were injected into the lane and can be aligned along the phaseguide without jumping over. Thus, the cells grow under a three-dimensional geometry by solidification-gelling of the hydrogels to form cell aggregates (Figure 1.8C). This is an additional advantage to the cell clusters embedded in hydrogels, because the cells can be protected from mechanical force, such as shear stress.

As mentioned in the previous section, representative techniques used in the compartmentalization of a microfluidic environment to separate the cell culture area from the medium flow region include the use of pillars, membranes, and artificial barriers. However, those geometries in microenvironments can impede the communication between the compartments due to insufficient diffusion and prevention of direct interaction. Since the height of the phaseguide does not exceed one-fourth of the channel height, nutrient supply, waste product export, and cell-cell communication can occur freely in this device.

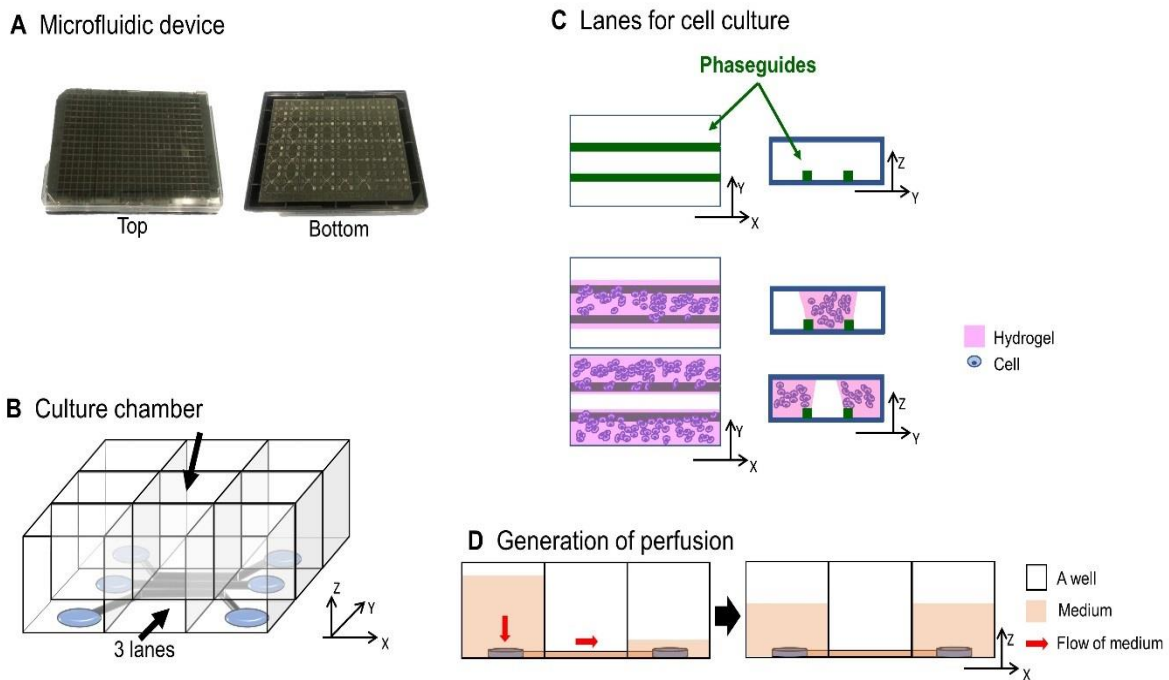


Figure 1.8 Schematic diagrams of a biochip based on a 384 wells plate embedded with microstructures for liver cell cultivation. (A) Top and bottom views of the biochip, (B) View of one culture chamber unit in a 3 lanes platform device. (C) Straight 3 lanes for cell culture with phaseguides placed between the lanes. Cells embedded in the hydrogel and the mixture (cells and hydrogel) can be aligned along the phaseguides, indicating the possibility of 3D cultures, (D) The principle of generation of perfusion without connection of additional pump setups.

1.4 Aim and outline of this thesis

1.4.1 Motivation and aim of the thesis

The liver has diverse functions including synthesis of proteins and various metabolic and detoxification processes, allowing the human body to maintain and sustain life. However, conventional monolayer culture models have limited use as *in vitro* models for observing various phenomena to predict toxic effects and to understand disease mechanisms. Also, *in vivo* animal experimental models have limited ability to serve as human disease models due to species differences, and thus often fail to match human clinical data. Therefore, there is an urgent need to develop an accurate and improved *in vitro* liver model. To date, most researchers have focused only on toxicological studies employing previously developed *in vitro* models, even though the liver also plays a critical role in inflammation.

In vivo, hepatocytes are surrounded by the space of Disse and by lined endothelial cells, and thereby are not exposed to blood flow directly. There are several advantages of using a phaseguide-based microfluidic platform to grow liver cells and also to mimic *in vivo* situations: i) liver cells can grow and be sustained under three-dimensional structures by embedding in hydrogel; ii) cells can freely communicate between adjacent regions (e.g. medium or cells) without physical compartmentalization; iii) liver cells do not directly contact perfusion since they are embedded in hydrogel; and iv) generated perfusion is beneficial to the cells, supplying nutrients and removing waste products. Therefore, we hypothesize that these unique new microenvironments might support the maintenance of hepatic cells in terms of morphology, diverse hepatic functions, and polarity *in vitro*.

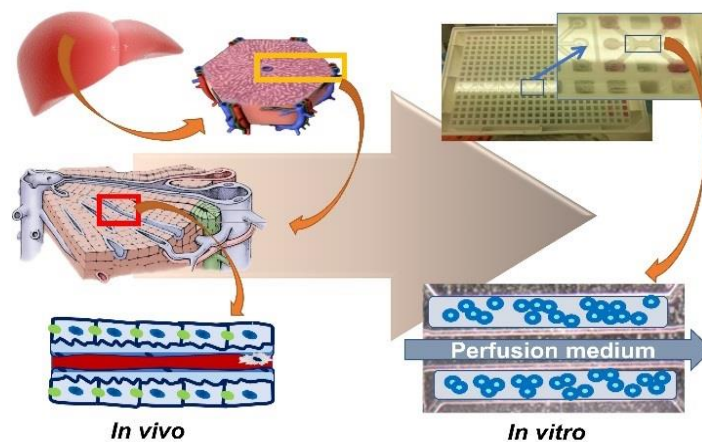


Figure 1.9. The motivation of this thesis to develop a new *in vitro* liver culture model using a microfluidic device by mimicking *in vivo* hepatocyte environments.

The aims of this thesis were to generate a new *in vitro* liver cell culture model using a commercial microfluidic device, and to evaluate various hepatic inflammation responses in the model. We used two types of hepatic cell lines (HepG2 and HepaRG cells) and evaluated their behaviour in new microenvironments, as well as their response to IL-6 treatment for inflammation stimulation. The following research questions are addressed below, and will be subsequently addressed in each chapter of this thesis.

1) What are the differences in the behavior of HepG2 cells in a microfluidic culture compared to static conventional 2D and 3D cultures?

2) How does a newly developed HepG2 cells-on-a-chip platform react to IL-6-induced inflammation and melatonin? Why and how does melatonin modify altered hepatic responses stimulated by IL-6?

3) For HepaRG cultivation in the biochip, how do ECM, flow, and DMSO affect the phenotype of the HepaRG cells? If HepaRG cells can differentiate to hepatocyte-like cells, can they produce CRP by stimulation of IL-6?

4) Are there differences in HepG2 and HepaRG cell behaviours during the microfluidic cultivation process? How similar is this new *in vitro* platform in comparison of the clinical or primary hepatocytes cultivation data?

1.4.2 Outline of this thesis

The thesis consists of five chapters. In Chapter 1, a general introduction was provided including information about the basic liver structures, functions, and roles in inflammation. Moreover, various *in vitro* microfluidics liver model platforms, as well as the final aims of the thesis, were introduced. In Chapters 2-4, more details and topic-specific introductions, methods and material parts, results, and discussions of findings will be presented in each chapter to answer the research questions:

In Chapter 2, a new *in vitro* liver cell cultivation model using an HepG2 cell line in the biochip will be characterized and evaluated. The new biochip cultivation model will be compared to conventional monolayer cultures and 3-D cultures by the characterization of the morphology, cell viability, lactate dehydrogenase (LDH) assay, albumin and urea production rates, bile canaliculi formation, and CYP1A induction. Finally, an acetaminophen-induced toxicity test as a proof-of-concept will be performed for the three different culture platforms, as well as a comparison of their LC50 values.

Chapter 1

In Chapter 3, although the liver plays vital roles in inflammation, most of the applications in new microfluidic *in vitro* liver platforms are limited to investigating drug-induced toxicity and metabolism. This prompted us to evaluate hepatic functions related to inflammation processes induced by IL-6 and melatonin in the newly developed *in vitro* HepG2 cells-on-a-chip platform (discussed in Chapter 2). Various hepatic functions, including detoxification, acute phase response, glucose metabolism, and mitochondrial functions will be explored. In addition, we also will investigate the expression level of several transcription factors that regulate acute phase response and detoxification.

In Chapter 4, the behaviour of HepaRG cells in microenvironments has not yet been fully elucidated up to date. Therefore, our motivation is to cultivate undifferentiated HepaRG cells directly in the biochip, observing their behaviour to test whether HepaRG cells can differentiate in this environment in order to save time, and to avoid the addition of DMSO for toxicology applications. To elucidate the behaviour of undifferentiated HepaRG cells in a new microenvironment, two different ECMs and two different types of perfusion flow—with or without DMSO treatment—will be compared for each experimental setup. The final choice of culture model will then be further investigated for polarization and CRP production by IL-6 stimulation.

The dissertation will be concluded in Chapter 5 with a summary, a conclusion, and an outlook for possible plans and directions in the future.

Chapter 2. On-chip 3D cell culture in phaseguides improves hepatocyte functions *In Vitro*.

This chapter has been published in the biomicrofluidics journal in 2015.

Publication: BIOMICROFLUIDICS 9, 034113, 2015

2.1 Introduction

2.1.1 Motivation and aims of this chapter

The main motivation of this chapter is to test our hypothesis that a 3D culture with a supply of flow contacting the cells indirectly might support the hepatic cells cultivation *in vitro* by using the commercial microfluidic device. Therefore, the aim of this chapter is to develop and to characterize a microfluidic based 3D hepatic cell cultivation system. The HepG2 cell line was chosen to investigate diverse cellular behaviors, including morphology and hepatic specific functions.

To answer the question of how HepG2 cells behave differently in the new microenvironments, Matrigel™-embedded HepG2 cells cultured in this biochip (3D with supply of the indirect flow) were compared with a static Matrigel™ culture (3D) and a monolayer culture (2D) models.

Therefore, the morphology of the cells, cell viability, hepatocyte-specific physiology functions, and acetaminophen-induced toxicity were characterized at least for two weeks. In addition, the intensive discussion will follow with regard to hepatic functions compared to clinical data, primary hepatocyte cultivation results, and other microfluidic hepatic culture models.

2.1.2 Introduction

As we mentioned in previous chapter, the liver plays pivotal roles in almost every field of metabolism such as glucose, nitrogen, and drug metabolism. In addition, the immune and coagulation systems such as the acute phase response has aroused interest in analyzing the special hepatocytes' functions since decades [110]. Nevertheless, the *in vitro* study of liver functions and liver cell-specific responses to external stimuli still deals with the problem to preserve the *in vivo* functions of primary hepatocytes and to depict the *in vivo* situation with stable immortal hepatocyte cell lines. For example, isolated and cultured liver cells display altered transcriptional and translational profiles other than their *in vivo* counterparts resulting in modified metabolism and cellular responses [2].

Hepatocyte's functions are strongly dependent on its morphology and polarization which is rarely achieved by conventional 2D culture [111]. This might lead to misinterpretation and the lack of transferability to the *in vivo* situation, therefore, strongly limits the validity of *in vitro* analysis of liver cell functionality. The embedding of hepatocytes in an extracellular matrix such as naturally derived Matrigel™ preserves cellular morphology and polarization [112]. By using perfusion systems, cells can adequately be supplied with nutrients and oxygen while wastes are removed permanently [113, 114]. The improvement of hepatocytes' proliferation and metabolism by a constant perfusion flow in a microfluidic reactor was shown previously [113]. Nevertheless, a strong flow does not reflect the *in vivo* situation as a hepatocyte in the liver is not in direct contact to blood circulation for endothelial cells and the space of Disse acting as filters to the hepatocytes. The negative impact of strong shear stress on hepatocytes' metabolism has been shown before [115].

Only few research groups have used artificial physical barriers to separate liver cells from flow such as tightly placed micropillars [96, 103], or micro scale walls [93, 94] using microfabrication techniques, or commercial membrane filters [97, 116]. However, those artificial physical barriers might prevent intercellular communication, diffusion of nutrients, waste metabolites clearance, and signaling molecules.

Therefore, to the best our knowledge, this is the first biochip combining several advantages for cultivation of hepatocytes compared to previously developed culture platforms. We hypothesis that following features of this new microfluidic culture model might support hepatic cells cultivation *in vitro* : i) the separation of the cells' culture area and the perfusion flow without any physical barrier, ii) indirect contact of HepG2 cells to the flow due to the polymerization of the extra cellular matrix working as a filter for the cells.

Although the principal suitability of HepG2 cells cultivation in the OrganoPlate was demonstrated [117], a profound basic characterization of hepatocytes cultured in this biochip is still lacking. In order to investigate cells's behavior in new microenvironment and pave the way for further studies with clinical importance, the present study aimed to assess hepatocytes' behavior considering multiple performance criteria: cellular morphology and cell viability over two weeks (clustering, bile canaliculi formation, viability), serum protein production rate (albumin), different metabolisms analysis (urea, CYP1A2 activity), and one clinically important toxicity assay (acetaminophen). The current study clearly demonstrates improved functioning of HepG2 cells in the microfluidic-based chip in comparison to static 2D and 3D cultures pertinent to normal hepatocyte metabolism and drug response.

2.2. Materials and methods

2.2.1. Cell culture conditions

The HepG2 (human hepatocellular carcinoma) cells were purchased from the German collection of microorganisms and cell cultures (DSMZ, Braunschweig, Germany). The cells were cultivated in William's E medium (Pan-Biotech GmbH, Aidenbach, Germany) supplemented with 10% FBS, penicillin (100 U/ml), and streptomycin (100 µg/ml) (Sigma-Aldrich, Munich, Germany) in a 75 cm² flask. They were incubated and maintained at 37°C and 5% CO₂ in a cell incubator (Binder, Tuttlingen, Germany).

The number of cells was counted by using a hemocytometer and the cell viability was assessed by trypan blue exclusion. For monolayer culture (2D), the cells were seeded in conventional 96-well plates (2x10⁴ cells per well). For static 3D culture, cells were mixed with Matrigel™ in the same concentration as for chip cultivation and were layered in 96-well plates as well (Figure 2.1).

The perfused 3D cultivation of HepG2 cells was carried out in the microfluidic platform purchased from MIMETAS company (Leiden, The Netherlands). The microfluidic chip is placed on the ice bucket before the cells are transferred into the device to protect solidification of matrigel. 50 µl of cold phosphate buffered saline (PBS) were added to the observation well to prevent evaporation. The number of HepG2 cells was counted and the appropriate amount was suspended with Matrigel™ (8.2mg/ml) at 4°C on ice to concentrations of 1x10⁷, 5x10⁷, and 1x10⁸ cells/ml. This mixture was injected and sucked by pipetting into the inner channel along the phaseguide by capillary forces. In the case of the 2-lanes device, the cell mixture at concentrations higher than 1x10⁷ was frequently not sucked

inside the lane by capillary force. Due to the difficulties of injecting the cell mixture, we finally chose a 3-lanes device. The cells were incubated at 37°C for 15 minutes to be gelled and 25 µl of the medium was added to the medium outlet. Further, second gelation incubation time to allow entire gelling was chosen for 5-6 hours (Figure 6.2 in appendix). The perfusion was started by adding 100 µl of medium to the inlet well. The medium was renewed every day. For further analysis, the concentration of 8×10^7 cells/ml was used. For experiment optimization, we tested also another perfusion setup: we cultivated HepG2 cells in the middle lane and generated the flow on the side lanes.

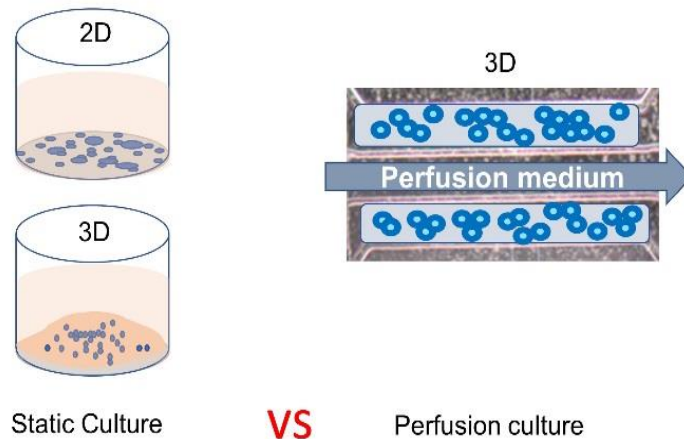


Figure 2.1 Different *in vitro* HepG2 cultivation models. 3D cultivation in the microfluidic device exhibiting phaseguides (in the presence of flow) is compared with static 2D and 3D culture (in the absence of flow) with regard to various cellular behaviors.

2.2.2. Cell morphology visualization

The cell clusters were monitored at day 3, 7, and 14 by using a light microscope. Area and length of cell clusters were measured using the Image J program (<http://imagej.nih.gov/ij>). Cellular plasma membrane and nucleic acids were stained with CellMask plasma membrane stain (5µg/ml, C10046, Invitrogen, Paisley, UK) and DAPI (200ng/ml, D9542, Sigma, Munich, Germany) in PBS, respectively. The cells were incubated with CellMask and DAPI working solution for 30 minutes at room temperature. Fluorescence was monitored using a Zeiss fluorescence microscope (excitation/emission: 365 nm / DAPI filter set for DAPI, 625 nm / Alexa fluor 633 filter set for cellular plasma membrane stain).

2.2.3. Bile canaliculi visualization

Bile canaliculi were visualized by using 5-carboxyfluorescein diacetate (5-CFDA, Sigma-Aldrich, Munich). This non-fluorescent dye is converted by intracellular esterases to the fluorescent carboxyfluorescein (CF) which in turn is excreted via the multidrug resistance associated protein (MRP) transporter expressed in the bile canaliculin [112]. The culture medium was exchanged, supplemented with 5 μ M 5-CFDA, and the cells were incubated for 30 minutes in the incubator. The medium with 5-CFDA was aspirated; the cells were washed 3 times and incubated with a dye free medium for 50 minutes. The 5-CFDA/CF efflux was observed by using a Zeiss fluorescence microscope with a 470 nm excitation and FITC filter set.

2.2.4. LDH activity measurement

The lactate dehydrogenase (LDH) activity in the medium was measured using the colorimetric Lactate Dehydrogenase Assay Kit (ab102526, Abcam, Cambridge, UK) according to the manufacturer's instructions. By using a microplate reader, the optical density was measured at 450 nm immediately after incubation at 37°C for 30 minutes.

2.2.5. Live/Dead staining/visualization

The cellular live/dead assay was performed by using Calcein Blue AM (eBioscience, Frankfurt, Germany) and Ethidium Homodimer III (EthD-III, Biotium, Hayward, USA) staining to determine cell viability. Briefly, the cells were washed three times with PBS buffer after incubated for 30 minutes with 4 μ M calcein AM Blue and 1 μ M EthD-III in PBS. Fluorescence images were taken by using a Zeiss fluorescence microscope (excitation/emission: 365 nm / DAPI filter set for Calcein Blue AM, 530 nm / PI filter set for Ethidium Homodimer III) and analyzed using the ImageJ software.

2.2.6. Albumin measurement

The cell culture medium from HepG2 cells was collected at indicated time points and stored at -80°C immediately. Albumin secreted by cells to the medium was determined using a human albumin ELISA Kit (E88-129, Bethyl Laboratories, Montgomery, Texas, USA). All procedures were followed by the manufacturer's instructions. Optical density at 450 nm was measured with a microplate reader. Experiments were performed in triplicate.

2.2.7. Urea measurement

Culture medium was collected during the cultivation period and stored at -80°C. The amount of urea in the cell culture medium was determined by using a colorimetric urea assay kit (ab83362, Abcam, Cambridge, UK). The procedure was ensued according to the manufacturer's instructions. The optical density at 570 nm was measured with a microplate reader.

2.2.8. Cytochrome P450 1A induction assay

The CYP1A assay was performed with resorufin ethyl ether (Sigma-Aldrich, Munich, Germany) as substrate which is converted by the cytochrome P450 monooxygenases CYP1A1 and CYP1A2 to a fluorescent resorufin product [118]. The HepG2 cells were cultivated with 5 µM 3-methylcholaten (3-MC, Sigma-Aldrich, Munich, Germany) dissolved in medium for 72 hours to induce CYP1A activity. Control cultures were treated with a vehicle solution (DMSO). After the cultivation start, the cells were incubated with 10 µM resorufin ethyl ether in a serum-free medium for 3 hours. Fluorescence was measured at 525/580-640 nm with a fluorescence microplate reader.

2.2.9. Acetaminophen Treatment

For the evaluation of liver toxicity, the cells were treated with acetaminophen (APAP; Sigma-Albrich, Munich, Germany). An APAP stock solution was prepared with DMSO and further diluted in growth medium to concentrations of 0.5-25 mM. As a control, DMSO was diluted in similar concentrations without APAP. 2D and perfused 3D HepG2 cells were cultured for 24 hours and 10 days, respectively. Cells were treated with different concentrations of APAP for 72 hours. Live and dead staining was performed as mentioned above. The measurement was performed in triplicate and a dose response analysis was done by using Origin Lab. The LC 50 value was calculated based on the fitting curve equation in logarithmic scaling.

2.2.10. Statistical analysis

Statistical analysis was performed with SPSS by using One Way ANOVA and with repeated measures for normally distributed data. $P < 0.05$ was considered significant. For the CYP1A induction assay, independent Student's T-test was used. For reasons of clarity and comprehensibility, all data are expressed as means \pm standard deviation (SD).

2.3 Results

2.3.1 Cell and culture morphology under different conditions

First of all, for optimization of chip-based culture, we tested the cultivation in the middle lane and perfusion flow generated at both side lanes. However, the spheroids of HepG2 cells did not retain their clustering morphology. After one week, most of the cells started collapsing their aggregation and showed monolayer-like morphology (Figure 2.2). After 2 weeks of cultivation, the cells did not maintain their aggregation, thereby cell clusters could not be formed at all, while the cells cultured in the side lanes formed cell clusters and well-maintained for 2 weeks. Therefore, we proceeded to cultivate the cells in both side lanes to generate stable cell clusters in the extracellular matrix with less contact of flow for further studies.

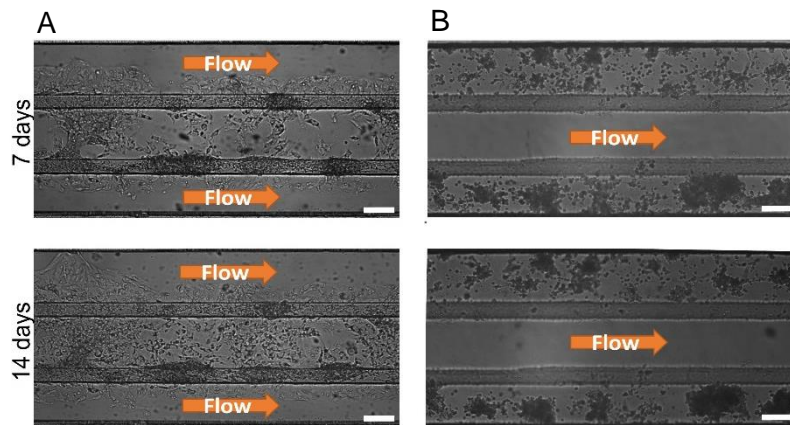


Figure 2.2 The morphology of HepG2 cells cultured in the middle lane (A) and in the side lanes (B) of the device after 7 and 14 days of the cultivation. Scale bars indicate 100 μ m.

After testing HepG2 cultivation in the different location in the chip, the cellular morphology was analyzed at day 7 after the cultivation in the different culture models (Figure 2.3). In the 2D culture, HepG2 cells displayed an epithelial morphology with a spread membrane. In contrast to this, the cells in the static and the perfused 3D culture lay tightly together and their membranes did not spread, whereas the shape was more globular (Figure 2.3A).

The formation and increase of HepG2 cell clusters in the chip cultivation at different cell seeding concentrations is demonstrated in Figure 2.3B. The cells aggregated and arranged themselves to clusters within three days and spheroids maintained more than two weeks. However, when seeding concentration was 1×10^7 cells/ml, matrix and cell clusters were flushed out by the perfusion flow after one week of cultivation in the biochip (Figure 6.3 in appendix). The cluster size differed between different cell seeding concentrations with a

maximum size of 70-80 μm for the culture with 1×10^7 cells/ml and up to 200 μm for 1×10^8 cells/ml at day 7. The formed cell clusters were stable for more than two weeks of cultivation, when the cells cultured in the both side lanes. To analyze the growth of each cluster, their area was measured at day 3, 7, and 14 for each concentration (Figure 2.3C). The cluster area of the 5×10^7 cells/ml culture was slightly higher in comparison to the 1×10^7 cells/ml culture ($3000 \mu\text{m}^2$ vs. $2000 \mu\text{m}^2$). In contrast, the cluster area of the 1×10^8 cells/ml cultured cells was considerably higher with approximately $6000 \mu\text{m}^2$. There were no significant changes between day 3 and day 14 for the 1×10^7 cells/ml and 5×10^7 cells/ml cultured cells. However, for the highest seeding concentration we detected an increase of the cluster area between day 3 and 7. For reasons of augmented adherence of cells in the inlet channel when using the highest concentration, an intermediate concentration of 8×10^7 cells/ml was chosen for further experiments.

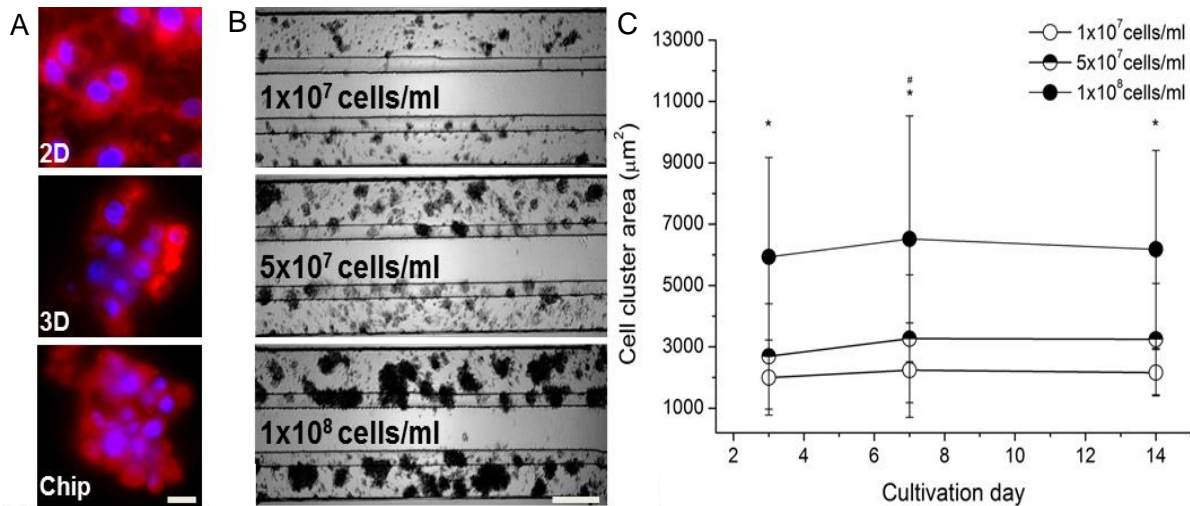


Figure 2.3 Comparison of HepG2 culture morphology in 2D and chip culture after 7 days of cultivation and formation of cell clusters in the perfused microfluidic device. (A) Membrane (red) and nuclei (blue) staining of HepG2 cells in different culturing systems visualized by fluorescence microscopy. Scale bar indicates $10 \mu\text{m}$. (B) Representative images of HepG2 clustering in low (1×10^7 cells/ml), middle (5×10^7 cells/ml), and high (1×10^8 cells/ml) concentrated cultures examined by light microscopy. Scale bar indicates $200 \mu\text{m}$. (C) Aggregation area of variably concentrated HepG2 cultures over time. Data are shown as mean \pm SD ($n = 3$). Significant differences ($p < 0.05$) are indicated as follows: * every concentration vs. the other two at the respective day, # within high-concentrated culture vs. day 3 and day 14.

2.3.2 Viability of HepG2 cells under different culturing conditions

The LDH concentration in the medium of 2D cultured HepG2 cells started to increase after 9 days and reached 5-times higher levels after two weeks in comparison to the respective baseline (Figure 2.4). By contrast, the LDH concentration in the medium of static and perfused 3D cultured cells remained low within 15 days with a slight increase after day 6. There was no significant difference between static 3D and perfused 3D cultures during the two weeks of cultivation.

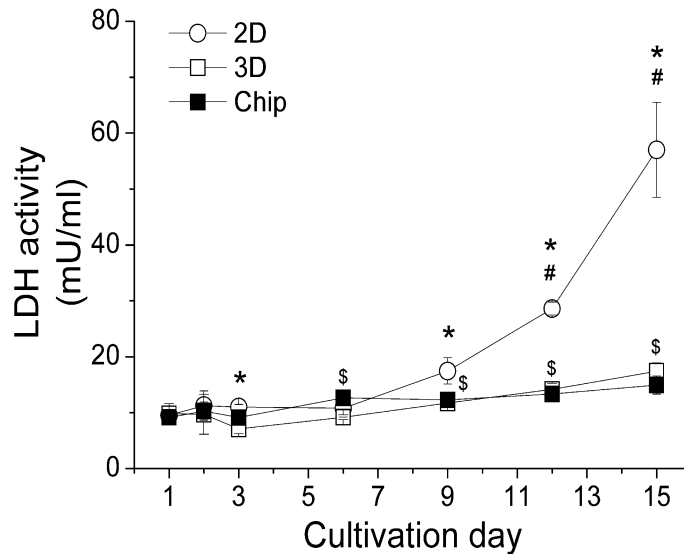


Figure 2.4 LDH release of HepG2 cells within two weeks in the different culture models. Data are shown as mean \pm SD ($n = 3$). Significant differences ($p < 0.05$) are indicated as follows: * 2D vs. chip culture at the respective day, # within 2D culture vs. day 1, 2, 3, 6, and 9, \$ within chip culture vs. day 1 and 3, & within static 3D culture vs. day 1, 2, 3, and 6.

In order to determine dead cells in the perfused 3D culturing system, HepG2 cells were cultivated for a period of three weeks and analyzed on day 7, 14, 18, and 21 (Figure 2.5A). Within the first two weeks, almost no EthD-III staining (red color) was visible. The cells in proximity to the perfused flow started to get damaged after two weeks of cultivation while the cells more distant to the flow survived a longer culturing time. We found only few dead cells inside the spheroids even after two weeks of cultivation (Figure 2.5B). The viability rate assessed by measuring the area of live and dead cells revealed that 80 % of the cells were alive up to three weeks in perfused 3D cultivation.

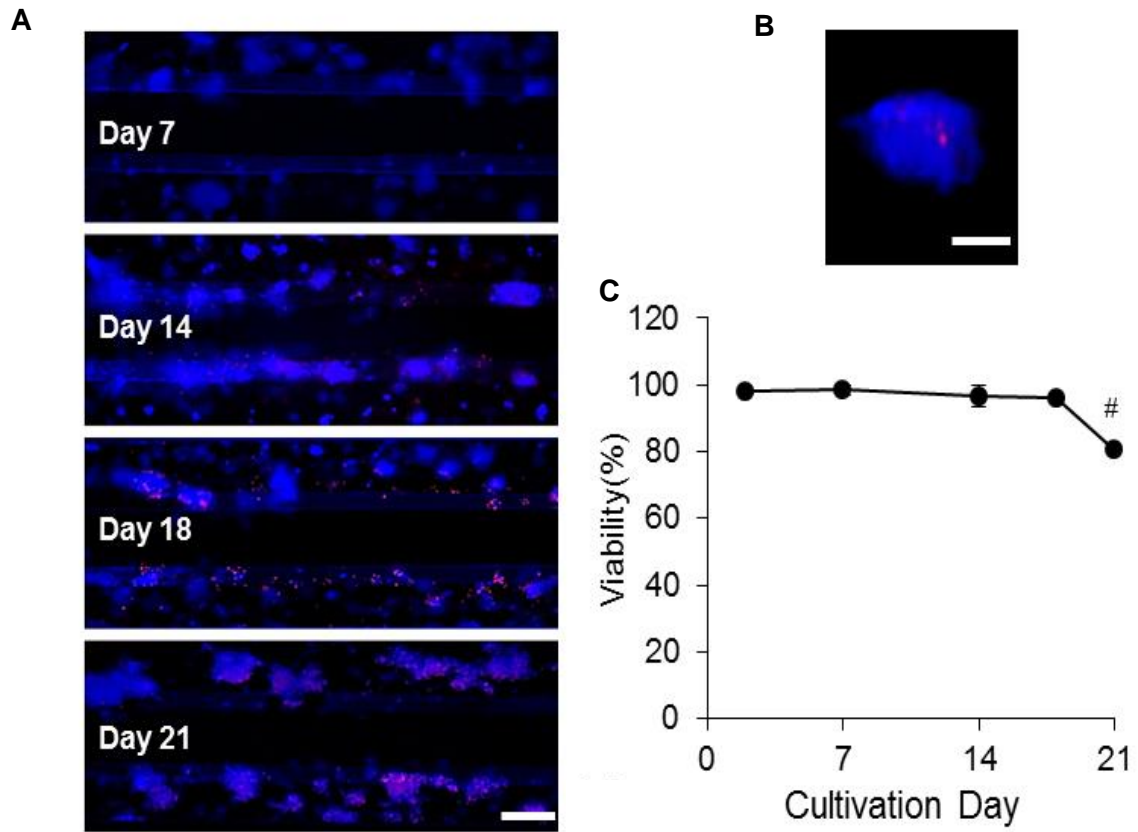


Figure 2.5 Cell viability of HepG2 cells cultured in the microfluidic device. (A) Representative images of live/dead (blue/red) stained cells after three weeks of cultivation. Scale bar indicates 200 μm . (B) Representative image of a spheroid with live/dead staining after two weeks of cultivation. Scale bar indicates 50 μm . (C) Determination of viability from three independent experiments. Data are shown as mean \pm SD ($n = 3$). Significant differences ($p < 0.05$) are indicated as follows: # vs. all other days.

2.3.3 Formation of bile canaliculi in static 2D, 3D, and chip culture

Figure 2.6 represented the formation of bile canaliculi in the different cultivation models. HepG2 cells in static 2D and 3D cultures showed diffuse weak fluorescence signal indicating intracellular location of the fluorescence dye carboxyfluorescein. Small spotted strong fluorescence signal was only seen infrequently in these culturing models. However, the 3D culture in the chip displayed with strong fluorescence within cell clusters indicating the frequent formation of bile canaliculi. This remained stable for more than two weeks.

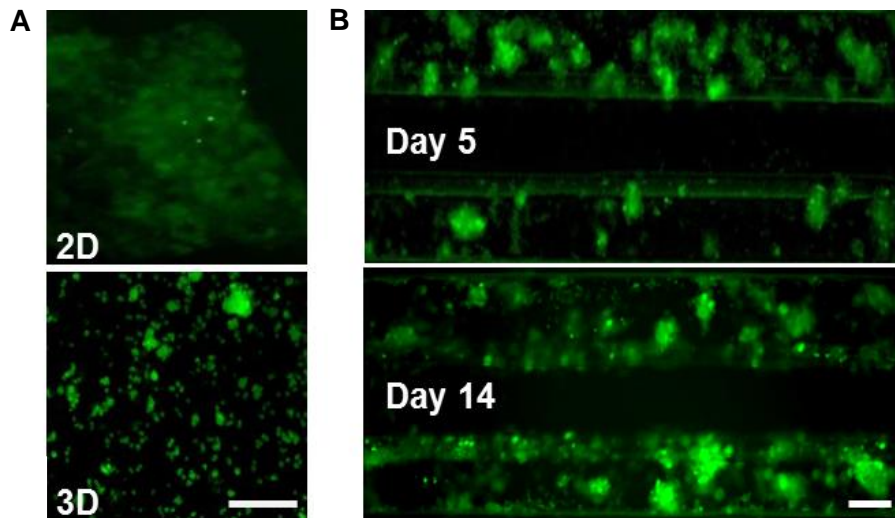


Figure 2.6 Representative images of bile canaliculi formation of HepG2 cells under different culturing conditions visualized by fluorescence microscopy. (A) Static 2D and 3D cultures on day 5. (B) Perfused 3D culture on day 5 and 14. Scale bar indicates 100 μm .

2.3.4 Metabolic activity of HepG2 cells under different culturing conditions

The amount of albumin production as a parameter of metabolic activity under different culturing conditions is shown in figure 2.7. For the entire cultivation period, the albumin concentration in the medium of HepG2 cells in the chip was consistently higher than in the medium of the static 2D and 3D cultures. Beginning with a concentration twice as much as in the static cultures (day 3), the albumin production raised strongly after 10 days of cultivation in the chip, reaching a maximum of 5-times higher levels on day 15 and a tendency to decrease on day 18. In comparison, the levels remained stable in the 2D culture over the whole observation period. In the static 3D culture, we measured a very low increase of albumin at day 12 and this elevated level remained until day 18. Beginning with a concentration twice as much as in the static cultures (day 3), the albumin production raised strongly after 10 days of cultivation in the chip, reaching a maximum of 5-times higher levels on day 15 and a tendency to decrease on day 18. In comparison, the levels remained stable in the 2D culture over the whole observation period. In the static 3D culture, we measured a very low increase of albumin at day 12 and this elevated level remained until day 18.

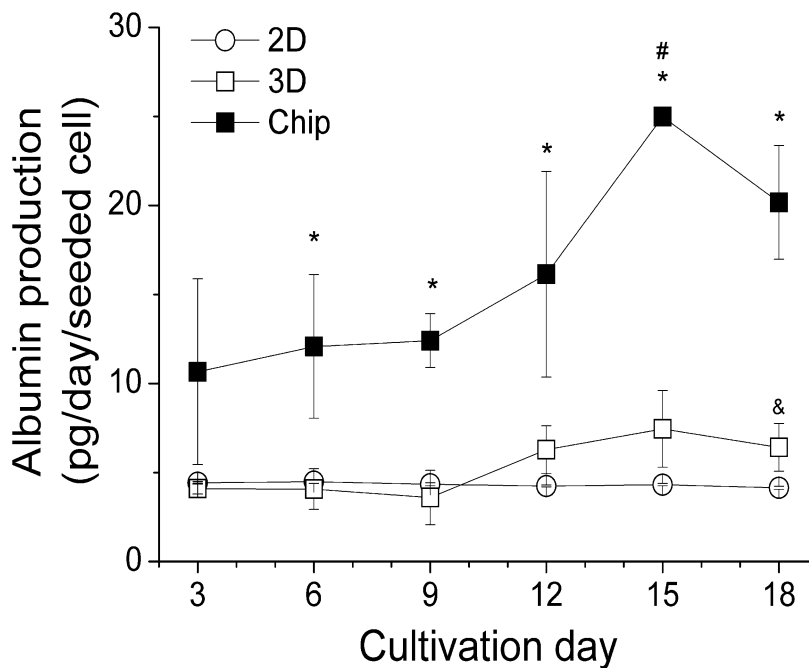


Figure 2.7 Albumin production within 18 days under different culturing conditions. Data are shown as mean \pm SD ($n = 3$). Significant differences ($p < 0.05$) are indicated as follows: * perfused 3D vs. static 2D and 3D cultures, & static 3D vs. 2D culture at the respective day, # within chip culture vs. day 3, 6, 9.

2.3.5 Detoxification capacity of HepG2 cells under different culturing conditions

The urea concentration in the medium of 2D and static 3D cultured HepG2 cells was consistently low over two weeks with approx. 6 nM and 20 nM per seeded cell, respectively. In contrast to this, HepG2 cells in the perfused chip produced a twelve-times (to 2D culture) and a three-times (to static 3D culture) higher amount of urea within 2-14 days of cultivation. A slight decrease of urea production was seen in the chip culture system being significant at day 14 (Figure 2.8A).

The CYP1A induction assay displayed doubled enzyme activity in the static 2D and 3D cultures in comparison to the respective uninduced control. In contrast, resorufin fluorescence intensity in the chip culture model increased 9-times, indicating higher CYP1A activity in comparison to the other culture models (Figure 2.8B).

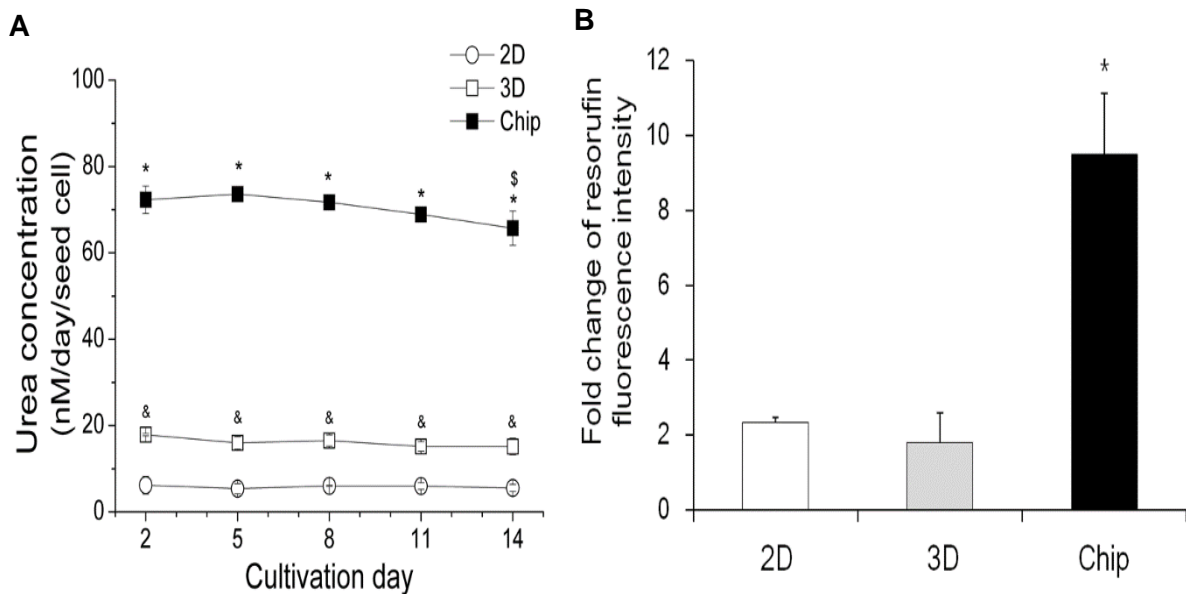


Figure 2.8 Metabolism of HepG2 cells under different culturing conditions. (A) Urea production within 14 days under different culturing conditions. Data are shown as mean \pm SD ($n = 3$). Significant differences ($p < 0.05$) are indicated as follows: * chip culture vs. static 2D and 3D cultures, & static 2D vs. 3D cultures at the respective day, \$ within chip culture vs. day 2 and 5. (B) CYP1A induction assay treated 3-MC for 72 h under different culturing conditions. Fluorescence intensity was normalized to the uninduced control within each culturing model. Data are shown as mean \pm SD ($n = 3$). Significant differences ($p < 0.05$) are indicated as follows: * vs. static 2D and 3D cultures.

2.3.6 Drug-induced HepG2 damage under different culturing conditions

To evaluate the applicability of the microfluidic-based chip culture system for drug-induced cell damage assays, HepG2 cells were exposed to acetaminophen (APAP). Representative pictures and a dose-response curve are presented in Figure 2.9. LC50 of 2D, static 3D, and chip cultures at day 10 were determined at 15.8 mM, 11.8 mM, and 7.1 mM, respectively. At day 5, LC50 of the chip culture was determined at 11 mM, and the cytotoxic effect was not homogenous (Figure 6.4 in appendix). Significantly reduced viability was observed at 5 mM for all culture systems and the treatment with 25 mM reduced the viability to 10% (chip culture), 20% (static 3D culture), and 30% (2D culture).

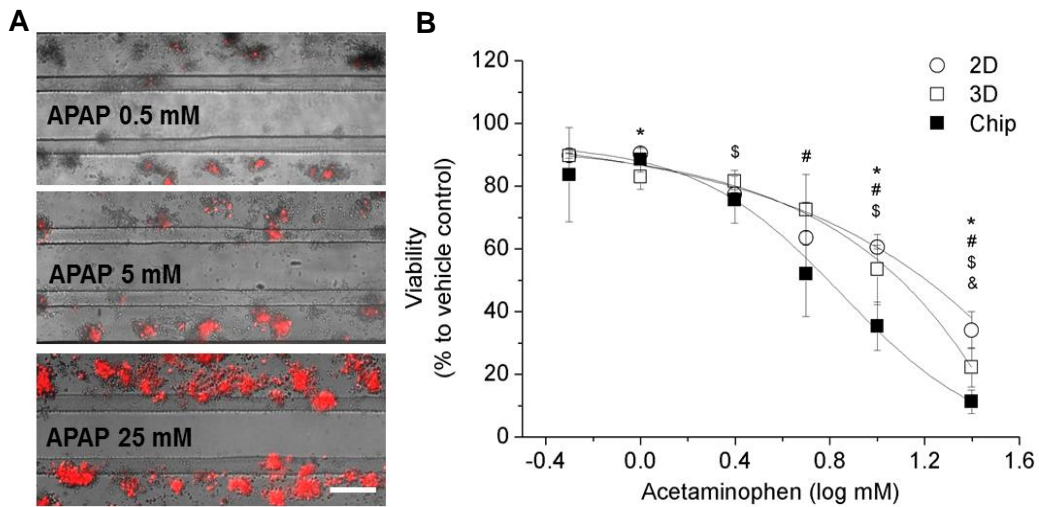


Figure 2.9 Acetaminophen response of HepG2 cells under different culturing conditions. (A) Representative images of HepG2 cells cultured 10 days in the perfused chip and exposed to different concentrations of acetaminophen. (B) Dose-response curve of HepG2 cells exposed to acetaminophen under different culturing conditions. Data are shown as mean \pm SD ($n = 3$). Significant differences ($p < 0.05$) are indicated as follows: * 2D vs. chip culture, \$ static 3D vs. chip culture, & 2D vs. static 3D culture at the respective concentration, # within 2D, static 3D, and chip cultures vs. their respective baseline (0.5 mM).

2.4 Discussion

The major challenge for the *in vitro* cultivation of hepatocytes is the maintenance of their typical morphological characteristics and cellular functions. The embedding of hepatocytes in extracellular matrix (ECM) including Matrigel™ has been demonstrated to prevent cellular dedifferentiation and to help maintain hepatocyte's characteristics [119]. Furthermore, different microfluidic systems have been developed in the past in which constant growth conditions were achieved by a perfusion flow of cell culture medium providing permanent sustenance with nutrients and oxygen as well as removal of waste metabolites [120, 121]. However, to our knowledge, there is still no system described where hepatocytes are cultivated with indirect flow without any physical barrier which would reflect the *in vivo* situation even better. In order to establish a useful cultivation system for the analysis of hepatocellular functions we tested the growth, differentiation, and metabolic behavior of HepG2 cells embedded in Matrigel™ in the OrganoPlate™ from MIMETAS company that combines these unique characteristics.

In our study, the Matrigel™-embedded HepG2 cells aggregated to cell clusters (spheroids) early after plating while the cells in 2D culture grew in a uniform monolayer with an epithelial morphology. These spheroid-like structures in the microfluidic based 3D cultures did not exceed a diameter of 150 µm which should allow sufficient sustenance of the inner cells [122]. The cluster area of the highest concentrated cells increased slightly within the first week of cultivation but the following week did not yield further augmentation which is rather likely due to reduced proliferation caused by contact inhibition [123]. A similar behavior was published previously about HepG2 cells grown as an organotypic culture in spheroid-like structures [124]. Nevertheless, the HepG2-cluster size in our study was not as uniform as the spheroid-size in the study from those authors.

The culture system seemed to preserve cellular viability and integrity over at least 15 days which we demonstrated with multiple performance criteria: i) the constant low LDH in the medium of chip-cultured cells in comparison to a strong increase in the medium of the monolayer cells clearly demonstrates integrity of the chip cells; ii) live/dead staining revealed first dying cells after 14 days of chip culturing and only few dying cells within spheroids; iii) the strong increase of albumin production until day 15 is not seen in the culture of the monolayer cells and less pronounced in the static 3D culture.

Albumin production has been shown to be influenced by the oxygen concentration and by flow-induced shear stress [125]. Considering the increase of albumin production within day 12 to 15 as well as the good viability of the cells within at least two weeks of cultivation, we

suggest that the cells do not suffer from oxygen or nutrient deprivation. In the literature, albumin secretion rates for hepatocytes cultivated in biochips range from 3.6 pg/cell/day (HepG2 cells) over 2.6-19 pg/cell/day (primary human hepatocytes) to 10-60 pg/cell/day (primary rat hepatocytes), and Török *et al.* estimated the *in vivo* secretion rate to 17,8 pg/cell/day [113, 116, 126]. Thus, the levels of albumin secreted from cells cultured in the OrganoPlate™ appear to be in a physiological range and obviously higher than the secretion rates determined for HepG2 cells by Baudoin *et al.* [113].

Some studies have been conducted to find out the effect of shear stress to hepatocyte cultures, all of them demonstrating a decrease of normal hepatocytes' metabolism with increasing flow rates. For example, Tilles *et al.* presented better metabolism of hepatocytes cultivated in a microchannel bioreactor with a flow pressure of 0.01-0.33 dyn/cm² in comparison to 5-21 dyn/cm² [115]. Dash *et al.* estimated physiological flow pressure to 0.6 dyn/cm², and applying this in a collagen sandwich culture improved the functions of their rat hepatocytes over two weeks [127]. Very low flow pressures were applied by Baudoin *et al.* with a range of 0.02-0.06 dyn/cm² which resulted in improved metabolism of their hepatocytes in comparison to static cultures [113]. In our experiments, the shear stress was determined within the channel to 0.3 dyn/cm² which is caused by the hydrodynamic resistance of the small connecting channels (unpublished information from Trietsch, S.J.). Therefore, it is not likely that shear stress poses a problem in this microfluidic chip system and still the flow should be adequate to ensure sufficient nutrient supply and removal of waste metabolites. Nevertheless, in our study, live/dead staining revealed a premature dying of the cells in the proximity of the perfusion channel, clearly indicating a negative influence of the perfusion flow on the HepG2 cells. The more distant cells seemed to be protected against this, probably due to the Matrigel™-embedding.

The strong positive staining of excreted 5-CF even for small clusters suggests differentiation of the chip-cultured hepatocytes in contrast to the static cultures. This is also supported by the higher capacity of nitrogen metabolism of the chip-cultured cells evidenced by considerably augmented urea concentration in the medium. Similar levels of urea secretion were also described by Khetani *et al.* for primary rat hepatocytes, but only when the cells were cultured together with fibroblasts [128]. Hegde *et al.* presented much lower levels of 10-60 pg/cell/day despite cocultivation conditions [116]. The *in vivo* urea secretion rate was stated by Bhatia *et al.* to 120-190 pg/cell/day [129]. Therefore, the culturing of HepG2 in this OrganoPlate™ seems to increase urea secretion to levels that *in vitro* were reached before only by cocultivation systems. Culturing the HepG2 cells in the microfluidic chip increased also their capacity of phase I metabolism (obvious by the increased activity of

CYP1A) in comparison to the conventional monolayer culture and static 3D system. Comparable results were recently described by Hegde *et al.* with six-times higher CYP1A activity in a perfused biochip system in comparison to a static culture [116].

Altogether, the results indicate optimal growth and differentiation of the HepG2 cells in the OrganoPlate™ between day 6 and 14, demonstrated by the slight increase of the cluster area until day 7, by the increase of bile canaliculi staining until day 14, by the decreased viability after day 18, by the increase of albumin production after day 12, and by the decrease of urea production at day 14.

As the toxicity of acetaminophen is one of the most frequent causes of drug-induced liver injuries world-wide [130]. As proof of concept, we used this cultivation model to evaluate the drug induced hepatotoxicity. The chip-cultured cells presented a higher sensitivity for the treatment of acetaminophen than the HepG2 cells grown in monolayer and static 3D culture. This was obvious after five days of cultivation but more pronounced after ten days in chip cultivation. Therefore, we suggested that the time point for toxicity studies should be between after 8 and 12 days of cultivation. This higher sensitivity in the chip cultivation is likely to be caused by the increased expression level of CYP1A and other cytochrome P450 monooxygenases that are necessary for the bioactivation of APAP [131]. In our study, significantly reduced viability was observed at 5 mM for all culture systems. Prot *et al* determined first deteriorations of cell proliferation at 1 mM APAP within their respective microfluidic biochip cultivation system [105]. In another microfluidic biochip used by Ma *et al.*, the viability was reduced to 30% with an APAP concentration of 10 mM which is similar to the results of our study [121]. Xia *et al.* observed that the cells grown in a laminar flow perfusion bioreactor were more sensitive for APAP-induced hepatotoxicity than the cells grown in a static 2D culture, and 60% of cell death was shown after 24 hours of treatment with 25mM of APAP [132]. Even though the APAP toxicity tested in our biochip cultivation model showed a similar result in comparison with other microfluidic hepatic culture models, nevertheless it is not consistent when compared to *in vivo* data exhibiting a toxic plasma level between 1-2mM.

In summary, this is the first report of HepG2 cultivation with indirect flow but without physical barrier. Our finding suggest that HepG2 cells cultured in the OrganoPlate™ from MIMETAS mimicking an *in vivo* hepatocyte environment showed improved and stable hepatic functions for at least two weeks in comparison to 2D and static 3D cultures. The performance criteria were largely comparable to *in vivo* data and in some parts superior to the reports from other perfused culture systems. However, there are still some disadvantages (difficulties of retrieving the cells from the device) and future challenges (co-cultivation with other cell types) which need to be addressed.

2.5 Conclusion

The results of this study clearly demonstrate the superiority of culturing HepG2 cells in a perfused 3D culture system using commercial microfluidic device in comparison to a conventional static 2D and 3D culture. Moreover, the suitability of the applied microfluidic chip for the cultivation of HepG2 cells is evidenced with a high survival rate, improved hepatic functions. This system, therefore, is ready to be used as a promising platform for further hepatic physiological and toxicological studies.

Chapter 3. New HepG2-on-a-chip platform for study of melatonin effects on various hepatic inflammatory responses stimulated by IL-6

3.1 Introduction

3.1.1 Motivation and aims of this chapter

As discussed in Chapter 1, hepatocytes exhibit diverse responses upon stimulation with interleukin IL-6, mainly in the context of inflammation and energy metabolism. Although hepatocytes are involved in inflammation process, previously developed *in vitro* liver models focused solely on drug-induced hepatotoxicity studies. Up to date, there is a lack of the investigation on the alterations of hepatic metabolism caused by inflammation using new *in vitro* systems. Moreover, melatonin has been shown to exert pleiotropic protective actions, such as anti-inflammation and anti-oxidative stress on many cell- and organ-types.

Therefore, after the characterization of HepG2 cells-on-a-chip in previous chapter (Chapter 2), we applied this new *in vitro* platform to evaluate its applicability to study for hepatic inflammatory reactions stimulated by IL-6 and melatonin, as well as to the question of how melatonin interacts with hepatic inflammation status.

The key roles of the liver, including maintaining homeostasis and metabolic regulation, will be evaluated in the context of acute phase response, detoxification, glycogen, and energy metabolism.

3.1.2 Introduction

Liver diseases are generally associated with increased inflammation accompanied by the rise of various pro- and anti-inflammatory cytokines. Hepatocytes react on inflammatory stimuli with diverse stress response mechanisms. One mechanism aiming to directly protect the respective cell from protein damage and dysfunction of cellular organelles can be noted as endoplasmic reticulum (ER) stress response including unfolded protein response (UPR), another mechanism acting globally to protect all affected cells and organs is innate immune response.

Interleukin 6 (IL-6) is a cytokine and secreted by activated immune cells, leading to elevated plasma levels found in multiple diseases, and also secreted by liver macrophages, thereby stimulating hepatocytes locally [133]. This cytokine stands out for very pleiotropic actions which are regulated by the composition of the complex that IL-6 forms with its receptors IL-6R and gp130 either in their soluble or in their membrane-bound forms [134]. IL-6 is involved in inflammation and acts as a major regulator for the APR, whereas other proinflammatory cytokines such as IL-1 and TNF- α could play a minor role due to their limited stimulation of major APR proteins [37, 135]. Some studies also indicate a link between IL-6 signaling, the UPR, and the induction of APR genes [67, 136, 137]. Other effects of IL-6 on hepatocytes are related to altered expression levels of cytochrome P450 monooxygenases and drug transporters, thereby modifying hepatic detoxification mechanisms [138, 139]. IL-6 also affects glucose metabolism in the liver, accompanying glycogen depletion [140]. A recent study discovered the translocation of signal transducer and activator of transcription 3 (STAT3) to the mitochondria of immune cells, thereby modifying the mitochondrial membrane potential and highlighting a new pathway of IL-6 signaling [141].

The hormone melatonin is particularly known for its main function in regulating the circadian clock. Moreover, melatonin has been shown to possess strong anti-inflammation and anti-oxidative stress organ-protective properties [57, 62, 142]. In previous studies, our collaboration group found evidence for the modification of cellular stress mechanisms by melatonin in the context of inflammation. For example, increased levels of gene expression involved in ER stress, such as protein kinase RNA-like endoplasmic reticulum kinase (PERK) and DNA damage-inducible transcript 3 (DDIT3) was observed in melatonin-treated septic animals [66]. Rats with hemorrhagic shock revealed that melatonin inhibited the shock-induced upregulation of UPR modifying proteins [143]. These studies also revealed that melatonin modifies the expression of the transcription factor CREBH that seems to be an important player for mediating the hepatic signaling of IL-6 via the ER stress response to

activate the APR [144]. Furthermore, regulatory effects on glucose metabolism by CREBH were described [145]. Therefore, it is very interesting to check whether melatonin involves the acute phase response regulation via CREBH. Although the anti-inflammatory function of melatonin is well known, to our knowledge there is no study relating APR and melatonin.

Mitochondria provide energy to the cell but are also a main organelle for free radical production during ATP production, resulting in oxidative stress. In addition, UPR induced overload of reactive oxygen species (ROS), calcium production in the ER, accompanying altered mitochondrial membrane potential [146]. Interestingly, melatonin is accumulated in mitochondria and exerts protective effects via scavenging reactive oxygen species (ROS) and inhibiting the mitochondrial permeability transition pore (MPTP) [147]. Therefore, mitochondria are considered as main target organelles for melatonin.

Still, most inflammation studies rely on animal experiments, even though the poor correlation with human conditions often misleads the physiological and genetic results on humans [102, 148]. Since a decade, various new *in vitro* liver platforms have been developed to reduce this gap. However, most applications focused on drug screening and drug induced hepatotoxicity studies. Nearby this detoxification function, the human liver is also involved in inflammation processes. Therefore, the need of developing precise and predictable *in vitro* human liver models to study inflammation is urgent. We developed a new cultivation system as a liver-on-a-chip platform which preserves a considerable range of human hepatic functions [149].

Therefore, it is very interesting to evaluate how this new system works for the study of liver cells in response to inflammation stimulated by IL-6 and the interplay of melatonin. The aim of this study is to evaluate the various inflammatory hepatocellular responses by IL-6/melatonin, including detoxification, APR, glycogen storage, and mitochondria functions in HepG2-on-a-chip.

3.2 Materials and methods

3.2.1 Cell culture conditions

The HepG2 (human hepatocellular carcinoma) cells were purchased from the German collection of microorganisms and cell cultures (DSMZ, Braunschweig, Germany). The cells were cultivated and maintained as previously described in chapter 2. The number of cells was counted by using a hemocytometer and the cell viability was assessed by trypan blue exclusion. In this study, we decreased the concentration of seeded cells to 5×10^7 cells/ml in matrigel and mixture of cells and matrigel were transferred to each chamber of the OrganoPlate™ (Mimetas company, The Netherlands) as previously described in chapter 2. The medium was renewed every two days. The average size of cell aggregates was shown $100 \pm 50 \mu\text{m}$.

3.2.2 IL-6 and melatonin treatment conditions

An IL-6 (Humanzyme, Chicago, USA) stock solution (10 $\mu\text{g/ml}$) was prepared with 0.1 % BSA (Sigma-Aldrich, Munich, Germany). Melatonin (Sigma-Aldrich, Munich, Germany) was dissolved in DMSO (1M) to be used as a stock solution and stored at -20°C . Working solutions were prepared freshly with similar amounts of BSA and DMSO. At the 10th day of cultivation in the chip, cells were treated with IL-6 (100 ng/ml), physiological melatonin concentration (1 nM) [150], IL-6 plus melatonin, or control (0.001 mg/ml BSA, 0.0000001 % of DMSO) solutions for 72 hours. The cytokine concentration was selected according to the preliminary result and literature reports [151]. From the preliminary experiments (Figure 3.1), 100ng/ml of IL-6 was chosen, which showed a significant change compared to control group.

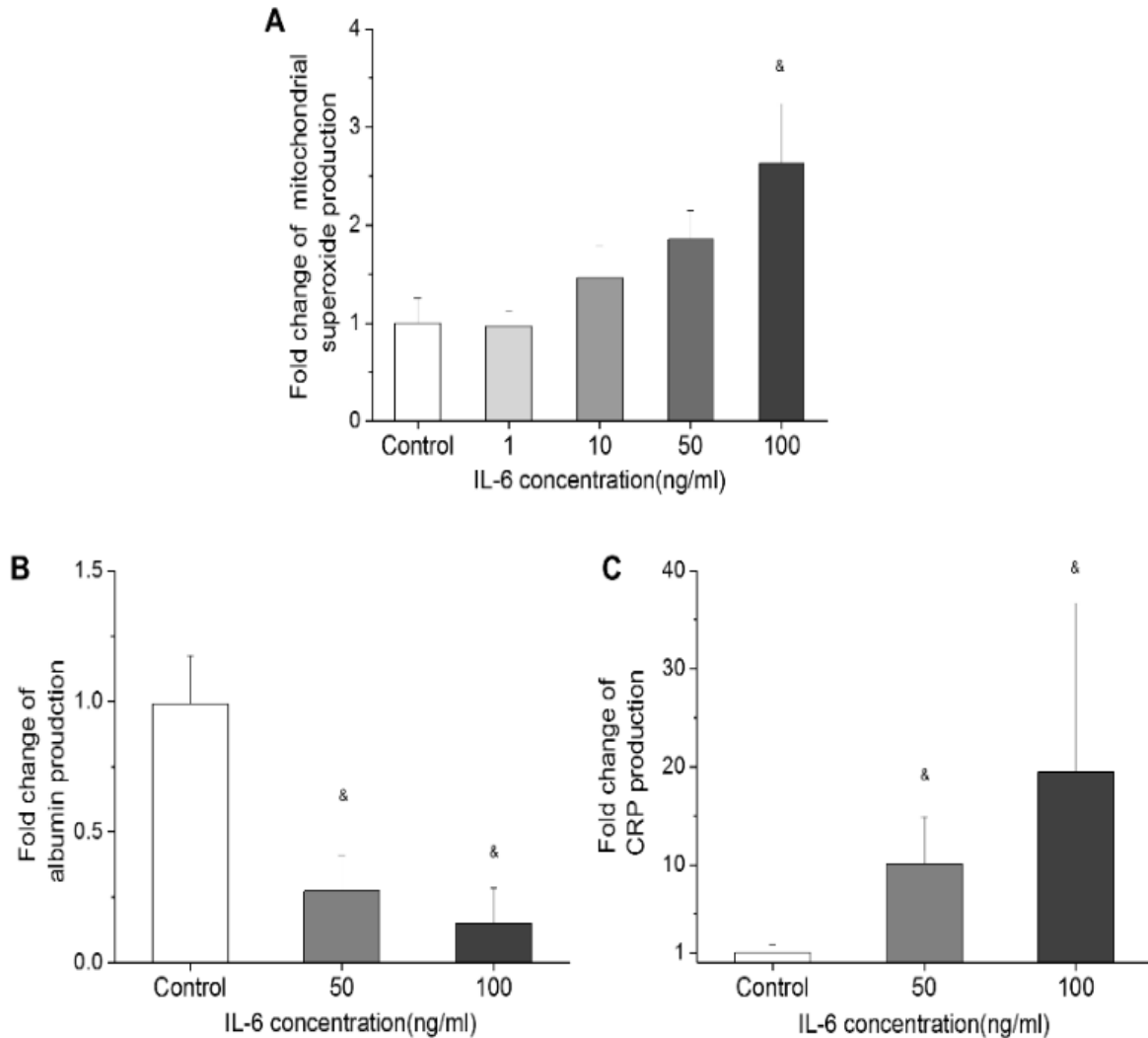


Figure 3.1 Fold change of mitochondrial superoxide production (A), albumin production (B), and CRP production (C) in HepG2 cells-on-a-chip stimulated by IL-6 (dose dependency). \$ indicates a significant difference ($p < 0.05$) versus control group. Experiments were performed three times and data are shown as mean \pm SD.

3.2.3 Efflux transport assays

Efflux transport assays were performed by using fluorescent substrates. 5-CFDA (Sigma-Aldrich, Germany) was used as a substrate for the multidrug resistance associated protein (MRP2). HepG2 cells in the chip were washed with uptake buffer [152] and then incubated for 30 minutes with 5 μ M of 5-CFDA. Cells were then washed three times with PBS buffer and immediately monitored under a fluorescence microscope (FITC filter set). MK-571 (Sigma-Aldrich, Germany) was used as an inhibitor for the efflux of MRP2. The cells were incubated with 50 μ M of MK-571 for overnight.

3.2.4 Expression of CYP1A (phase I metabolism cytochromes)

The CYP1A assay was performed with resorufin ethyl ether (Sigma-Aldrich, Munich, Germany) as a substrate which is converted by the cytochrome P450 monooxygenases CYP1A1 and CYP1A2 to a fluorescent resorufin product. After the treatment of IL-6 and melatonin for 72 hours, the cells were incubated with 10 μ M of 7-ethoxyresorufin in a serum-free medium for 4 hours. Fluorescence intensity was measured at 525/580–640 nm by using a fluorescence microplate reader.

3.2.5 Immunofluorescence staining

The protein expression levels of MRP2, the pregnane X receptor (PXR), CREB3L3 for ER stress and hepcidin for positive APR were determined by immunostaining. Cells in the microfluidic device were fixed in 4 % paraformaldehyde for 30 minutes at room temperature and permeabilized with 0.2 % solution of Triton X-100 in PBS for 30 minutes. After blocking with 1 % BSA for 30 minutes, the cells were incubated with a primary antibody for hepcidin (1:100, ab30760, Abcam, Cambridge, UK), MRP2 (1:50, ab3373, Abcam), PXR (10 μ g/ml, ab118336, Abcam), and CREB3L3 (1 μ g/ml, ab150865, Abcam, Cambridge, UK) at 4 °C overnight. Subsequently, the cells were stained with the secondary antibody DyLight 488 goat anti rabbit (1:100, ab96899, Abcam, Cambridge, UK) and with Hoechst 33345 (Sigma-Aldrich, Germany) for nucleic acids staining for 1 hour at room temperature. After washing with PBS three times, images were acquired using a Zeiss fluorescent microscope (485 nm LED and FITC filter sets). All fluorescent images were quantified using Image J and normalized to total cell area.

3.2.6 Albumin and CRP measurement

Commercially available ELISA kits were used to determine the amount of albumin (Human Albumin ELISA Kit, E88–129, Bethyl Laboratories, Montgomery, Texas, USA) and CRP (Human C-Reactive Protein ELISA Kit, KHA0031, Life technology, Frankfurt, Germany). The culture medium was collected at indicated time points and stored at -80 °C until usage. All procedures were followed by the manufacturer's instructions. Optical density at 450 nm was measured with a microplate reader.

3.2.7 Assays on mitochondrial integrity

The JC-1 mitochondrial membrane potential kit (No. 10009172, Cayman chemical, Tallinn, Estonia) was used according to the manufacturer's instructions. The cells were washed with PBS and incubated for 20 minutes with the freshly prepared JC-1 working solution (3 μ g/ml) in a CO₂ incubator at 37°C. The cells were washed with PBS, the fluorescence of JC-1

aggregates (red) and monomers (green) were measured microscopically (Texas Red, 530/590 nm; FITC, 485/520 nm), and the red to green ratio was calculated.

MitoSOX™ Red (M36008, Molecular probes, Karlsruhe, Germany) was used to determine the mitochondrial superoxide production. According to the manufacturer's instructions, a 5 mM stock solution in DMSO was further diluted to 2.5 µM in PBS as a working solution. Cells were incubated 10 minutes and gently washed three times with warm PBS buffer. After washing, cells were examined under a Zeiss fluorescent microscope (Texas Red filter set). All fluorescent images were quantified using Image J and normalized to the total cell area.

3.2.8 Alteration in glucose metabolism (glycogen content)

For the determination of the amount of stored glycogen in HepG2 cells clusters the Periodic Acid-Schiff (PAS) Staining Kit (No. 395B, Sigma-Aldrich, Munich, Germany) was used. Staining was performed according to the manufacturer's instructions. Briefly, cells were fixed with FAA (formalin-acetic-alcohol) for 3 minutes and washed three times with water, incubated with the PA solution for 5 minutes, washed four times, and placed in Schiff's reagent for 15 minutes. After continuous washing with water, cells were stained with hematoxylin for 1 minute. Ten cell clusters from each group were selected and the PAS stained area was quantified using Image J.

3.2.9 Statistics

All data are presented as fold change to the respective control group. Statistical analysis was performed using SPSS (IBM, Ehningen, Germany) by using One Way ANOVA for normally distributed data, otherwise Kruskal-Wallis One Way ANOVA on ranks, followed by Tuckey's range test for pairwise multiple comparisons. $P < 0.05$ was considered significant. For reasons of clarity all data are expressed as means \pm standard deviation (SD).

3.3 Results

3.3.1 IL-6 reduced the detoxification capacity of HepG2 cells

3.3.1.1 MRP2 expression level and efflux activity

To investigate whether the expression level and functional activity of MRP2 are maintained under IL-6 and/or melatonin treatment, immune staining and a specific substrate (5-CFDA) for MRP2 were used. Representative fluorescent images for the staining of MRP2 expression and the respective quantified results are shown in figures 3.2 A+B. IL-6 treatment markedly decreased MRP2 expression (40 % of the control). Interestingly, melatonin alone seemed to increase MRP2 expression (120% of the control), nevertheless, this was not significant. In the case of co-treatment of melatonin and IL-6, MRP2 expression levels were comparable to basal levels and significantly higher than in to the group that received IL-6 alone.

Furthermore, we determined the functional activity of MRP2 transporters by measuring the accumulation of 5-CF intracellularly and at the bile canaliculi after excretion through MRP2. Clusters of HepG2 cells in the control and melatonin groups showed accumulation of exported 5-CF green fluorescence in the middle of the cell spheroid and only little intracellular fluorescence, indicating high transporter activity. In contrast to this, in the presence of IL-6, only intracellular fluorescence was observed. The MRP2 inhibitor MK571 served as control. Cells in presence of MK571 showed only diffused and blurred intracellular fluorescence (Figure 3.2C).

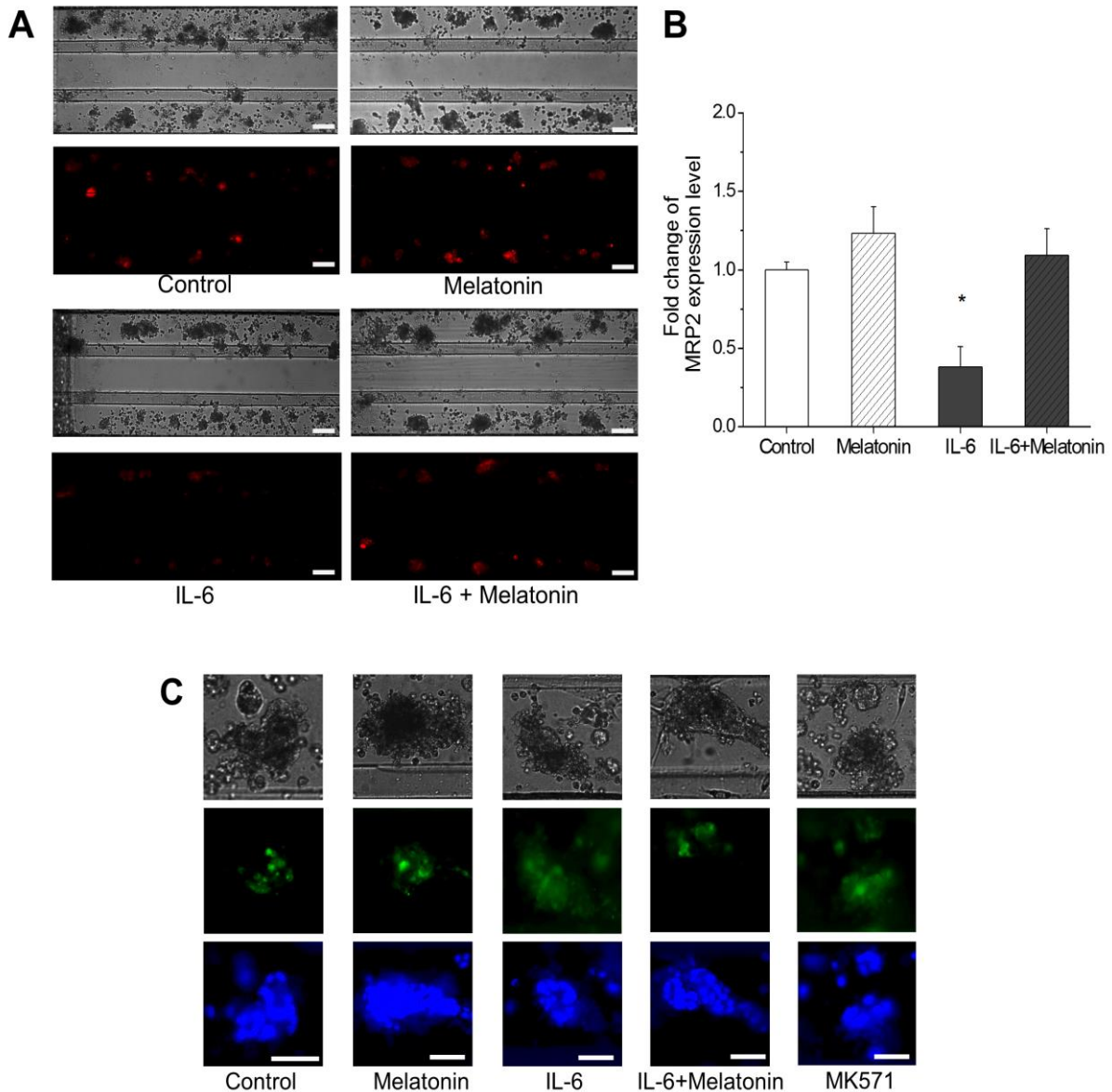


Figure 3.2 MRP2 expression levels and its transporter efflux assay on HepG2 cells after IL-6 and/or melatonin treatment. (A+B) MRP2 expression presented by representative light and fluorescent images and quantified by the calculated fluorescent intensity per total cell area. Scale bar indicates 100 μm . Data are shown as mean \pm SD ($n = 4$). Significant differences ($p < 0.05$) are indicated as follows: * vs. Control, Melatonin, IL-6+Melatonin. (C) Representative images of the MRP2 efflux activity assay of each group. The HepG2 spheroids were observed by phase contrast and fluorescence microscopy. The light images (first horizontal line in C), excreted 5-CF (middle horizontal line in C), nucleic acids staining (last horizontal line) are shown of each group. Scale bar indicates 50 μm .

3.3.1.2 Effect of IL-6 and melatonin on PXR expression

Furthermore, we investigated whether PXR expression levels are influenced by IL-6 and melatonin, since PXR is known to be a major regulator for MRP2 expression [153]. Representative fluorescent images for PXR protein expression and the respective quantified results are shown in figure 3.3. When treating with melatonin alone, PXR expression levels did not change (92 % of the control). However, IL-6 administration induced significantly decreased PXR expression levels, while melatonin co-treatment reversed this IL-6-induced reduction (80 % of the control).

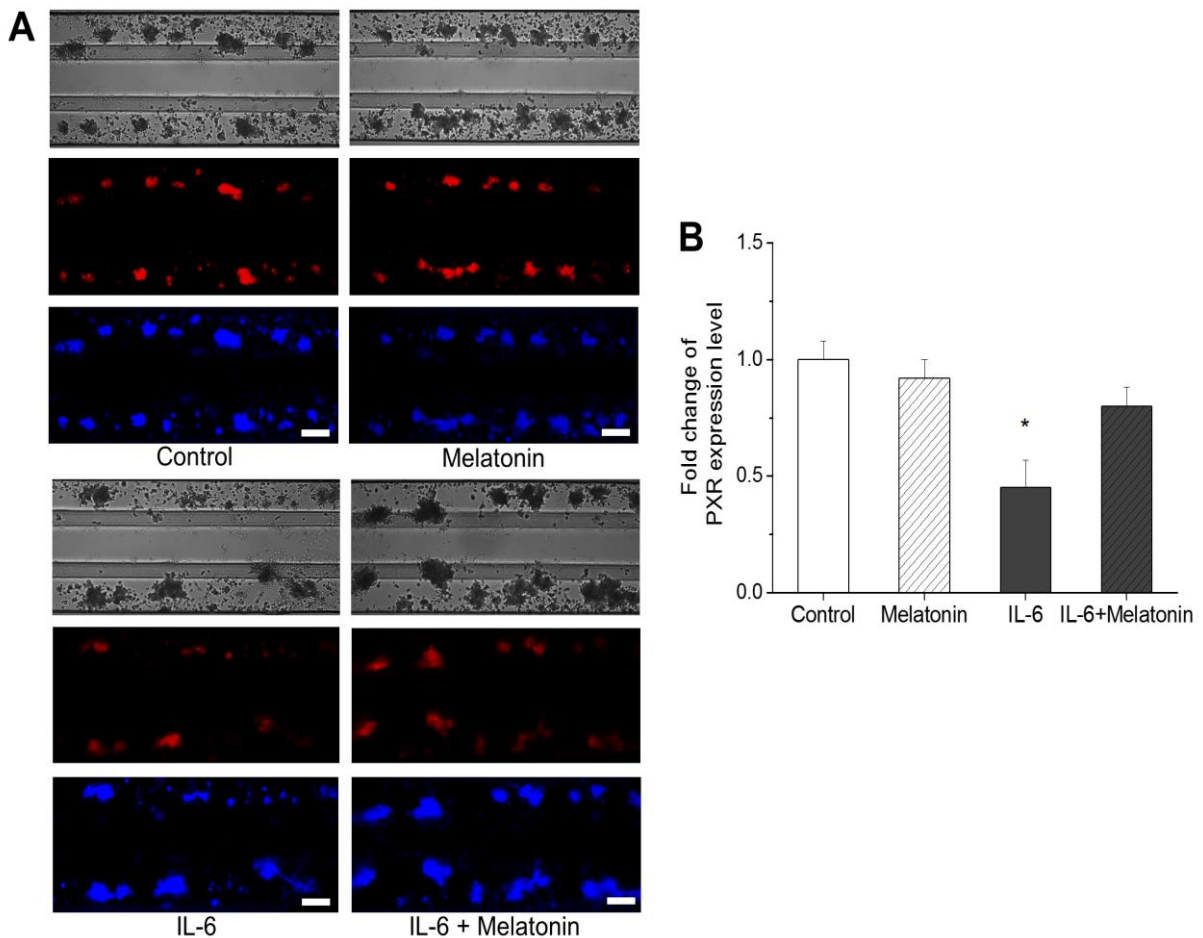


Figure 3.3 PXR expression level on HepG2 cells after IL-6/and or melatonin treatment. (A) PXR expression presented by representative light and fluorescent images and (B) quantified by the calculated fluorescent intensity per total cell area. Scale bar indicates 100 μm. Data are shown as mean ± SD ($n = 3$). Significant differences ($p < 0.05$) are indicated as follows: * vs. Control, Melatonin, IL-6+Melatonin.

3.3.1.3 Effects of IL-6 and melatonin on the activity of CYP1A

The addition of IL-6 to HepG2 cell clusters in the Organoplate™ for 72 hours resulted in a significant 10-15% reduction of CYP1A activity in comparison to the control group, as indicated by 7-ethoxy resorufin-O-deethylase (EROD) activity (Fig. 3.4). On the other hand, when cells were treated simultaneously with melatonin, CYP1A activity levels were comparable to basal levels. A slight tendency of lowered activity was seen by melatonin administration alone (95% of the control).

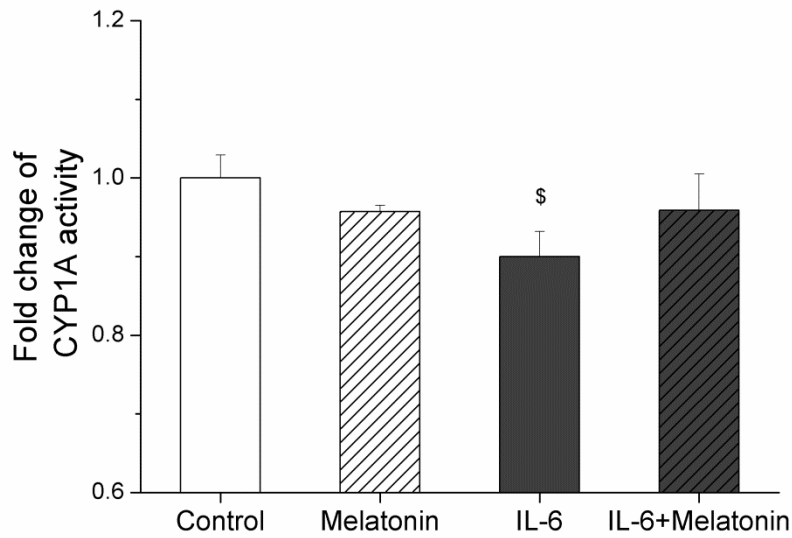


Figure 3.4 CYP1A activity in HepG2 cells after IL-6 and/or melatonin treatment estimated by EROD activity. Data are shown as mean \pm SD (n = 6). Significant differences ($p < 0.05$) are indicated as follows: \$ vs. Control.

3.3.2 Melatonin modified CREB3L3 expression levels and the IL-6-induced acute phase response

Albumin production was strongly reduced after administration of IL-6 (15% of control, Fig. 3.5A). Simultaneous melatonin administration tended to reduce the albumin repression, but with high intergroup variability resulting in a high standard deviation. Melatonin alone did not increase albumin production over basal levels of the control group.

C-reactive protein (CRP) production by HepG2 cells was increased 19-fold change in cultures treated with IL-6 (Fig. 3.5B). Melatonin did not alter CRP levels markedly, neither when given alone nor in combination with IL-6. Hepcidin expression levels were also elevated by IL-6 administration (2,2-fold over control, Fig. 3.5C+D). Opposed to CRP, melatonin prevented this upregulation entirely.

In order to determine the impact of IL-6 and melatonin on CREBH, the ER-bound transcription factor representing the possible link between IL-6 signaling, the ER stress response and the APR, its expression levels were determined in the different treatment groups. CREBH protein expression was significantly reduced by IL-6 treatment to 40% in comparison to the control (Fig. 3.6). Melatonin alone did not alter the protein amount of this transcription factor, but clearly counteracted the lowered expression observed in the IL-6 group.

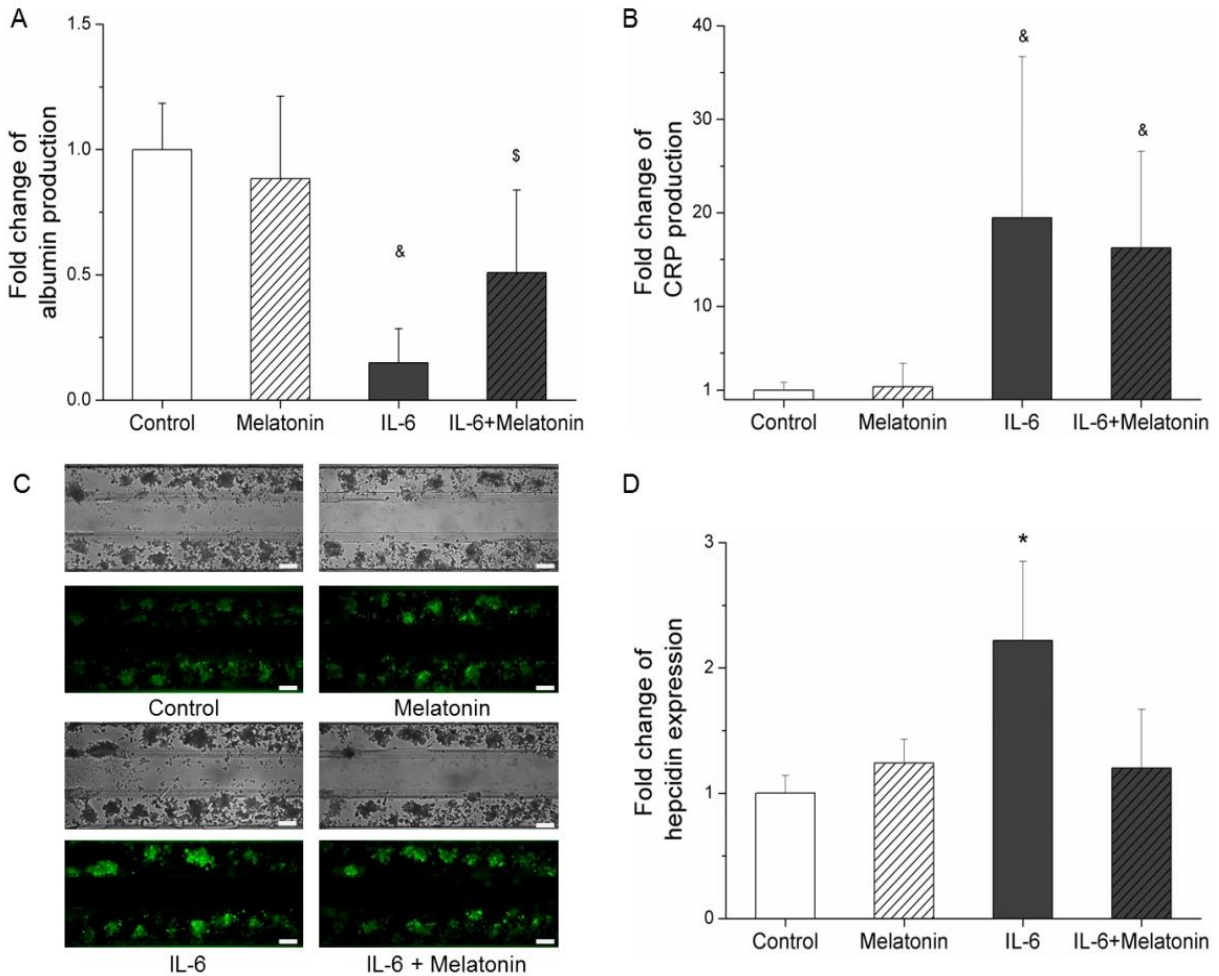


Figure 3.5 Acute phase response of HepG2 cells 72 hours after IL-6 and/or melatonin treatment. (A+B) Albumin and CRP levels determined by ELISA and normalized to fold change to control. Data are shown as mean \pm SD (n = 5). (C+D) Hepcidin expression presented by representative light microscopical and fluorescent images and quantified by the calculated fluorescent intensity per total cell area. Data are shown as mean \pm SD (n = 4). Significant differences ($p < 0.05$) are indicated as follows: * vs. Control, Melatonin, IL-6+Melatonin; \$ vs. Control; & vs. Control, Melatonin.

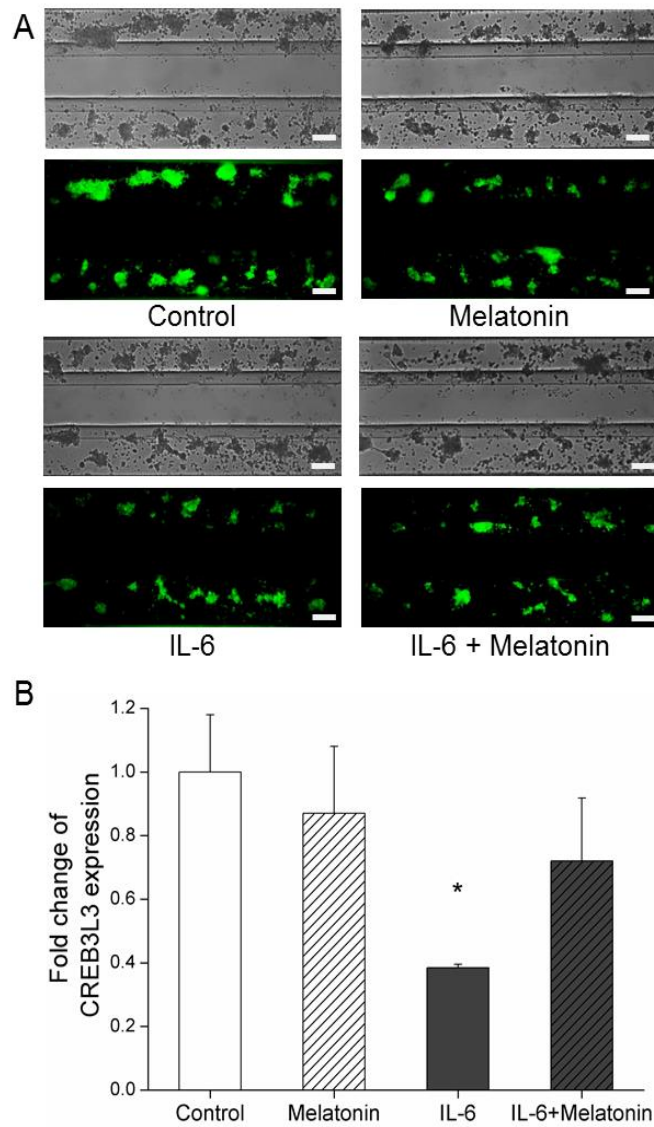


Figure 3.6 CREBH expression in HepG2 cells after IL-6 and/or melatonin treatment. (A) Representative images via transmitted light microscopy and immune fluorescent imaging of HepG2 cells cultured in the OrganoPlate™. Scale bar indicates 100 μ m. (B) Quantification of the fluorescent intensity per total cell area. Data are shown as mean \pm SD (n = 4). Significant differences ($p < 0.05$) are indicated as follows: * vs. Control, Melatonin, IL-6+Melatonin.

3.3.3 Alterations of mitochondrial functions in HepG2 cells

Mitochondrial functions were determined on the basis of alterations in the mitochondrial membrane potential (MMP) and the production of mitochondrial superoxide, by employing fluorescent probes. The MMP of HepG2 cells was constant within repeated control experiments. IL-6 treatment consistently reduced the red/green fluorescence ratio of JC-1 by half in comparison to the control (Fig. 3.7A). Simultaneous melatonin treatment mitigated the IL-6-induced reduction of the MMP, but did not elevate the MMP to basal levels (70 % of control). Melatonin alone did not considerably change the MMP although the values scattered considerably stronger than in the control group.

Mitochondrial superoxide production was also affected. IL-6 treatment increased the levels 2.6-fold while cells co-treated with melatonin had almost basal superoxide levels (Fig. 3.7B). Moderately increased values (<1.7-fold) were obtained when cells were treated with melatonin alone, although this was not significant.

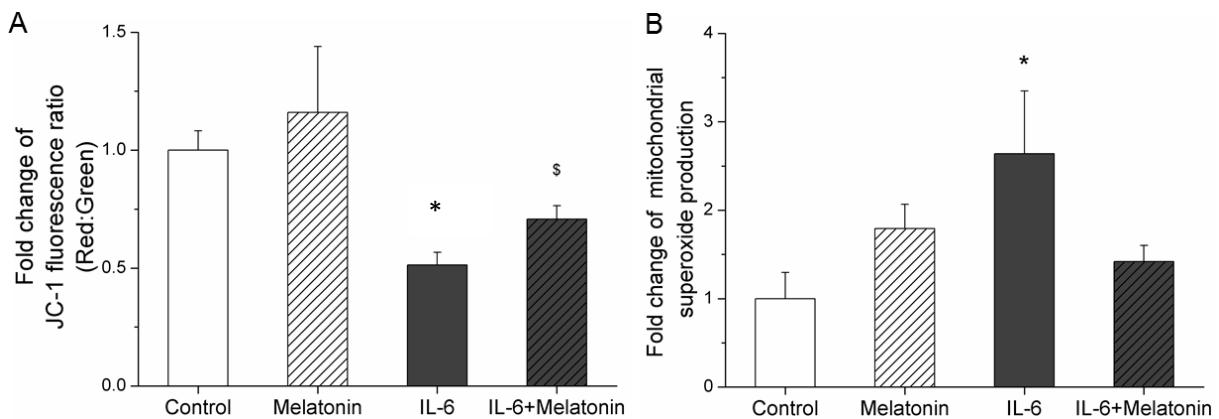


Figure 3.7 Mitochondrial functions of HepG2 cells assessed by measuring the MMP and superoxide production after IL-6 and/or melatonin treatment. (A) Fold change of red/green ratio of JC-1 for the assessment of the MMP. Data are shown as mean \pm SD (n = 3). (B) Mitochondrial superoxide production assessed by MitoSOXTM staining. Data are shown as mean \pm SD (n = 4). Significant differences (p < 0.05) are indicated as follows: * vs. Control, Melatonin, IL-6+Melatonin; \$ vs. Control.

3.3.4 Reduced glycogen storage of IL-6 treated HepG2 cells

In order to assess the impact of IL-6 and melatonin on glucose metabolism, glycogen storage was determined in the differently treated cultures. While most vehicle and melatonin treated cells exhibited strong glycogen staining visible by the dark purple color, only 65 % were darkly stained in the IL-6 treatment group while the majority of other cells remained clear (Fig. 3.8).

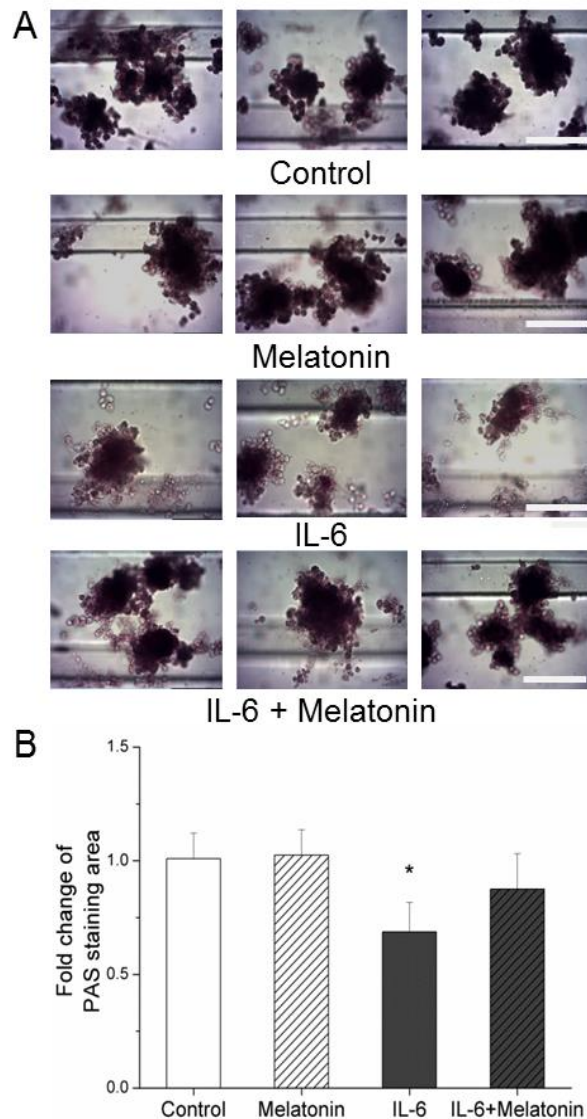


Figure 3.8 Glycogen staining of HepG2 cells after IL-6 and/or melatonin treatment. (A) Representative images via transmitted light microscopy of HepG2 cells cultured in the OrganoPlate™ after PAS staining. Scale bar indicates 100 μ m. (B) Quantification of the glycogen staining intensity per cluster. Data are shown as mean \pm SD (n = 2). Significant differences ($p < 0.05$) are indicated as follows: * vs. Control, Melatonin, IL-6+Melatonin.

3.3.5 STAT3 phosphorylation of IL-6 and melatonin treated HepG2 cells

In order to assess whether IL-6 and melatonin modify STAT3 signal pathway in the HepG2 cells platform, the expression of total STAT3 and serine phosphorylation of STAT3 were observed in different treated cultures (Figure 3.9). IL-6 activates STAT3 signal pathway in the new *in vitro* platform significantly compared to control and melatonin alone group by the confirmation of the expression of serine phosphorylation in nucleus. Melatonin co-treatment group does not show a significant change for phosphorylated STAT3 as well as total STAT3.

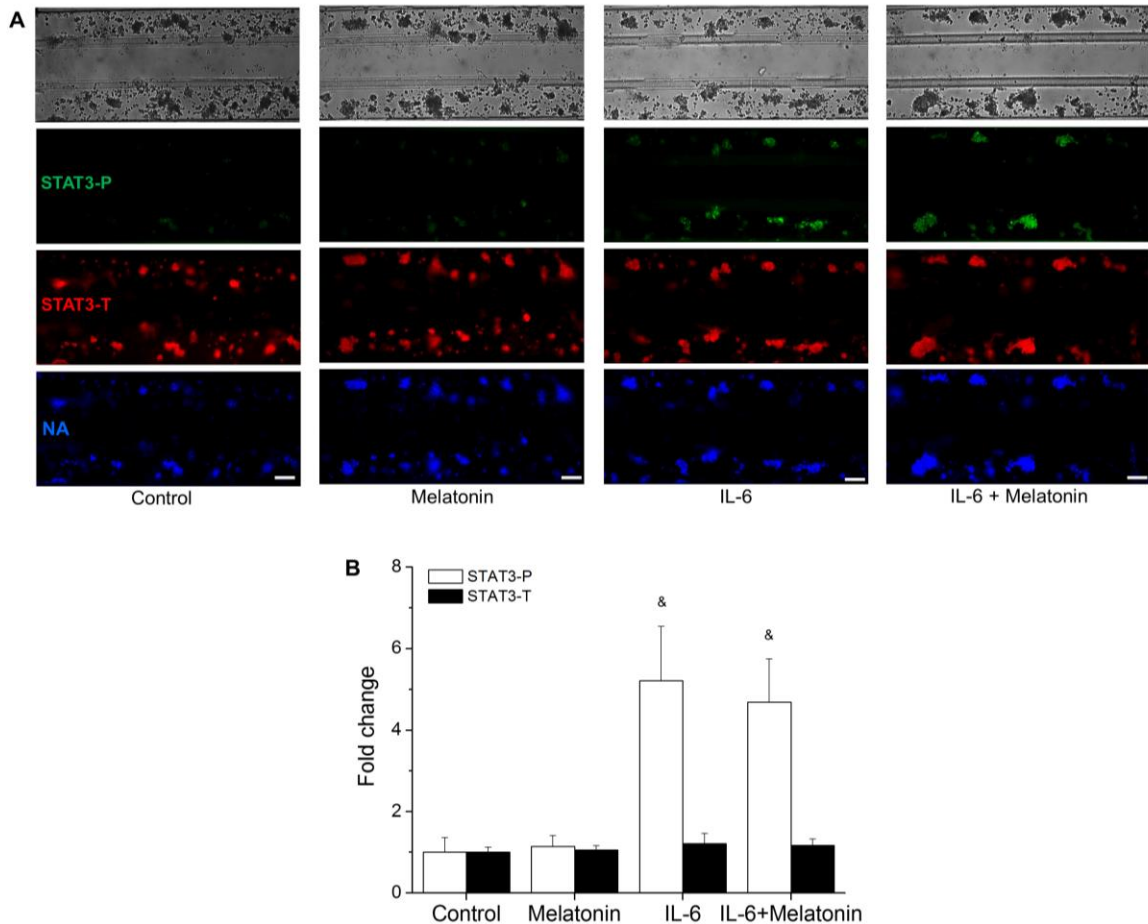


Figure 3.9. (A) Representative fluorescent microscope images with immunostaining for total STAT3 and serine phosphorylation of STAT3 (STAT3-P) in HepG2 cells-on-a-chip after IL-6 and or melatonin treatment. Light microscope images (first horizontal line) and fluorescent images for staining of phosphorylated serine727 residue of STAT3 (second horizontal line), staining of total STAT3 (third horizontal line), and staining of nucleic acids (last row) (B) Quantification of fluorescent microscope images by the ratio of fluorescent intensity to total cell area. All values were normalized to fold change of control. Scale bar indicates 100 μ m. Experiments were performed three times and data are shown as mean \pm SD. & indicates a significant difference ($p < 0.05$) versus control, melatonin group.

3.4 Discussion

The experiments of this study show alterations in a wide range of hepatic functions in response to inflammation stimulation by IL-6 and melatonin using a new HepG2 chip platform. While some of these changes stimulated by IL-6 might impair proper liver function (downregulation of detoxification and glycogen storage, increasing oxidative stress), others are likely to be aimed at protecting the organ and ameliorate the situation (increasing APR). Interestingly, simultaneous melatonin administration counteracted most of the detected alterations, although not always to basal levels, suggesting the assumption that melatonin might attenuate IL-6 induced cellular responses without completely inhibiting them.

Multidrug resistance-associated protein 2 (MRP2) is localized on the canalicular membrane of hepatocytes and transports a wide range of compounds as part of the hepatic detoxification process. MRP2 expression in HepG2 spheroids was shown in previous literature [123]. Reduced expression and activity of this transporter was observed, for example, during inflammation, drug-induced liver injury, or after ischemia with reperfusion, and this might further contribute to aggravated liver damage [154–156]. We determined significantly reduced MRP2 expression levels and efflux activity in response to IL-6 treatment. These results are mainly comparable with some previous studies on primary human hepatocytes cultivated in sandwich cultures upon IL-6 treatment, showing downregulated MRP2 mRNA and protein expression levels [151, 157]. The expression of MRP2 is mainly regulated by the pregnane X receptor (PXR) [153].

Down-regulated expression of PXR by IL-6 stimulation has already been demonstrated in human hepatocyte cultures [33, 34]. Interestingly, melatonin was shown to attenuate lipopolysaccharides(LPS)-induced down-regulated PXR expression in mouse liver in previous literature [160]. Our results also demonstrate reduced expression of MRP2 as well as PXR after IL-6-stimulation. Both effects were counteracted by melatonin administration suggesting the assumption that melatonin's effects might act via this PXR-axis. In the context of relation of CYP1A activity and IL-6 stimulation, previous studies demonstrated that IL-6 downregulated the expression and activity of CYP1A in human primary hepatocytes [161]. Previous literature has shown reduced EROD activity in response to melatonin in extracted human liver microsomes [162]. The results of this study do not allow a clear interpretation of the actions of melatonin treatment on HepG2 cells alone or in combination with IL-6.

Acute phase response induced by IL-6 was already well documented in previous research. IL-6 is a main mediator causing alterations in the expression of positive and negative APR proteins such as the reduction of albumin, the strong increase of CRP, and the elevated

hepcidin levels [144, 163–165]. Melatonin counteracted the reduced albumin production along with the elevated hepcidin levels assuming that the administration of this hormone might ameliorate the detrimental consequences of an overwhelming APR. Previous studies demonstrated that melatonin treatment significantly increased serum albumin levels reduced by doxorubicin and gamma-irradiation in *in vivo* rat model [166, 167]. Those *in vivo* results are in accordance with our study as well. CREBH (Creb3l3), a mediator of the ER stress response, is known to increase the CRP transcription, and these signaling pathways seem to interact closely with IL-6-signaling in hepatocytes [136]. Surprisingly, in our study the protein expression of CREBH was lowered by IL-6. This might negate the hypothesis of a positive regulation of CRP transcription by this transcription factor. Nevertheless, we did not analyze the activation of CREBH which is known to occur upon ER stress by proteolytic cleavage, subsequent detachment from the ER membrane, and translocation of the N-terminal fragment to the nucleus [67]. CREBH cleavage was described earlier as arising in response to IL-6 probably synergistically with other elements of the UPR [136]. Shin *et al.* reported the activation of CREBH by IL-6 treatment of HepG2 cells [144]. Additionally, they found direct evidence for the transcriptional regulation of CRP and hepcidin by CREBH. This is especially interesting when considering that in our study the co-administration of melatonin prevented the IL-6-induced upregulation of hepcidin but did not alter the increased CRP levels. The main mediators of hepcidin transcriptional activation are STAT3 and SMAD via JAK and BMP signaling pathways, respectively [45, 168]. According to our knowledge, there is no evidence for transcriptional regulation of CRP by BMP/SMAD signaling. In addition, melatonin did not counteract the strong increase of IL-6-induced STAT3-phosphorylation (Fig 3.9). Therefore, we were not yet able to clarify the different mechanisms that lead to hepcidin but not CRP regulation by melatonin.

In the context of glycogen storage, Ritchie *et al.* found direct evidence that the hepatic glycogen metabolism is altered by IL-6 stimulation, resulting in the release of glucose from glycogen in rat hepatocytes [169]. Others also observed reduced glycogen content upon IL-6 treatment and they correlated it with decreased activation of the Akt/GSK pathway in mouse and human hepatocytes [170, 171]. Forkhead box protein O1 (FOXO1) is a known transcription factor and regulates G6Pase, which mediates the last step of glycogenolysis (break down of glycogen) [172]. It is already well known that insulin-mediated activation of the Akt signaling pathway induces the degradation of FOXO1 by its phosphorylation, resulting in an increase of glycogen synthesis. Interestingly, melatonin was shown to increase the activity of Akt signaling in a rat model [173] and in HepG2 cells thereby increasing glycogen synthesis [150]. Surprisingly, Kodama *et al.* proposed that PXR acts as a repressor of FOXO1 [174], thereby decreasing glycogenolysis. In addition, inhibition of the

PI3K/Akt pathway directly downregulated MRP2 mRNA [175]. Therefore, this might explain the proposed mechanism that melatonin alleviates reduced MRP2 and glycogen storage by the modulation of PXR expression and Akt signaling via FOXO1 and G6Pase. This assumption indicates that there might be a link between detoxification mechanism and glucose metabolism regulated by PXR. However, it would be desirable to analyze IL-6 signaling, Akt signaling, FOXO1, and PXR within the interplay of IL-6 and melatonin in further studies.

The particular role of mitochondria in providing energy to the cell but also controlling intracellular signaling pathways such as apoptosis prevention or initiation and its close interaction with the ER, prompted us to evaluate mitochondrial functions in the context of IL-6 and/or melatonin. The MMP of the HepG2 cells in our culturing systems was lowered by IL-6 administration. Similar results from Berthiaume *et al.* on primary rat hepatocytes in a sandwich culture system were also reported [176]. The authors postulated based on their comprehensive studies that in IL-6 treated hepatocytes processes to stabilize the MMP are favored over processes generating ATP which might lead to limited energy availability for hepatocellular functions. They determined increased flux via the electron transport chain but reduced flux via the ATP synthase complex. Mitochondrial superoxide is predominantly generated at complex I and III of the electron transport chain. Therefore, this is in accordance with the elevated superoxide levels we determined in our setup. Melatonin administration counteracted both the reduced MMP and the increased mitochondrial superoxide as well, suggesting that cellular energy supply might be improved and oxidative stress could be alleviated by this hormone. Evidence for this was described previously. For example, Reyes-Tosco *et al.* concluded from their experiments that melatonin is able to attenuate excessive oxygen consumption of liver mitochondria and consequently protects them from oxidative damage [177, 178]. Also, melatonin was described to modulate the mitochondrial respiratory activity via increasing the action of complex I and III thereby altering the generation of reactive oxygen species [179]. Additionally, Lopez *et al* proved that melatonin decreased mitochondrial superoxide production directly and increased the activity of respiratory complex I and III [180]. Apart from its action as a ligand to the membrane-bound melatonin receptors, its localization within mitochondria and nuclei was shown [57, 179]. Taken together, melatonin seems to be able to exert protective activities at different sites within the cell, thereby being capable of modifying a wide range of cellular stress responses.

This study shows the interplay of melatonin actions and inflammation stimulated by IL-6 in a newly developed HepG2 cells-in-a-chip platform model, which allows quantitative

measurements of various hepatic functions including detoxification mechanisms, the acute phase response, and glucose metabolism. In addition, results from this new *in vitro* platform were well comparable with previous literature on primary hepatocyte and *in vivo* models, which might overcome the limitation of typical HepG2 culture models. However, our data cannot fully explain the complex molecular pathways that are mediated by melatonin and IL-6 in human liver. Nevertheless, we conclude that our new *in vitro* platform allows to study hepatic inflammation responses.

3.5 Conclusions

The results of this study clearly demonstrate that IL-6 modifies hepatic inflammatory responses including detoxification, APR proteins, glucose metabolism, and mitochondrial functions in a new *in vitro* platform. Thereby, we proposed this new platform as a tool to study hepatic inflammation responses. Melatonin alleviated IL-6-induced reduction of MRP2 expression, the lowered production of albumin, increased expression of hepcidin, reduced glycogen storage, and the diminished mitochondrial functions. This study provides further evidence of the positive properties of this hormone and proposes a new candidate pathway.

Chapter 4. Differentiation of human liver progenitor cell line (HepaRG cell) directly on a biochip.

4.1 Introduction

4.1.1 Motivation and aim of this chapter

HepaRG cells are the hepatic stem cell line and can differentiate toward hepatocyte-like and biliary-like cells. However, the entire cultivation process requires one month and relies on the addition of 2% dimethyl sulfoxide (DMSO). In addition, the behaviour of HepaRG cells cultured in a microenvironment has not yet been fully elucidated

Therefore, the purpose of this research is to differentiate HepaRG cells (progenitor cells and undifferentiated cells) toward hepatocyte-like cells by minimizing the cultivation time and without DMSO treatment, using a microfluidic device combined with the following specific cultivation parameters: i) comparison of extracellular matrixes (matrigel and collagen I); ii) types of flow (one or both sides); and iii) effects of DMSO.

Cell morphology, the population of cells between hepatocyte-like cells and biliary-like cells, diverse hepatic functions, and cell polarity were evaluated after 2 weeks of cultivation in the chip. CRP production is measured by the stimulation of IL-6 to test its applicability for hepatic inflammatory reaction.

4.1.2 Introduction

Primary human hepatocytes, the main parenchymal cells of the liver, were considered a gold standard for *in vitro* models in cell biology and pharmaceutical research to evaluate the hepatic metabolism and toxicity of drugs and xenobiotics [181]. However, due to their many limitations such as a high variation between donors, restricted accessibility, fast loss of their hepatic functions after isolation from liver tissue, and a lack of proliferation [182], the HepaRG cell line has therefore been increasingly proposed as an alternative to primary hepatocytes and HepG2 cells to study the toxicology [183], the xenobiotic metabolism [184], and inflammations [139]. Unlike other immortal hepatic cell lines, HepaRG cells show pronounced similarity to primary human hepatocytes, as evidenced by the analysis of gene expression profiling and their metabolic activity [75].

The HepaRG cell is a bipotent liver progenitor cell line that differentiates into both hepatocyte-like cells and biliary-like cells. They show liver progenitor-like cells under their proliferation state. When the cells reach confluent, approximately one week after seeding, they start to commit into both hepatocyte and biliary epithelial-like cells. At 2 weeks of cultivation, superconfluent HepaRG cells can start to differentiate toward hepatocyte by addition of dimethyl sulfoxide (DMSO) [185]. However, the entire cultivation process takes 4 weeks and relies on the treatment of a high concentration of 2% of DMSO for differentiation [71, 72]. Sumida *et al.* found that the gene expression of human and rat hepatocytes can be affected by 0.5% (v/v) of DMSO [186]. In addition, recent research has addressed negative effects of DMSO treatment for the differentiation of HepaRG cells due to a decrease of the cell viability and the hepatic functions except xenobiotic detoxification [187]. Consequently, it is important to investigate the effects of DMSO on the behavior of HepaRG cells in a new *in-vitro* environment.

Organs on chips, a new class of *in vitro* models, have been introduced to recapitulate *in vitro* models by mimicking the structural properties of tissues and organs *in vivo*. Generally, they are multi-channels microfluidic cell culture devices, in which cells or tissue can be cultured in such a way that it can replicate an *in vivo* environment, such as tissue-tissue interface, spatiotemporal gradients, and geometry [188, 189]. To date, only few studies have incorporated HepaRG cells in microfluidic devices for long-term based co-culture models and toxicity tests [97, 190, 191]. In these cases, already fully differentiated HepaRG cells were used by addition of 2% of DMSO in flask cultivation during one month and transferred into their own microfluidic devices. However, the behavior of HepaRG cells in micro-environment has not been extensively clarified yet. Furthermore, stem and progenitor cells have been shown to differentiate into mature liver cells in presence of fluid in the bioreactor [192].

Chapter 4

Previously, we have demonstrated that 3D culture of HepG2 cell in a microfluidic device combined with phaseguides showed improved hepatic specific functions compared with static 2D and 3D cultures in chapter 2. Therefore, we hypothesize that this phaseguide-based microfluidic device can be used as a tool, offering 3D culture and fluid flow, to differentiate HepaRG cells into hepatocyte-like cells without the addition of DMSO and to additionally reduce their differentiation process time.

In order to understand the behavior of HepaRG cells in a new microfluidic device, we employed four strategies to differentiate HepaRG cells into hepatocyte-like cells. First, two seeding time points have been chosen for the cultivation in the microfluidic device to reduce differentiation time: i) when the HepaRG cells show progenitor cell lineage at 5 days; ii) when the cells are at 14 days of cultivation, showing highly confluent with a not fully differentiated status. Second, two commercial extra cellular matrices (ECM), i.e. matrigel and collagen I, have been compared for the differentiation of HepaRG cells in the microfluidic device, as they are considered the closest representatives of naturally derived hydrogels for cultivation of hepatic cells *in vitro* [123]. To the best of our knowledge, there is no existing research on the direct comparison of matrigel and collagen I cultivation in the presence of flow with hepatic cell line cultures. Third, two different types of flow toward the cell culture area (one side and both sides) were compared. Fourth, with or without DMSO cultivation were characterized for 14 days of cultivation. Finally, we evaluated the polarity of final differentiated HepaRG cells cultured in a microfluidic device and their ability of C-reactive protein (CRP) production stimulated by IL-6 in order to use this platform as a tool for inflammation studies. Our results clearly demonstrate that Matrigel is suitable for HepaRG cells differentiation in the microfluidic device, and the flow can influence the size of the formed cell clusters and bile canaliculi formation. Furthermore, the DMSO treatment induces a significant cell damage and represses various hepatic functions during the cultivation.

4.2 Materials and Methods

4.2.1 HepaRG Cell culture

The cryopreserved HepaRG cells (catalog number: HPRGC10) were purchased from Thermo Fisher Scientific and maintained according to the manufacturer's instruction. For maintenance cultivation, HepaRG cells were seeded at a density of 2×10^4 cells/cm² in a 25cm² flask and cultivated in William's E medium (Thermo Fisher Scientific, Hamburg, Germany), supplemented with 10% FBS, 100U/ml penicillin and streptomycin (Sigma-Aldrich, Munich, Germany), 2mM Glutamax (Gibco, Darmstadt, Germany), 50µM hydrocortisone hemisuccinate (Sigma-Aldrich, Munich, Germany), and 4µg/ml insulin (Life-technology, Germany) in a humidified cell incubator (Binder, Tuttlingen, Germany). First passage of HepaRG cells were fully differentiated by addition of 2% of DMSO in the medium for 4 weeks of cultivation. The HepaRG cells were subcultured every 2 weeks.

4.2.2 Experimental set up for differentiation of HepaRG cells in microfluidic device

- Selection of seeding time of HepaRG cells for microfluidic cultivation

Two different seeding times of HepaRG cells were chosen for the further cultivation process in the microfluidic device. HepaRG cells at 5 days (progenitor like cells: PGC) and 14 days (not fully differentiated cells: NFDC) of cultivation were mixed with extra cellular matrix and transferred into the microfluidic device (OrganoPlate™, Mimetas company, The Netherlands) at a seeding concentration of 4×10^7 cells/ml. The further cultivation procedure was performed according to the previously described publication [149] and the medium was renewed every two days.

- Set up 1 (Different extra cellular matrix)

The neutralization of an acidic collagen I solution (Gibco, Life technology, Germany) was achieved by adding 10X PBS and sterile 1N NaOH on ice by following the manufacturer's instructions. Frozen matrigel (Corning, Wiesbaden, Germany) was stored in ice at 4°C for overnight to be fully melted. HepaRG cells were suspended in matrigel and neutralized collagen I solution on ice, respectively. A mixture of matrigel and cells was injected into the upper channel of the chip, while the collagen I mixture was injected in the lower channel. In both cases, the mixture aligned itself along the phaseguide under the capillary force. The cells were incubated at 37°C for 35 minutes to be gelled, and 25 µl of the medium was added to the medium outlet. After further incubation for 5-6 hours for entire gelling, the perfusion was started by adding 100 µl of medium to the inlet well.

- Set up 2 (Type of flow)

After we characterized the HepaRG cells with matrigel and collagen I cultivation, a further cultivation process was performed using matrigel only. To check whether the type of flow can have an effect on the formation of cell clusters, perfusion flow was generated in both sides (both sides of flow) and in the middle of the channel (one side of flow) with the same seeding concentration of HepaRG cells.

- Set up 3 (with and without DMSO treatment)

For DMSO supplement cultivation, the medium including 1% of DMSO has been replaced after 3 days of cultivation in the microfluidic device. From 5 days of cultivation, 2% of DMSO in medium was supplied continuously for the rest of the cultivation. Each experiment setup was illustrated in Figure 4.1.

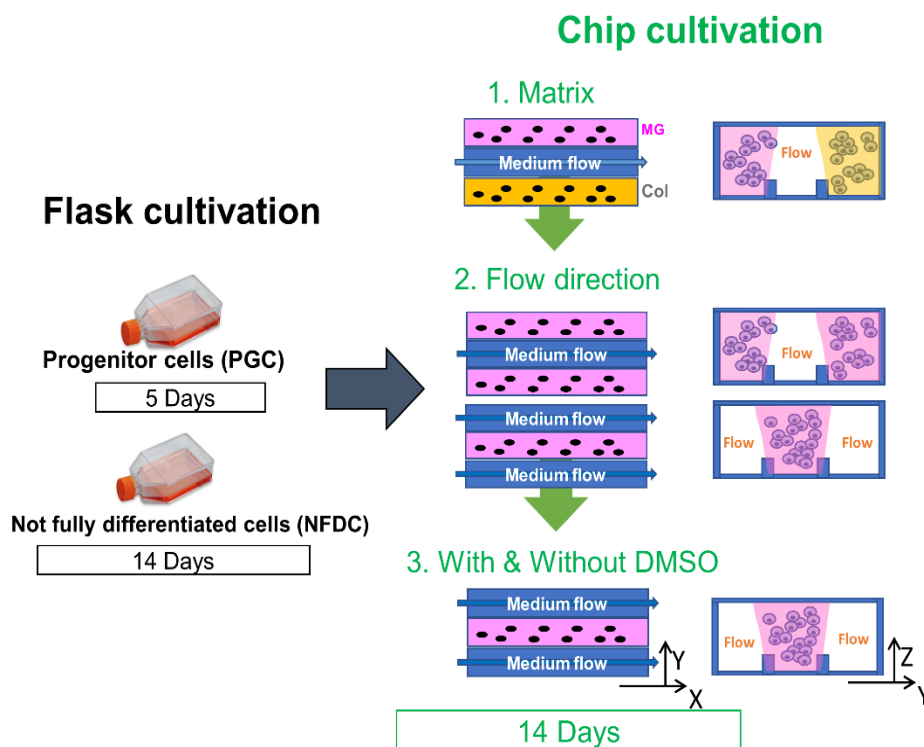


Figure 4.1 A schematic diagram of experiment set up for HepaRG cells cultivation in the microfluidic device. Progenitor cells (PGC) and not fully differentiated cells (NFDC) from flask cultivation were cultivated further in microfluidic device according to three optimization process to differentiate HepaRG cells into hepatocytes. 1. Difference of matrix (Collagen I vs. Matrigel) 2. Types of flow (one side of flow vs. both sides of flow) 3. Comparisons of with or without DMSO supplement (with vs. without DMSO) cultivation. After 14 days of chip cultivation, various assays have been fulfilled.

4.2.3 Cell viability assay

The cellular live/dead assay was performed by staining with Calcein Blue AM (eBioscience, Frankfurt, Germany) and Ethidium Homodimer III (EthD-III, Biotium, Hayward, USA) to determine cell viability. Briefly, the cells were washed three times with PBS buffer after incubating for 15 minutes with 5 μ M calcein AM Blue and 1 μ M EthD-III in PBS. Fluorescence images were taken by using a Zeiss fluorescence microscope (excitation/emission: 365 nm / DAPI filter set for Calcein Blue AM, 530 nm / PI filter set for Ethidium Homodimer III) and analyzed using the ImageJ software for the quantitative analysis.

4.2.4 CYP1A induction assay

The quantitative determination of CYP1A activity was performed using an ethoxyresorufin-O-deethylase (EROD) assay with resorufin ethyl ether (Sigma-Aldrich, Munich, Germany) as a substrate. The cells were incubated with 5 μ M of 3-methylcholaten (3-MC) for 72 hours to induce CYP1A activity, and the control group cells were treated with a vehicle solution (DMSO). After the induction of CYP1A, the cells were cultivated with 2 μ M resorufin ethyl ether in a serum-free medium for 30 minutes. The medium was then collected and the fluorescence was measured at 525/580-640 nm with a fluorescence microplate reader. The fold changes were calculated as the ratio between the values of the 3-MC treatment group and the control group.

4.2.5 Bile canaculi formation analysis

The bile canaliculi formation and function was observed by using a substrate, 5-carboxyfluorescein diacetate (5-CFDA) (Sigma-Aldrich, Germany), for the multidrug resistance associated protein (MRP2) [193], which is located at the bile canaliculi in the apical domain. The non-fluorescent 5-CFDA entering the cells by diffusion were cleaved by intracellular esterase to form the fluorescent 5-CF metabolites. The 5-CF were exported at the bile canaliculi by the MRP2 protein. After washing with an uptake buffer (136mM NaCl, 5.3mM KCl, 1.1mM KH₂PO₄, 0.8mM MgSO₄, 1.8mM CaCl₂, 11mM D-glucose, 10mM HEPES, pH7.4) the cells in the chip were incubated for 30 minutes with 5 μ M of 5-CFDA, then washed with PBS buffer and the accumulated 5-CF in the bile canaliculi were observed under a fluorescence microscope.

4.2.6 Immunostaining

Cells were fixed with 4% of paraformaldehyde for 30 minutes and permeabilized with 0.2% of tritonX-100 for 30 minutes. After blocking with 1% of BSA for 30 minutes, the cells were incubated overnight at 4°C with the following primary antibodies: Albumin (1:200, mouse

monoclonal, abcam) CK19 (1:200, rabbit monoclonal, abcam), CK18 (1:50, mouse monoclonal, abcam), MRP2 (1:50, mouse monoclonal, abcam), ZO-1 (1:100, rabbit monoclonal, abcam), NTCP (1:100, rabbit monoclonal, abcam), CYP3A4 (1:50, rabbit monoclonal, Santa Cruz technology). After washing with PBS three times, the cells were stained with the secondary antibody DyLight 488 goat anti rabbit (1:100, ab96899, Abcam, Cambridge, UK), Alexa Fluor 647 goat anti mouse (1:200, ab150115, Abcam, Cambridge, UK), and with Hoechst 33345 (Sigma-Aldrich, Germany) for nucleic acids staining for 1 hour at room temperature. After washing with PBS three times, the cells were monitored under a fluorescent microscope or a confocal microscope (Carl Zeiss, Tholey, Germany).

4.2.7 Albumin and CRP production measurement

The cell culture medium was collected at indicated time points and stored at -80°C immediately. The amount of albumin and CRP secreted in the medium was determined using a human albumin ELISA Kit (Bethyl Laboratories, Montgomery, Texas, USA) and a CRP ELISA kit (Thermo Fisher Scientific, Germany), respectively. All procedures followed the manufacturer's instructions.

4.2.8 Processing and quantification Images and statistical test

Fluorescent images were analyzed using Icy (<http://icy.bioimageanalysis.org/>) and ImageJ Fiji [194] and quantified using ImageJ (<https://imagej.nih.gov/ij/>, 1997-2016) software. For statistical tests, one-way ANOVA and a Student's-t test were performed for normally distributed groups, while Kruskal-Wallis and Mann-Whitney tests were carried out for non-normally distributed groups to compare data between the four or two groups of culture models, respectively. All data values correspond to the average \pm standard deviation (SD).

4.3 Results

4.3.1 HepaRG cultivation: comparison of extracellular matrices (matrigel vs. collagen I)

To compare the differentiation toward hepatocyte-like cells from HepaRG cells between matrigel and collagen I gel cultivation in microfluidic environment, the cell morphology and expression of albumin and CK19 were observed after 2 weeks of chip cultivation, as shown in Figure 4.2. The average diameter of PGC cell clusters was 20-40 μ m, while NFDC cell clusters showed a bigger diameter (30-80 μ m). However, we found plenty of single cell units, suggesting that both types of cells did not form aggregates efficiently. Surprisingly, both cells (PGC, NFDC) with collagen I cultivation showed an elongated shape rather than cell cluster formation. Interestingly, those elongated cells aligned uniformly along the direction of flow, similar to cord-like structures. To determine whether cells differentiated into hepatocyte or biliary-like cells immunostaining of albumin as a hepatocyte marker and cytokeratin 19 (CK19) as a biliary cell marker, were performed. A high albumin expression occurred only in a few of cell aggregates in matrigel, not in collagen I cultivation. Elongated cells with a cord-like structure in collagen I cultivation showed higher CK19 than albumin expression, suggesting that those cells differentiated into biliary cells rather than hepatocytes. Cell clusters in matrigel co-expressed with albumin and CK19, suggesting that they differentiate into hepatocytes and biliary cells together. In this culture system, we demonstrated that both of PGC and NFDC in matrigel differentiated into hepatocyte and biliary cells together, whereas collagen I cultivation differentiated most likely into biliary cells.

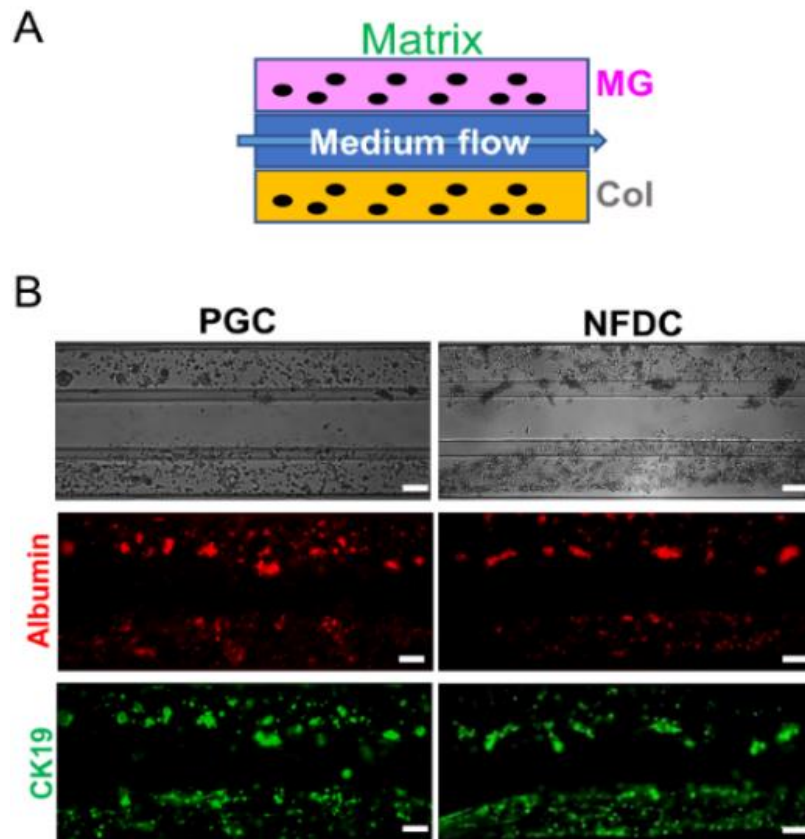


Figure 4.2 (A) Comparison of Matrigel (MG : upper lane) and collagen I (Col : bottom lane) cultivation of PGC and NFDC on 14 days in microfluidics device. (B) Representative images of phase contrast and fluorescent immunostaining for albumin (red) and CK19 (green). Scale bars represent 100 μ m.

4.3.2 HepaRG cultivation: comparison of types of flow (both vs. one side)

From our first result, PGC and NFDC differentiated toward hepatocytes only in a matrigel matrix. However, the cells were not likely to form aggregates efficiently due to the following reasons: 1) the size of the cell clusters is not sufficiently large, 2) plenty of single cell units remain in the matrix. We hypothesize that this problem might arise from insufficient flow to the cells, because *in vivo* liver progenitor cells are found in the canal of herring, in which a bile flow exists and which belongs to the portal triads field [195]. In a healthy human liver, this portal triad shows the highest pressure, produced by the flow, which continuously decreases until the hepatic vein [196].

To test whether the flow can affect the formation of cell aggregations, we tested two types of flow (one side flow, both sides of flow) and conducted further experiments, including a measurement of the cell cluster area (Figure 4.3A+B) and the formation of bile canaliculi using 5-CFDA staining at 14 days of chip cultivation (Figure 4.3C).

The size of cell clusters was affected by the type of flow in both cases, i.e. PGC and NFDC. The cell clusters formed by both side of flow showed enlarged sizes compared to only one side flow. In particular, NFDC formed larger cell clusters than PGC, showing in a range of 50-100 μ m in diameter, while the diameter of PGC clusters measures 40-80 μ m.

A 5-CFDA/5-CF efflux assay was used to observe the bile canaliculi formation. In this assay, the non-fluorescent 5-CFDA rapidly diffuses inside the cells, then it is cleaved to fluorescent 5-CF by intracellular esterase and located at the bile canaliculi by the MRP2 transport protein [193]. In the one side flow culture, we found that the majority of cells showed a diffused intracellular fluorescence and almost no fluorescent dye exported into the bile canaliculi, since the cells did not form aggregates. In contrast, the cells in both sides of flow cultivation showed an accumulation of excreted fluorescence 5-CF into the bile canaliculi at the cell-cell contact areas, suggesting that a both sides of flow supports the formation of cell aggregates and cell-cell contact. Therefore, both side of flow for PGC and NFDC in microfluidic cultivation was chosen for further studies.

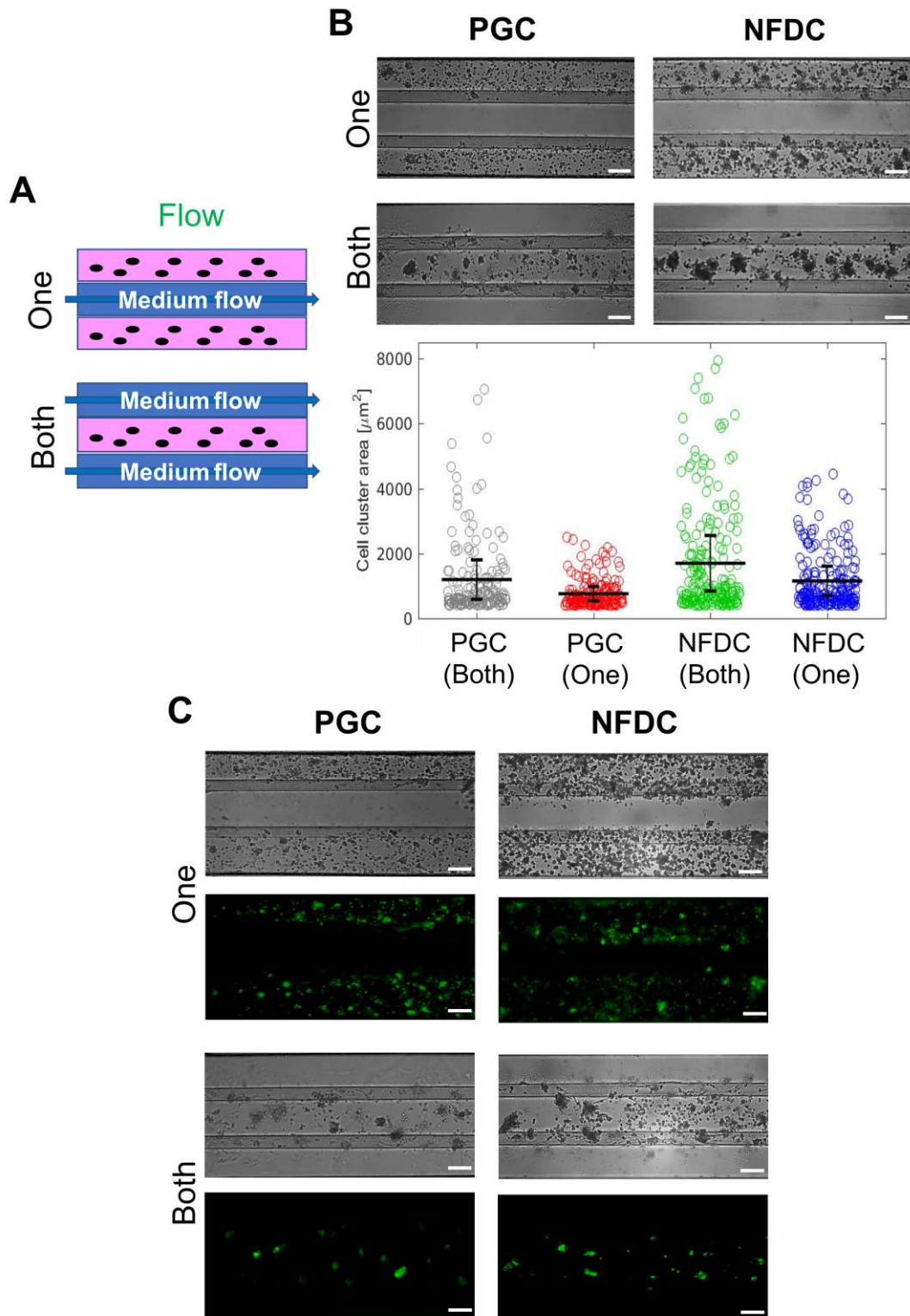


Figure 4.3 (A) Comparison of one side (One) and both side of flow (Both) cultivation of PGC and NFDC on 14 days in microfluidics device. (B) Representative images of phase contrast and size of cell aggregates were presented. (C) Excretory activity of MRP2 at bile canalicular of HepaRG cells was assessed by 5-CFDA. Scale bars indicate 100 μm .

4.3.3 Cell viability and liver specific functions (with vs. without DMSO treatment)

In the next step, we investigated whether DMSO affects the cell viability and population (hepatocyte-like cells vs. biliary-like cell) of HepaRG cells in the microfluidic cultivation. First, we checked the cell viability by live and dead staining at 14 days of microfluidic cultivation (Figure 4.4A+B). Here, PGC showed a higher cell survival rate than NFDC in both with and without DMSO cultivation. In more detail, PGC and NFDC in absence of DMSO showed $88\% \pm 2\%$ and $67\% \pm 3\%$ of cell survival, whereas with DMSO treatment reduced cell viability significantly, showing $63\% \pm 9\%$ and $50\% \pm 1\%$, respectively. These results suggest that DMSO promoted a significant cell death, which was proven by a significantly reduced cell viability in both PGC and NFDC cells.

After checking the cell viability, we further investigated the distribution of the cell population between hepatocyte-like cells *versus* biliary-like cells by quantification of immunostaining of cytokeratin 18 (CK18) and cytokeratin 19 (CK19), since they are markers for hepatocyte and biliary cells respectively [72, 197]. The final ratio of CK18 and CK19 in the total cell area was calculated and is shown in Figure 4.4C and D. PGC expressed $70\% \pm 5\%$ of CK18 and $24\% \pm 4\%$ of CK19 in the absence of DMSO and $53\% \pm 3\%$ of CK18 and $17\% \pm 2\%$ of CK19 in the presence of DMSO. The CK18 and CK19 expressions were both significantly reduced by 16% and 8% for DMSO in PGC. In the case of NFDC, CK18 and CK19 showed $48\% \pm 8\%$ and $22\% \pm 3\%$ of expression in the absence of DMSO and $40\% \pm 5\%$ and $14\% \pm 2\%$ in the presence of DMSO, respectively. Only the CK19 expression was suppressed significantly in NFDC. Therefore, our results suggest that DMSO influences the viability of both of hepatocyte-like cells and biliary-like cells. Furthermore, PGC without DMSO showed the highest cell viability and hepatocyte marker CK18 expression level in our microfluidic device.

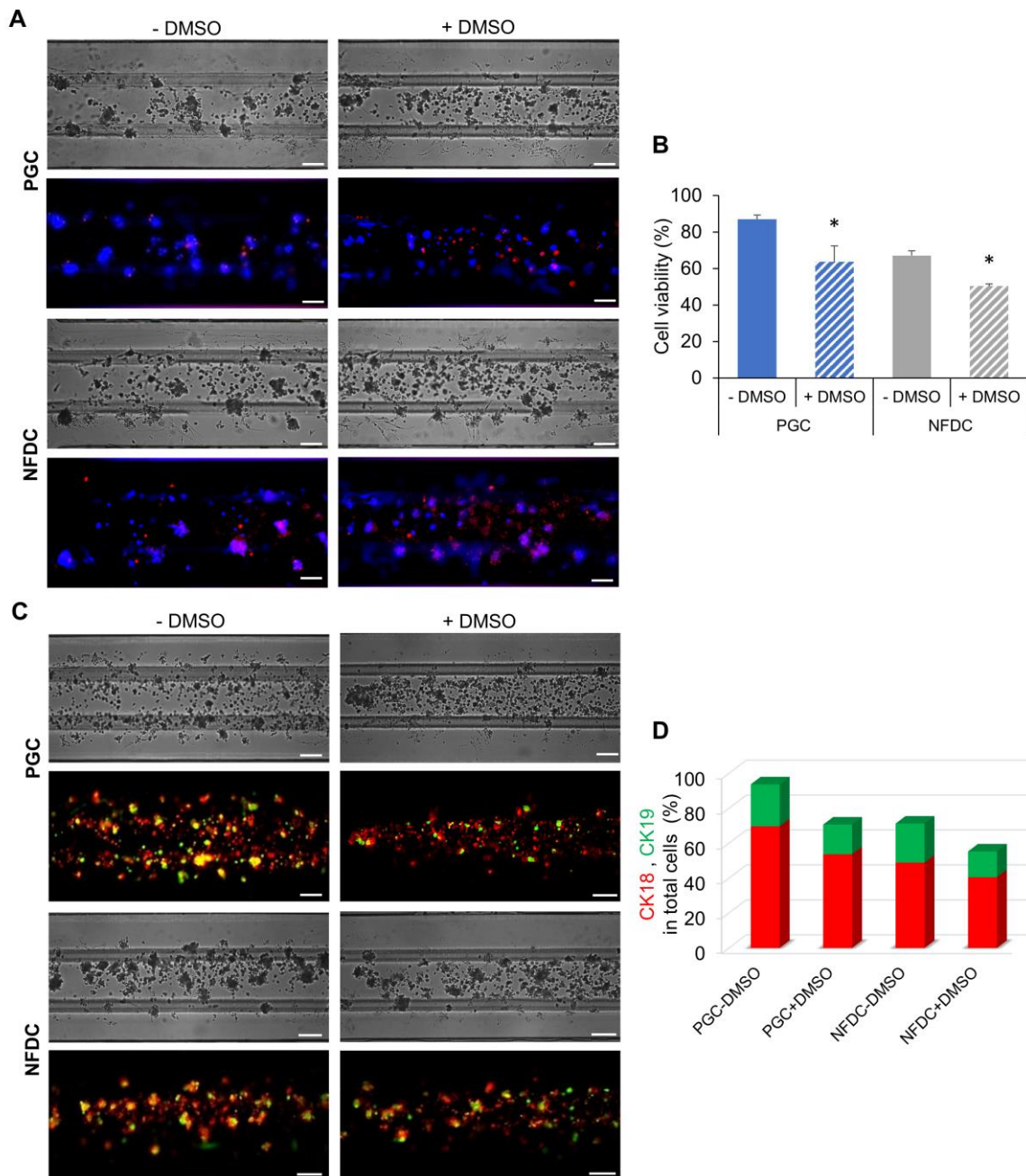


Figure 4.4 Comparison of with and without the addition of DMSO cultivation of PGC and NFDC after 14 days in microfluidic device. (A) Cell viability was assessed by fluorescent live(blue) / dead(red) staining at 14 days of cultivation. (B) Determination of cell viability by quantification of fluorescent images. Data are the average \pm SD of at least 6 independent cultures. (* indicates significant difference versus -DMSO group, $*P < 0.05$) (C) Population of hepatocyte and biliary-like cells in PGC and NFDC by immunostaining of CK18 (hepatocyte-like cells) and CK19 (biliary-like cells). (D) The fluorescent area of CK18 and CK19 was quantified and normalized to total cell area. Data are the average \pm SD of at least 6 independent cultures.

Chapter 4

We further investigated liver specific functions including the albumin production, CYP1A induction assay, and immunostaining of CYP3A4 and albumin in PGC and NFDC with and without DMSO treatment in the microfluidic device (Figure 4.5).

In the context of albumin production (Figure 4.5A), only PGC showed an augmented production rate, with 13-fold (in the presence of DMSO) and 7.6-fold change (in the absence of DMSO) compared to 3 days of cultivation before the cells were treated with DMSO, suggesting that PGC can be differentiated toward hepatocyte-like cells efficiently in a microfluidic device, whereas NFDC continuously showed a significantly reduced albumin production during whole culture period. Interestingly, a DMSO treatment induced a significantly reduced albumin production only in the PGC cultivation but not in NFDC cultivation.

Regarding the CYP1A induction assay (Figure 4.5B), PGC in the absence of DMSO showed the highest induction rate (3.5-fold change) among the groups, however the CYP1A induction rate reduced significantly in the PGC in DMSO supplement cultivation. Surprisingly, DMSO does not affect the CYP1A induction rate in the case of NFDC.

Furthermore, we performed an immunofluorescence double staining of CYP3A4 and albumin (Figure 4.5C). Expression of albumin and CYP3A4 was co-localized in both PGC and NFDC cultivation. The albumin expression was suppressed by DMSO supplement in both of PGC and NFDC, whereas CYP3A expression was not dramatically changed by the DMSO treatment and was distributed homogenously.

Therefore, we conclude that PGC in the absence of DMSO cultivation in microenvironment outperformed the cultivation in the presence of DMSO regarding the differentiation into hepatocyte-like cells, since they showed the highest cell viability and liver functionalities, thereby this culture model was selected for further studies.

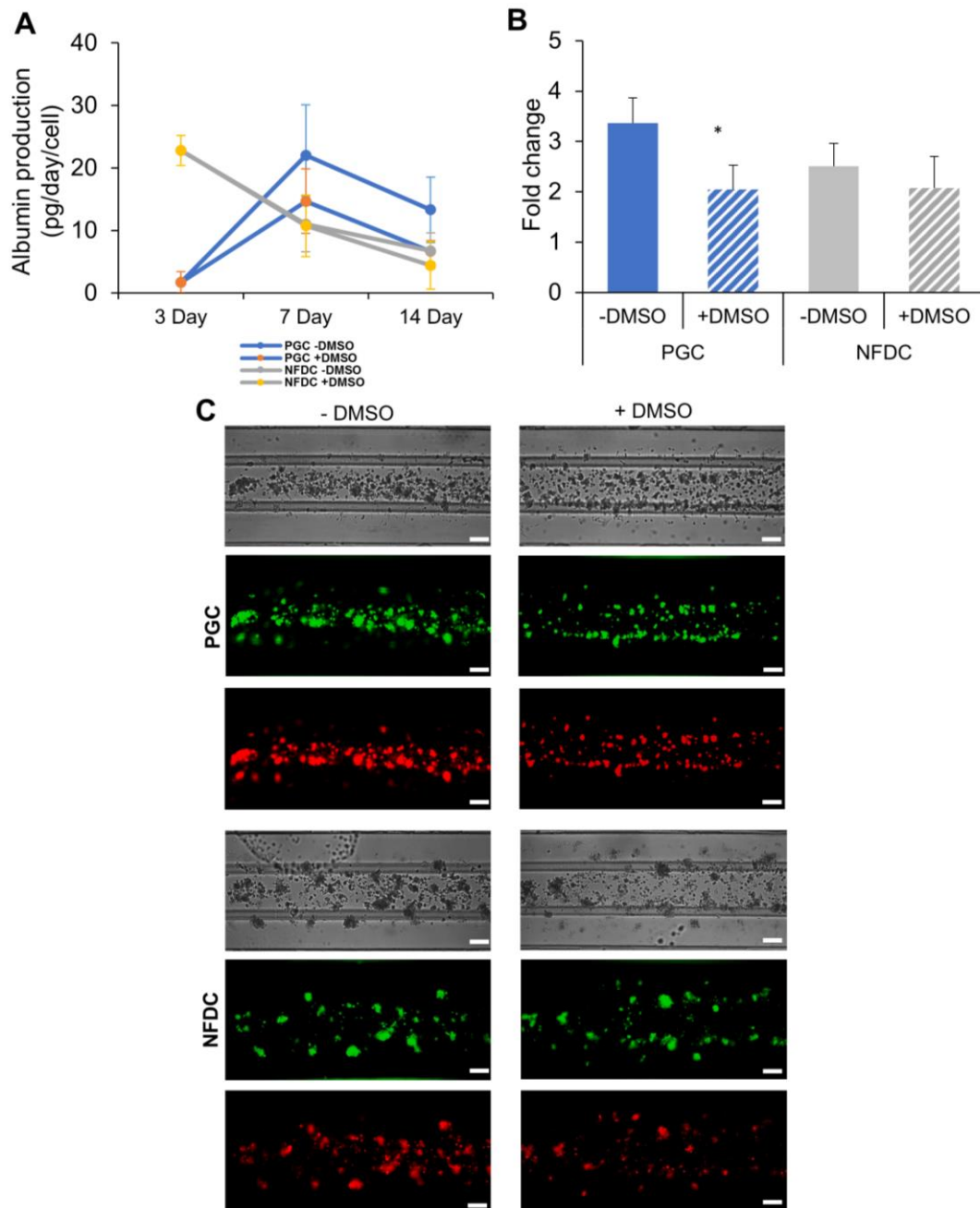


Figure 4.5 Comparisons of liver specific functions between PGC and NFDC in presence and absence of DMSO culture. (A) Time-dependent secretion of albumin. Cells were cultured for 14 days in microfluidic device and the culture medium was collected at day 3, 7, and 14 (before treatment of DMSO) during the culture period. Data are the average \pm SD of at least 5 independent cultures. (B) CYP1A induction assay was evaluated at the 14days of microfluidic cultivation. Data are the average \pm SD of 5 independent cultures. (* indicates significant difference versus -DMSO group, * $P < 0.05$) (C) Immunofluorescence microscopy of CYP3A4(green), albumin(red), and light microscope images (top) at the 14 days of cultivation. Scale bars represent 100µm.

4.3.4 Localization and polarization of PGC cell clusters in microfluidic device.

We further investigated the localization of cell population (hepatocyte-like cells and biliary-like cells) in PGC cell clusters after 14 days of cultivation in the microfluidic device. A confocal fluorescent microscope was used to investigate the distribution of cell populations in regard of the depth by employing immunostaining of CK18 and CK19. Interestingly, cells located at the height of 30 μ m to 80 μ m formed clusters, whereas cells located higher than 100 μ m did not form clusters, showing a spreading shape. CK19 was shown to be expressed in the inner area of the cell cluster, whereas CK18 expression is located at the overall area of the cell cluster (Figure 4.6A), suggesting that biliary-like cells are localized within cell spheroid, while hepatocyte-like cells are homogeneously distributed.

In *In vivo*, hepatocytes are arranged in three dimensional structures (3D) in the presence of flow, forming cell-cell contacts, which is important for maintaining specific polarity and also for intracellular functions [198]. Therefore, in order to elucidate whether differentiated PGC cells on 14 days of cultivation in the microfluidic device without DMSO supplement indicated the polarity, cell clusters were observed by immunostaining of NTCP for the basal membrane, ZO-1 for the lateral membrane, and MRP2 for the apical membrane (Figure 4.6B+C). Surprisingly, differentiated PGC cell clusters showed an abundant expression of NTCP in a range of 30-100 μ m of height, and NTCP was localized to the sinusoidal membrane domain. Regarding of the apical and lateral domains, MRP2 was localized at the cell-cell contact region and showing a capillary-like shape surrounded by the tight junction proteins (ZO-1), confirming that cell clusters constitute distinct apical and basolateral domains. With these observations, we offer evidences that differentiated PGC in microfluidic device can be highly polarized without supplement of DMSO.

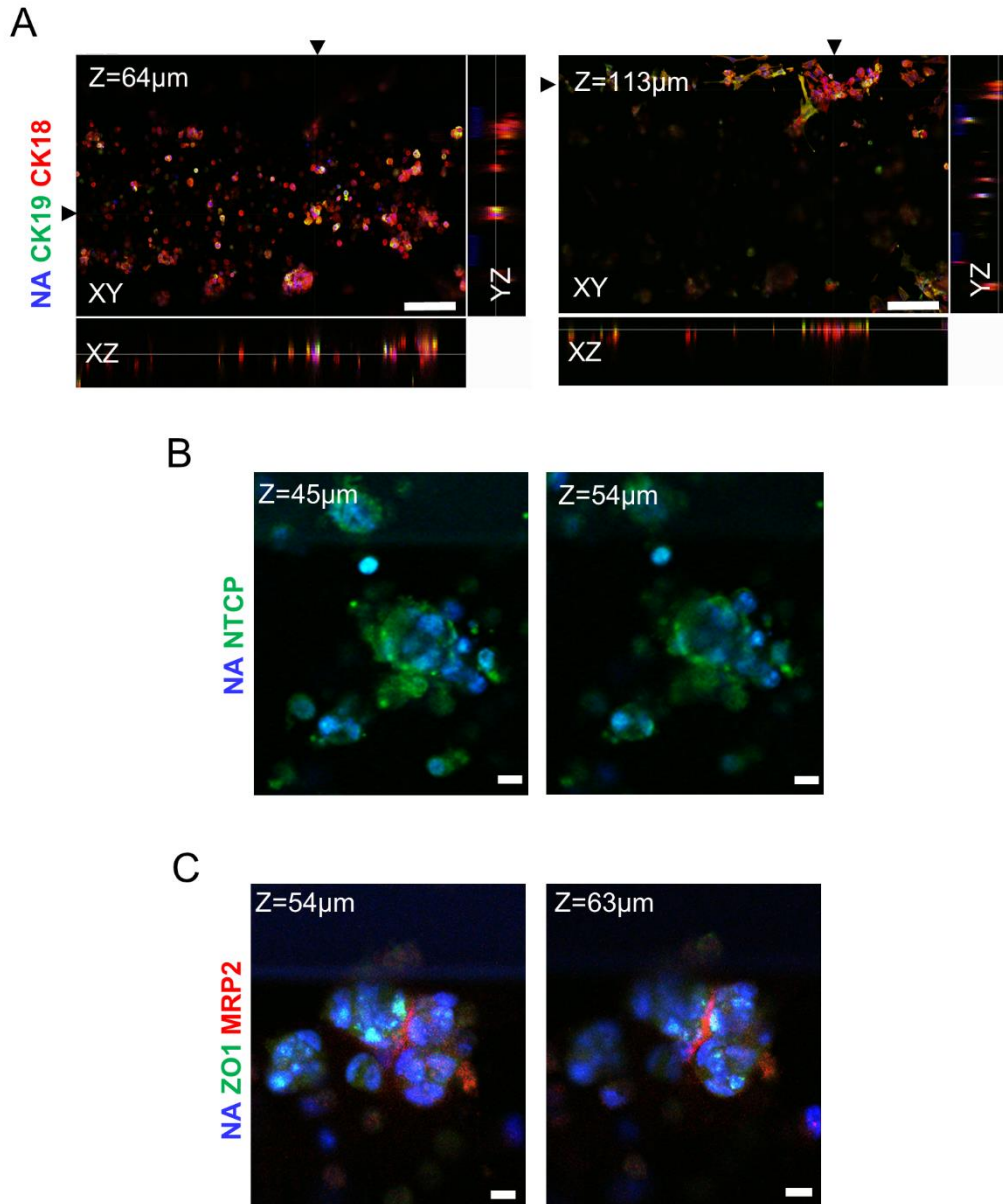


Figure 4.6 Immunofluorescence and confocal analysis of (A) CK18(red) and CK19(green) and localization of (B) NTCP(green) (C) ZO-1(green) MRP2(red) and NA(nuclei, blue) in cell aggregates indicates spatial segregation of these apical and basolateral markers as a sign of cell polarization. Scale bars represent 100µm in figure A and 10µm in figure B and C respectively.

4.3.5 CRP production stimulated by IL-6

For the validation of the final optimized PGC cultivation in our microfluidic device we tested whether differentiated hepatocyte-like cells can be stimulated by IL-6 to produce CRP. It has already been proven that fully differentiated HepaRG cells in 2D cultures in the presence of DMSO are a useful model for inflammation studies [199]. Therefore, we compared the CRP production level in differentiated PGC in the microfluidic device with fully differentiated HepaRG cells in a 2D cultivation. To calculate the CRP production accurately, the final quantified CRP level was normalized by the number of hepatocyte-like cells (Figure 4.7). IL-6 induced an increase of CRP production in both 2D culture *and* differentiated PGC in the microfluidic cultivation. Also, a dose dependent response on the tested concentrations of IL-6 (10ng/ml, 50ng/ml) was observed in the CRP production in the PGC microfluidic cultivation model. Surprisingly, the amount of produced CRP per hepatocyte-like cell in the PGC cultivation in microfluidic device (57 ± 17 fg/cell) were in very good agreement with the 2D culture data (62 ± 13 fg/cell).

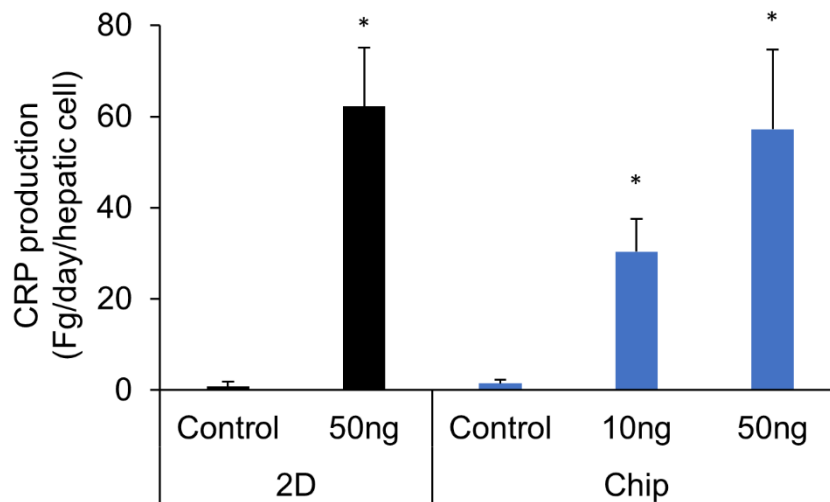


Figure 4.7 Level of CRP production stimulated by IL-6 treatment from fully differentiated HepaRG cells in 2D culture and from differentiated PGC in the microfluidic cultivation. 0ng/ml(control), 10ng/ml, and 50ng/ml of IL-6 concentration was applied. Data are expressed as average \pm SD of 3-5 independent culture samples. (* indicates significant difference *versus* control group in each cultivation, *P<0.05)

4.4 Discussion

HepaRG cells are considered a surrogate for human primary hepatocytes, since they show relatively similar levels of gene expression and metabolic activities in comparison of human primary hepatocytes. HepaRG cells can differentiate toward hepatocytes and biliary-like cells by supplemented with 2% of DMSO in monolayer cultures for 4 weeks. In this study, using a recently developed commercial biochip, we provide a unique culture model for the differentiation of HepaRG toward hepatocyte-like cells for two weeks without DMSO by optimizing following strategies. First, we selected undifferentiated HepaRG cells when they are shown under two distinct states: i) liver progenitor (PGC) and ii) not fully differentiated (NFDC). Second, we compared three parameters: i) extra cellular matrix (ECM) between matrigel and collagen I, ii) one *versus* both sides of flow, iii) with and without addition of DMSO during the cultivation. Our results clearly show that matrigel supported HepaRG cells to differentiate toward hepatocyte-like cells and both sides of flow promoted aggregation of cells, and DMSO influenced the cell viability and various hepatic functions. Furthermore, we investigated the polarity of the final selected culture model (PGC without DMSO) and validated its applicability for inflammation stimulation by IL-6.

In the context of the first previously mentioned step that compare between matrigel and collagen I, our results clearly demonstrated that PGC and NFDC in a microfluidic device exhibit both hepatocyte and biliary-like cell phenotypes in matrigel, which is evidenced by albumin and CK19 protein staining (Figure 2). Matrigel was regularly used in previous studies for hepatic differentiation from human pluripotent stem cells [200] and primary hepatocytes [201]. Tanimizu *et al.* found that Dlk⁺ hepatoblasts from mouse fetal liver, showing the same capacity for bi-directional differentiation as HepaRG, differentiate into hepatocytes in a matrigel-embedded gel cultivation. In contrast, these cells showed tube-like structures in collagen I gel cultivation with a high CK19 expression [202]. In addition, in *in vivo*, basement membrane proteins, including laminin and collagen IV, are mostly concentrated around the periportal area, which is considered as the place where liver progenitors are situated [202]. Whereas, the main ECM in the parenchymal area, where mature hepatocytes are located, are collagen I and fibronectin, often lacking basement membrane proteins [26]. Surprisingly, in our microfluidic environment, both PGC and NFDC cells in collagen I lost their cell-cell contact, showing a well aligned elongated shape along the flow stream with strong expression of CK19. This phenomenon of alignment of collagen I has been observed only in the presence of flow in microenvironments in previous research. e.g. collagen I aligned in microfluidic channels of widths in the 10-200 μ m range, whereas it randomly distributed in normal multi well plates in absence of flow [203]. Since the channel width in our microfluidic

device is 200 μm , it falls well into the range of alignment for collagen I. Therefore, the HepaRG cells grew in aligned collagen I, resulting in the formation of rope-like shape showing biliary-like cells.

In the comparison of one side *versus* both sides of flow, cells aggregated more efficiently and formed bigger spheroids in both side flow rather than one side flow cultivation, suggesting that the mechanical force provided by the flow might have an influence on cell-matrix interaction and promote cell-cell contact, resulting in an increased bile canaliculi formation as well. Previously, a 3D bioreactor in presence of flow supported the differentiation of human fetal liver cells into hepatocytes by forming small cell aggregates within 10 days [192]. Moreover, in clinical studies, sinusoidal shear stress generated by increase of portal pressure, where liver progenitor cells were located, was identified as an important factor for the initiation of liver regeneration *in vivo* [204]. In this microfluidic device, the cells might be influenced differently according to their distance from the flow region. In the case of one side flow, cells adjacent to the flow region might be influenced stronger by the fluid's mechanical force than cells close to the wall. In contrast, cells cultured in both side of flow might be influenced homogeneously, resulting in the promotion of cell aggregation in the overall cultivation area. Similar sizes of cell clusters of PGC were observed as compared with previous publications on progenitor cells derived from HepaRG cultured in alginate microencapsulation [205] and in hydrogel such as nanofibrillar cellulose and hyaluronan gelatin [206]. Interestingly, previous studies demonstrated a relation between the bile canaliculi area and the diameter of rat hepatocyte aggregates cultured in a 3D collagen gel microcavity device [207]. When the diameter of the cell aggregates lay between 60 μm and 80 μm , the formation of bile canaliculi showed an enhancement compared to conventional cultures. The HepaRG cell clusters formed in both sides of flow cultivation showed diameters of 40-80 μm and 50-100 μm for PGC and NFDC, respectively, suggesting that an appropriate size of HepaRG clusters enhanced the bile canaliculi formation. To our knowledge, this is the first report that a mechanical fluid force can affect the efficiency of the formation of HepaRG cell aggregations. Therefore, a homogeneous fluid mechanical force could play an important role in the formation of cell aggregates and thereby influence the bile canaliculi formation in undifferentiated HepaRG cultures in a microfluidic environment.

DMSO addition in 2D culture model is a necessary step to differentiate hepARG cells toward hepatocyte and biliary-like cells, resulting in a 1:1 ratio of population [74]. As we already mentioned in the introduction part, previous research addressed the negative effects of DMSO on primary hepatocytes and HepaRG cell cultivation, since DMSO induces a decrease of the cell viability and homeostasis functions [186, 187, 208]. Our results also

clearly demonstrate that DMSO induces a significant decrease of the cell viability and influences the distribution of hepatocyte and biliary-like cells population in both cases, i.e. PGC and NFDC. In the case of this 3D microfluidic culture model, cells were always embedded in matrigel, thereby dead cells remain and cannot be flushed out during perfusion. On the contrary, dead cells are removed by medium replacement in monolayer culture systems. Therefore, PGC without DMSO culture model was chosen due to its high cell viability and outstanding liver functionality. 70% of the total cells were identified as hepatocyte-like cells by immunostaining of CK18. This is in general agreement with previous studies using and alginate microencapsulated cultivation model for liver progenitor cells from HepaRG [205].

With regard to cell viability and liver specific functions in PGC without DMSO, our results are also comparable with previous research. Alginate encapsulated progenitor cell state of HepaRG cells showed a 89% cell survival rate at 14 days of culture without DMSO supplement [205]. The albumin production was dramatically increased during the cultivation and it corresponded to a high expression of albumin by immunostaining at 14 days of cultivation. This albumin level was even higher than fully differentiated HepaRG cells in 2D culture [209] and previous 3D culture platform [205, 210] or in a similar range to human fetal liver cells cultured in a 3D perfusion bioreactor [192]. For the functionality of the metabolic machinery, PGC without DMSO showed the highest CYP1A induction (3.4 fold change) and it is in line with previous research in 2D fully differentiate HepaRG culture model (2-3.9 fold change) [211]. In contrast, the PGC with DMSO and NFDC group showed a decreased CYP1A induction (2-2.5 fold change). Co-localized expression of CYP3A4 and albumin indicated a reconfirmation of a differentiation toward hepatocytes but did not exhibit zone specific phenotypes in this culture model. Interestingly, NFDC cells are likely to be less sensitive than PGC for the effects of DMSO, since NFDC indicated no significant changes in albumin production and CYP1A induction activity between the with and without DMSO treatment group. It might be explained that the population of hepatocyte-like cells in NFDC culture did not change significantly with DMSO *versus* without DMSO, whereas PGC significantly reduced the hepatocyte-like cell population.

Our culture model for PGC differentiated in a microfluidic device without DMSO clearly indicated a sufficient population of hepatocyte-like cells by co-staining of CK18 and CK19 and a distinct polarized organization, which is evidenced by the observance of MRP2 for apical membrane, and NTCP and ZO-1 for basolateral membrane. In our system, cholangiocytes (biliary cells) were observed in the core of the cell clusters and hepatocyte-like cells were distributed in the overall area of the cell clusters. Leite *et al* reported similar

observation for the localization of biliary cells that are located at the core part of HepaRG spheroid cultured in the stirred bioreactor [210]. It has already been demonstrated that differentiated HepaRG cells by administration of DMSO in 2D culture show a high expression of NTCP [212]. However, it has been proposed that HepaRG cells in 2D culture model do not fully recapitulate the polarization since they are limited the formation of canalicular at the apical membrane. We proved that the combination of matrigel for 3D cultures and supply of both sides of flow facilitates a hepatic differentiation by sufficient expression of tight junction (ZO-1) next to MRP2, promoting a correct assembly of cell-cell contact. It has been suggested that stable maintenance of cell-cell interaction and communication including paracrine signaling might be a critical factor for the differentiation of hepatic phenotypes [205, 213]. Importantly, since NTCP was identified as a receptor for the hepatitis B virus (HBV) and MRP2 supports the efficiency of the HBV infection, our PGC in a microfluidic 3D culture platform without the addition of DMSO can be a powerful tool to study the HBV infection *in vitro*.

IL-6 was shown to be a potent regulator for synthesis of acute-phase response proteins in primary hepatocytes [37]. Here, we also demonstrated that differentiated PGC in our microfluidic chip produced increased levels of CRP by IL-6 stimulation. Furthermore, the CRP production rate in the chip cultivation was comparable with fully differentiated 2D cultures after normalization of hepatocyte-like cell number.

In summary, the described strategies manifested the differentiation toward hepatocyte-like cells from undifferentiated HepaRG cells (liver progenitor cell) in a microfluidic environment by selection of ECM (matrigel), types of flow (both sides) and DMSO effects (without DMSO). Moreover, the entire cultivation process required 18 days without DMSO addition. Finally, 70% of the cells differentiated into hepatocyte-like cells whose hepatic functions are consistent with previous literature. This culture model can be applied for the cultivation of other cell types such as pluripotent stem cells and biliary cells and to be a relevant platform for the understanding of the physiology and regeneration of the liver.

4.5 Conclusion

The cultivation of undifferentiated HepaRG cells in the microfluidic device under different cultivation parameters showed a different population of the cells. The progenitor HepaRG cells cultured with matrigel, both sides of flow, and without the addition of DMSO showed a highest hepatocytes population, cell viability, and liver specific function. Moreover, differentiated hepatocyte-like cells in the biochip were highly polarized and produced CRP by stimulation of IL-6. Our results provide the possibility of the cultivation and the differentiation of stem cells in the microfluidic devices and this new *in vitro* platform can be applied to study hepatocyte physiology and toxicity including inflammatory reactions.

Chapter 5. Conclusion

5.1 Summary

In this thesis, we introduced a new *in vitro* liver model using a commercial microfluidic device that can be applied to investigate diverse hepatic physiological functions and hepatic inflammatory responses stimulated by IL-6. The phaseguides in the device allowed us to mimic the *in vivo* hepatocyte environment and support the cultivation of liver hepatic cell lines due to the following unique features: i) The cells are surrounded by ECMs and cultivated in 3-D, ii) The medium flow does not contact the cells directly, iii) The height of the phaseguides is one-quarter of the culture chamber height, allowing a free exchange of substances between the cell culture areas and the medium flow regions.

The work in this thesis focused on the characterization of two human hepatic cell lines—HepG2 and HepaRG—cultured in a new microfluidic device (Chapters 2 and 4). Furthermore, diverse inflammatory hepatic responses stimulated by IL-6 (Chapter 3 and 4), as well as the interplay with melatonin (Chapter 3), were studied.

In Chapter 2, HepG2 cells were cultivated in a new microfluidic device and multi-well plates, for conventional 2D and 3D cultures, and the behaviours of the HepG2 cells were compared in terms of the cell morphology, cell viability, liver-specific functions, and acetaminophen-induced toxicity. Here, it was demonstrated that HepG2 cells formed multiple clusters in each lane and maintained their aggregation. HepG2 cell clusters showed a high cell viability (>90%), with little necrosis in the core part, and improved liver function with regard to albumin and urea production, CYP1a activity, and bile canaliculi formation for two weeks in the new microenvironment, when compared to conventional 2D and 3D cultures. Furthermore, the biochip cultivation model showed the lowest LC50 value for acetaminophen-induced toxicity in comparison with the static 2D and 3D cultures. Thereby, it

was shown that the new *in vitro* platform can be employed to study liver physiological and toxicological applications.

After characterization of the new *in vitro* HepG2 cells-on-a-chip platform, which showed improved hepatic functions compared to static 2D and 3D culture models (Chapter 2), we further tested its applicability to the investigation of diverse hepatic inflammation responses stimulated by IL-6, as well as the interplay with the hormone melatonin (Chapter 3). IL-6 induced a reduction of the detoxification mechanisms (the expression of MRP2, its activity and CYP1A activity), glycogen synthesis, and mitochondrial homeostasis, and stimulated the regulation of positive and negative APR proteins. Interestingly, melatonin normalized most observed hepatic responses stimulated by IL-6, except for the CRP production. Furthermore, melatonin altered the expression level of CREBH and PXR, but did not change the total STAT3 and phosphorylated STAT3 level. Since CREBH and PXR are transcription factors that regulate APRs and the detoxification process in hepatocytes, our results suggest new candidate pathways for further studies to elucidate the hepatic protective effects of melatonin. In addition, we also observed similar inflammatory hepatic responses in our new *in vitro* platform compared to previously published results using human hepatocyte culture and *in vivo* models. Therefore, this new HepG2-on-a-chip platform can be applied for the investigation of hepatic inflammation responses and offers additional evidence of hepatic-protective functions of melatonin under pro-inflammatory stimulation.

As discussed in Chapter 4, HepaRG cells were cultivated in the same microfluidic device, and we compared their behaviour according to three different cultivation parameters: ECMs, types of flow, and DMSO. In order to reduce the length of the differentiation process, two different seeding times were chosen when HepaRG showed two distinct phenotypes: liver progenitor and not fully differentiated status in flask cultivation. HepaRG cultured in matrigel under one side flow formed only a few cell clusters and showed co-expression of albumin and CK19, whereas cells in collagen I cultures showed an elongated shape and did not form aggregates with a high expression of CK19. By applying both sides of flow, a more efficient formation of cell aggregates was observed, resulting in enlarged cell clusters and an enhanced bile canaliculi formation. The addition of DMSO significantly reduced cell viability and influenced the cell populations of both hepatocyte-like cells and biliary-like cells. Interestingly, the progenitor cell type of HepaRG was more sensitive in response to DMSO treatment regarding the liver specific functions (albumin production and CYP1A activity) than were the not fully differentiated HepaRG cells. The progenitor cell type of HepaRG cells cultured with matrigel, both sides of flow, and in absence of DMSO, were finally chosen for the differentiation of hepatocyte-like cells in the new microenvironment. Furthermore, the

differentiated progenitor HepaRG cells in the microfluidic device showed a highly polarized organization and produced similar levels of CRP, compared to fully differentiated monolayer cultures of HepaRG. Therefore, we concluded that the HepaRG microfluidic cultures could be used for the investigation of hepatic physiology and hepatic inflammatory responses as well as for the differentiation of other types of stem cells.

Interestingly, HepG2 and HepaRG cells cultured in the biochip showed different behaviours, including differences in the morphology and liver-specific functions. HepG2 cell clusters were sustained under supply of one side of flow, whereas HepaRG cell clusters formed efficiently under both sides of flow and showed smaller sizes than HepG2 cell clusters in the device. Both HepG2 and HepaRG showed a high cell viability, similar albumin production rate, and the formation of bile canaliculi, while HepG2 showed a higher CYP1A activity than HepaRG cells. In addition, a higher fold change of CRP production stimulated by IL-6 was observed in HepaRG than in HepG2 cell cultivation.

5.2 Conclusion and outlook

Diverse microfluidic devices for *in vitro* liver models have been introduced; however, standardized devices and protocols did not exist prior to now. Furthermore, installation of most microfluidic cell culture devices required additional complicated experimental setups which are unfamiliar to the average cell biology researcher [214]. By focusing on the use of one easily handled, commercial microfluidic device which can function without any other additional experimental setups, standardized methods and the evaluation of various hepatic functions were investigated in this thesis.

We provided evidence that both types of hepatic cells (HepG2 and HepaRG) cultured in this unique microenvironment showed well-maintained hepatic functions with a high cell survival rate for two weeks. However, the two hepatic lines, cultured in the biochip, showed behavioural differences in morphology and hepatic functions. This suggests that the unique microfluidic device with phaseguides not only supports the cultivation of hepatic cells, but also provides important new insights regarding their complex cellular behaviour.

Furthermore, HepG2 cells behaved differently in the microfluidic environment compared to conventional 2D and 3D models, showing various well-maintained hepatic physiological functions. The aggregation of HepaRG cells formed differently according to the exposed types of the flow in the device. This finding suggests that the flow significantly influences the behaviour of cells and should therefore be considered a critical parameter for hepatocyte cultivation in microenvironments. Our findings also suggest in-depth knowledge of the behaviour of hepatic cells in microenvironments.

Altogether, this new microfluidic culture model may be a promising *in vitro* liver tool to study hepatic physiology, overcoming typical limitations of traditional static monolayer and 3D culture models, as our culture model showed improved diverse hepatic functionality and polarity. This microfluidic cultivation model can be applied to interpret various hepatic toxicity mechanisms and liver disease models which require a highly-polarized hepatocyte platform. We also provided evidence for the applicability of this new *in vitro* hepatic model to the study of hepatic inflammatory responses, as well as its use as a tool to differentiate stem cells. Although the presented system operated successfully, there are still improvements to be made regarding the *in vitro* liver organ level culture mode as well as the additional compartments of the device for further study.

To improve the liver equivalent, co-cultivation with NPCs—such as fibroblasts, endothelial cells, and Kupffer cells—is suggested for the next *in vitro* liver model, as the NPCs are also

involved in the regulation of hepatic functions and inflammation responses via paracrine signalling. In this thesis, our hepatic microtissues from HepG2 and HepaRG cells (cultured in a single type of extracellular matrix such as matrigel or collagen I) did not show zone-specific functions. However, the liver contains complex ECM environments according to its zonation, and the composition of different ECMs will be proposed for further cultivation models. Since a difference in oxygen concentration is considered a critical parameter for liver zonation, the supply of an oxygen gradient might also be necessary in the future.

Concerning improvements to the microfluidic device used in this study, multiple organs-on-a-chip model can be suggested for the future with the addition of extra lanes in the culture chamber or connections to adjacent wells using an additional experimental setup, so that researchers can observe cell-cell communication and interactions of multiple organs that occur in the same manner as in the human body *in vivo*. Installation of upper part of phaseguide can be also suggested for support of the maintenance of cell aggregation, since we observed flattened shape in upper layers of cell culture area. Furthermore, electrical probes acting as sensors or extra compartments for a high-throughput screening system can be integrated to the present biochip platform, which will allow online monitoring for various applications.

Although the number of publications related to microfluidic cell culturing, including liver organ models is rapidly increasing, current studies cannot fully conclude the standardization of methods and nor explain in-depth biological characterization, such as metabolic, genetic, and signal transduction pathways. In this thesis, we attempted to understand and explain how melatonin influences the inflammation response stimulated by IL-6 from a molecular biology standpoint. Although it was not possible to fully elucidate such a complex biological phenomenon, we proposed new candidate pathways. Additionally, we were curious that how traditional *in vitro* platforms react differently on hepatic inflammation, therefore few experiments were performed for further studies. Interestingly, this microfluidic device platform showed more sensitive effects than traditional culture model (Figure 6.5 in appendix).

Therefore, the next challenges in the field of microfluidic cell biology are not merely to develop new biomimetic devices but also to address mechanisms in diverse disease models, cell differentiation, and cell signaling in new *in vitro* environments and to compare critically among various *in vitro* models and *in vivo* clinical data.

Reference

1. Kmiec Z (2001) Cooperation of liver cells in health and disease. *Adv Anat Embryol Cell Biol* 161:III–XIII, 1-151.
2. Godoy P, Hewitt NJ, Albrecht U, et al (2013) Recent advances in 2D and 3D in vitro systems using primary hepatocytes, alternative hepatocyte sources and non-parenchymal liver cells and their use in investigating mechanisms of hepatotoxicity, cell signaling and ADME. *Arch Toxicol*. doi: 10.1007/s00204-013-1078-5
3. Thurman RG, Kauffman FC, Jungermann K (1986) *Regulation of Hepatic Metabolism : Intra- and Intercellular Compartmentation*. Springer US
4. Jungermann K, Kietzmann T (2000) Oxygen: modulator of metabolic zonation and disease of the liver. *Hepatology* 31:255–260. doi: 10.1002/hep.510310201
5. Kietzmann T, Dimova EY, Flügel D, Scharf J-G (2006) Oxygen: modulator of physiological and pathophysiological processes in the liver. *Z Gastroenterol* 44:67–76. doi: 10.1055/s-2005-858987
6. Kietzmann T, Jungermann K (1997) Modulation by oxygen of zonal gene expression in liver studied in primary rat hepatocyte cultures. *Cell Biol Toxicol* 13:243–55.
7. Turner R, Lozoya O, Wang Y, et al (2011) Human hepatic stem cell and maturational liver lineage biology. *Hepatology* 53:1035–45. doi: 10.1002/hep.24157
8. Wisse E, De Zanger RB, Charels K, et al The liver sieve: considerations concerning the structure and function of endothelial fenestrae, the sinusoidal wall and the space of Disse. *Hepatology* 5:683–92.
9. Flisiak R (1997) Role of Ito cells in the liver function. *Pol J Pathol* 48:139–45.
10. Dixon LJ, Barnes M, Tang H, et al (2013) Kupffer cells in the liver. *Compr Physiol* 3:785–97. doi: 10.1002/cphy.c120026
11. Iwakiri Y, Groszmann RJ (2007) Vascular endothelial dysfunction in cirrhosis. *J Hepatol* 46:927–934. doi: 10.1016/j.jhep.2007.02.006
12. Wu J, Meng Z, Jiang M, et al (2010) Toll-like receptor-induced innate immune responses in non-parenchymal liver cells are cell type-specific. *Immunology* 129:363–374. doi: 10.1111/j.1365-2567.2009.03179.x
13. Katz N, Teutsch HF, Jungermann K, Sasse D (1977) Heterogeneous reciprocal localization of fructose-1,6-bisphosphatase and of glucokinase in microdissected periportal and perivenous rat liver tissue. *FEBS Lett* 83:272–6.
14. Jungermann K (1986) Functional heterogeneity of periportal and perivenous hepatocytes. *Enzyme* 35:161–80.
15. Gandhi CR (2011) *Molecular Pathology of Liver Diseases*. 5:81–95. doi: 10.1007/978-1-4419-7107-4
16. Ghafoory S, Breitkopf-Heinlein K, Li Q, et al (2013) Zonation of Nitrogen and Glucose Metabolism Gene Expression upon Acute Liver Damage in Mouse. *PLoS One* 8:e78262. doi: 10.1371/journal.pone.0078262
17. Häussinger D, Lamers WH, Moorman AF (1992) Hepatocyte heterogeneity in the metabolism of amino acids and ammonia. *Enzyme* 46:72–93.
18. Gebhardt R, Baldysiak-Figiel A, Krügel V, et al (2007) Hepatocellular expression of glutamine synthetase: An indicator of morphogen actions as master regulators of zonation in adult liver.

Prog Histochem Cytochem 41:201–266. doi: 10.1016/j.proghi.2006.12.001

19. Zanger UM, Schwab M (2013) Cytochrome P450 enzymes in drug metabolism: regulation of gene expression, enzyme activities, and impact of genetic variation. *Pharmacol Ther* 138:103–41. doi: 10.1016/j.pharmthera.2012.12.007
20. Jungermann K, Keitzmann T (1996) Zonation of Parenchymal and Nonparenchymal Metabolism in Liver. *Annu Rev Nutr* 16:179–203. doi: 10.1146/annurev.nu.16.070196.001143
21. Omiecinski CJ, Vanden Heuvel JP, Perdew GH, Peters JM (2011) Xenobiotic metabolism, disposition, and regulation by receptors: From biochemical phenomenon to predictors of major toxicities. *Toxicol Sci*. doi: 10.1093/toxsci/kfq338
22. Amacher DE (2010) The effects of cytochrome P450 induction by xenobiotics on endobiotic metabolism in pre-clinical safety studies. *Toxicol Mech Methods* 20:159–66. doi: 10.3109/15376511003690307
23. Ramadoss P, Marcus C, Perdew GH (2005) Role of the aryl hydrocarbon receptor in drug metabolism. *Expert Opin Drug Metab Toxicol* 1:9–21. doi: 10.1517/17425255.1.1.9
24. Martinez-Hernandez A, Amenta PS (1995) The extracellular matrix in hepatic regeneration. *FASEB J* 9:1401–10.
25. Susick R, Moss N, Kubota H, et al (2001) Hepatic progenitors and strategies for liver cell therapies. *Ann N Y Acad Sci* 944:398–419.
26. Martinez-Hernandez A, Amenta PS (1993) The hepatic extracellular matrix. II. Ontogenesis, regeneration and cirrhosis. *Virchows Arch A Pathol Anat Histopathol* 423:77–84.
27. McClelland R, Wauthier E, Uronis J, Reid L (2008) Gradients in the liver's extracellular matrix chemistry from periportal to pericentral zones: influence on human hepatic progenitors. *Tissue Eng Part A* 14:59–70. doi: 10.1089/ten.a.2007.0058
28. Lozoya OA, Wauthier E, Turner RA, et al (2011) Regulation of hepatic stem/progenitor phenotype by microenvironment stiffness in hydrogel models of the human liver stem cell niche. *Biomaterials* 32:7389–7402. doi: 10.1016/j.biomaterials.2011.06.042
29. Wang Y, Susando T, Lei X, et al (2010) Current development of bioreactors for extracorporeal bioartificial liver (Review). *Biointerphases* 5:FA116-FA131. doi: 10.1116/1.3521520
30. Treyer A, Müsch A (2013) Hepatocyte Polarity. In: *Compr. Physiol.* John Wiley & Sons, Inc., Hoboken, NJ, USA, pp 243–87
31. Slim CL, Lázaro-Diéguez F, Bijlard M, et al (2013) Par1b Induces Asymmetric Inheritance of Plasma Membrane Domains via LGN-Dependent Mitotic Spindle Orientation in Proliferating Hepatocytes. *PLoS Biol* 11:e1001739. doi: 10.1371/journal.pbio.1001739
32. Braiterman LT, Hubbard AL Hepatocyte Surface Polarity: Its Dynamic Maintenance and Establishment. In: *Liver.* John Wiley & Sons, Ltd, Chichester, UK, pp 73–105
33. Crispe IN (2009) The Liver as a Lymphoid Organ. *Annu Rev Immunol* 27:147–163. doi: 10.1146/annurev.immunol.021908.132629
34. Nemeth E, Baird AW, O'Farrelly C (2009) Microanatomy of the liver immune system. *Semin Immunopathol* 31:333–343. doi: 10.1007/s00281-009-0173-4
35. Robinson MW, Harmon C, O'farrelly C (2016) Liver immunology and its role in inflammation and homeostasis. *Cell Mol Immunol* 13:267–276. doi: 10.1038/cmi.2016.3
36. Epstein FH, Gabay C, Kushner I (1999) Acute-Phase Proteins and Other Systemic Responses to Inflammation. *N Engl J Med* 340:448–454. doi: 10.1056/NEJM199902113400607
37. Heinrich PC, Castell J V, Andus T (1990) Interleukin-6 and the acute phase response. *Biochem J* 265:621–636. doi: 10.1042/bj2650621

38. Nessler N, Launey Y, Aninat C, et al (2012) Clinical review: The liver in sepsis. *Crit Care* 16:235. doi: 10.1186/cc11381
39. Cray C, Zaias J, Altman NH (2009) Acute phase response in animals: A review. *Comp Med* 59:517–526. doi: 10.1002/ece3.1939
40. CASTELL J V., GEIGER T, GROSS V, et al (1988) Plasma clearance, organ distribution and target cells of interleukin-6/hepatocyte-stimulating factor in the rat. *Eur J Biochem* 177:357–361. doi: 10.1111/j.1432-1033.1988.tb14383.x
41. Castell J V., Gómez-Lechón MJ, David M, et al (1989) Interleukin-6 is the major regulator of acute phase protein synthesis in adult human hepatocytes. *FEBS Lett* 242:237–239. doi: 10.1016/0014-5793(89)80476-4
42. Hirano T, Yasukawa K, Harada H, et al (1986) Complementary DNA for a novel human interleukin (BSF-2) that induces B lymphocytes to produce immunoglobulin. *Nature* 324:73–76. doi: 10.1038/324073a0
43. Mihara M, Hashizume M, Yoshida H, et al (2012) IL-6/IL-6 receptor system and its role in physiological and pathological conditions. *Clin Sci (Lond)* 122:143–59. doi: 10.1042/CS20110340
44. Kishimoto T (2010) IL-6: from its discovery to clinical applications. *Int Immunol* 22:347–352. doi: 10.1093/intimm/dxq030
45. Wrighting DM, Andrews NC (2006) Interleukin-6 induces hepcidin expression through STAT3. *Blood* 108:3204–3209. doi: 10.1182/blood-2006-06-027631
46. Schmidt-Arras D, Rose-John S (2016) IL-6 pathway in the liver: From physiopathology to therapy. *J Hepatol* 64:1403–15. doi: 10.1016/j.jhep.2016.02.004
47. Mülberg J, Schooltink H, Stoyan T, et al (1993) The soluble interleukin-6 receptor is generated by shedding. *Eur J Immunol* 23:473–480. doi: 10.1002/eji.1830230226
48. Mackiewicz A, Schooltink H, Heinrich PC, Rose-John S (1992) Complex of soluble human IL-6-receptor/IL-6 up-regulates expression of acute-phase proteins. *J Immunol* 149:2021–7.
49. Tillet WS, Francis T (1930) SEROLOGICAL REACTIONS IN PNEUMONIA WITH A NON-PROTEIN SOMATIC FRACTION OF PNEUMOCOCCUS. *J Exp Med* 52:561–71. doi: 10.1084/JEM.52.4.561
50. Nicolas G, Chauvet C, Viatte L, et al (2002) The gene encoding the iron regulatory peptide hepcidin is regulated by anemia, hypoxia, and inflammation. *J Clin Invest* 110:1037–1044. doi: 10.1172/JCI15686
51. Heming N, Montravers P, Lasocki S (2011) Iron deficiency in critically ill patients: highlighting the role of hepcidin. *Crit Care* 15:210. doi: 10.1186/cc9992
52. Cerón, JJ, Eckersall, PD, Martínez-Subiela S (2005) Acute phase proteins in dogs and cats: current knowledge and future perspectives. *Vet Clin Pathol* 34:85–99. doi: 10.1111/j.1939-165X.2005.tb00019.x
53. Tothova C, Nagy O, Kovac G (2014) Acute phase proteins and their use in the diagnosis of diseases in ruminants: a review. *Vet. Med. (Praha)*.
54. Lerner A, Case J, Takahashi Y (1958) Isolation of melatonin, the pineal gland factor that lightens melanocyteS1. *J*.
55. Reiter RJ, Tan DX, Osuna C, Gitto E Actions of melatonin in the reduction of oxidative stress. A review. *J Biomed Sci* 7:444–58. doi: 25480
56. Ljubisavljevic S, Stojanovic I, Cvetkovic T, et al (2014) Erythrocytes' antioxidative capacity as a potential marker of oxidative stress intensity in neuroinflammation. *J Neurol Sci* 337:8–13. doi: 10.1016/j.jns.2013.11.006

57. Mathes AM (2010) Hepatoprotective actions of melatonin: Possible mediation by melatonin receptors. *World J Gastroenterol* 16:6087–6097.
58. Ambriz-Tututi M, Rocha-González HI, Cruz SL, Granados-Soto V (2009) Melatonin: A hormone that modulates pain. *Life Sci* 84:489–498. doi: 10.1016/j.lfs.2009.01.024
59. Costa EJ, Shida CS, Biaggi MH, et al (1997) How melatonin interacts with lipid bilayers: a study by fluorescence and ESR spectroscopies. *FEBS Lett* 416:103–6.
60. Jou M-J, Peng T-I, Yu P-Z, et al (2007) Melatonin protects against common deletion of mitochondrial DNA-augmented mitochondrial oxidative stress and apoptosis. *J Pineal Res* 43:389–403. doi: 10.1111/j.1600-079X.2007.00490.x
61. Tan D-X, Hardeland R, Manchester LC, et al (2014) Cyclic-3-hydroxymelatonin (C3HOM), a potent antioxidant, scavenges free radicals and suppresses oxidative reactions. *Curr Med Chem* 21:1557–65.
62. Carrillo-Vico A, Lardone PJ, Naji L, et al (2005) Beneficial pleiotropic actions of melatonin in an experimental model of septic shock in mice: Regulation of pro-/anti-inflammatory cytokine network, protection against oxidative damage and anti-apoptotic effects. *J Pineal Res* 39:400–408. doi: 10.1111/j.1600-079X.2005.00265.x
63. Şener G, Toklu H, Kapucu C, et al (2004) Melatonin Protects Against Oxidative Organ Injury in a Rat Model of Sepsis. *Surg Today* 35:52–59. doi: 10.1007/s00595-004-2879-1
64. Gonciarz M, Gonciarz Z, Bielanski W, et al (2012) The effects of long-term melatonin treatment on plasma liver enzymes levels and plasma concentrations of lipids and melatonin in patients with nonalcoholic steatohepatitis: a pilot study. *J Physiol Pharmacol* 63:35–40.
65. Mathes AM, Kubulus D, Waibel L, et al (2008) Selective activation of melatonin receptors with ramelteon improves liver function and hepatic perfusion after hemorrhagic shock in rat. *Crit Care Med* 36:2863–2870. doi: 10.1097/CCM.0b013e318187b863
66. Kleber A, Kubulus D, Rössler D, et al (2014) Melatonin modifies cellular stress in the liver of septic mice by reducing reactive oxygen species and increasing the unfolded protein response. *Exp Mol Pathol* 97:565–71. doi: 10.1016/j.yexmp.2014.10.009
67. Zhang K, Shen X, Wu J, et al (2006) Endoplasmic reticulum stress activates cleavage of CREBH to induce a systemic inflammatory response. *Cell* 124:587–99. doi: 10.1016/j.cell.2005.11.040
68. Brown MS, Ye J, Rawson RB, Goldstein JL (2000) Regulated intramembrane proteolysis: a control mechanism conserved from bacteria to humans. *Cell* 100:391–398. doi: 10.1016/S0092-8674(00)80675-3
69. van Midwoud PM, Verpoorte E, Groothuis GMM (2011) Microfluidic devices for in vitro studies on liver drug metabolism and toxicity. *Integr Biol (Camb)* 3:509–521. doi: 10.1039/c0ib00119h
70. Gerets HHJ, Tilmant K, Gerin B, et al (2012) Characterization of primary human hepatocytes, HepG2 cells, and HepaRG cells at the mRNA level and CYP activity in response to inducers and their predictivity for the detection of human hepatotoxins. *Cell Biol Toxicol* 28:69–87. doi: 10.1007/s10565-011-9208-4
71. Gripon P, Rumin S, Urban S, et al (2002) Infection of a human hepatoma cell line by hepatitis B virus. *Proc Natl Acad Sci U S A* 99:15655–60. doi: 10.1073/pnas.232137699
72. Cerec V, Glaise D, Garnier D, et al (2007) Transdifferentiation of hepatocyte-like cells from the human hepatoma HepaRG cell line through bipotent progenitor. *Hepatology* 45:957–967. doi: 10.1002/hep.21536
73. Parent R, Marion MJ, Furio L, et al (2004) Origin and Characterization of a Human Bipotent Liver Progenitor Cell Line. *Gastroenterology* 126:1147–1156. doi: 10.1053/j.gastro.2004.01.002
74. Sahu SC (2016) Stems cells in toxicology and medicine. WILEY-VCH Verlag GmbH

75. Hart SN, Li Y, Nakamoto K, et al (2010) A comparison of whole genome gene expression profiles of HepaRG cells and HepG2 cells to primary human hepatocytes and human liver tissues. *Drug Metab Dispos* 38:988–94. doi: 10.1124/dmd.109.031831
76. Yoon No D, Lee K-H, Lee J, Lee S-H (2015) 3D liver models on a microplatform: well-defined culture, engineering of liver tissue and liver-on-a-chip. *Lab Chip* 15:3822–3837. doi: 10.1039/C5LC00611B
77. Katt ME, Placone AL, Wong AD, et al (2016) In Vitro Tumor Models: Advantages, Disadvantages, Variables, and Selecting the Right Platform. *Front Bioeng Biotechnol* 4:12. doi: 10.3389/fbioe.2016.00012
78. 3D Biomatrix - 3D Cell Culture: Spheroid Cultures for Cancer Research, Stem Cell Research, and Drug Discovery. <https://3dbiomatrix.com/>. Accessed 13 Mar 2017
79. InSphero | Assay-Ready 3D Microtissue Models and Services. <https://www.insphero.com/>. Accessed 13 Mar 2017
80. Curcio E, Salerno S, Barbieri G, et al (2007) Mass transfer and metabolic reactions in hepatocyte spheroids cultured in rotating wall gas-permeable membrane system. *Biomaterials* 28:5487–5497. doi: 10.1016/j.biomaterials.2007.08.033
81. Lee KY, Mooney DJ (2001) Hydrogels for tissue engineering. *Chem Rev* 101:1869–79.
82. Lee S-A, No DY, Kang E, et al (2013) Spheroid-based three-dimensional liver-on-a-chip to investigate hepatocyte-hepatic stellate cell interactions and flow effects. *Lab Chip* 13:3529–37. doi: 10.1039/c3lc50197c
83. Yamada M, Utoh R, Ohashi K, et al (2012) Controlled formation of heterotypic hepatic micro-organoids in anisotropic hydrogel microfibers for long-term preservation of liver-specific functions. *Biomaterials* 33:8304–8315. doi: 10.1016/j.biomaterials.2012.07.068
84. Lee KH, No DY, Kim S-H, et al (2011) Diffusion-mediated in situ alginate encapsulation of cell spheroids using microscale concave well and nanoporous membrane. *Lab Chip* 11:1168–73. doi: 10.1039/c0lc00540a
85. Manz A, Graber N, Widmer HM (1990) Miniaturized total chemical analysis systems: A novel concept for chemical sensing. *Sensors Actuators B Chem* 1:244–248. doi: 10.1016/0925-4005(90)80209-I
86. Young EWK, Beebe DJ (2010) Fundamentals of microfluidic cell culture in controlled microenvironments. *Chem Soc Rev* 39:1036–48. doi: 10.1039/b909900j
87. Powers MJ, Domansky K, Kaazempur-Mofrad MR, et al (2002) A microfabricated array bioreactor for perfused 3D liver culture. *Biotechnol Bioeng* 78:257–269. doi: 10.1002/bit.10143
88. Sivaraman a, Leach JK, Townsend S, et al (2005) A microscale in vitro physiological model of the liver: predictive screens for drug metabolism and enzyme induction. *Curr Drug Metab* 6:569–91. doi: 10.2174/138920005774832632
89. Domansky K, Inman W, Serdy J, et al (2010) Perfused multiwell plate for 3D liver tissue engineering. *Lab Chip* 10:51–8. doi: 10.1039/b913221j
90. Sin A, Chin KC, Jamil MF, et al (2004) The Design and Fabrication of Three-Chamber Microscale Cell Culture Analog Devices with Integrated Dissolved Oxygen Sensors. *Biotechnol Prog* 20:338–345. doi: 10.1021/bp034077d
91. Chao P, Maguire T, Novik E, et al (2009) Evaluation of a microfluidic based cell culture platform with primary human hepatocytes for the prediction of hepatic clearance in human. *Biochem Pharmacol* 78:625–632. doi: 10.1016/j.bcp.2009.05.013
92. Novik E, Maguire TJ, Chao P, et al (2010) A microfluidic hepatic coculture platform for cell-based drug metabolism studies. *Biochem Pharmacol* 79:1036–1044. doi: 10.1016/j.bcp.2009.11.010

93. Lee PJ, Hung PJ, Lee LP (2007) An artificial liver sinusoid with a microfluidic endothelial-like barrier for primary hepatocyte culture. *Biotechnol Bioeng* 97:1340–1346. doi: 10.1002/bit
94. Nakao Y, Kimura H, Sakai Y, Fujii T (2011) Bile canaliculi formation by aligning rat primary hepatocytes in a microfluidic device. *Biomicrofluidics* 5:22212. doi: 10.1063/1.3580753
95. Gori M, Simonelli MC, Giannitelli SM, et al (2016) Investigating Nonalcoholic Fatty Liver Disease in a Liver-on-a-Chip Microfluidic Device. *PLoS One* 11:e0159729. doi: 10.1371/journal.pone.0159729
96. Toh Y-C, Lim TC, Tai D, et al (2009) A microfluidic 3D hepatocyte chip for drug toxicity testing. *Lab Chip* 9:2026. doi: 10.1039/b900912d
97. Wagner I, Materne E-M, Brincker S, et al (2013) A dynamic multi-organ-chip for long-term cultivation and substance testing proven by 3D human liver and skin tissue co-culture. *Lab Chip* 13:3538–47. doi: 10.1039/c3lc50234a
98. Maschmeyer I, Lorenz AK, Schimek K, et al (2015) Lab on a Chip co-culture of human intestine , liver , skin and. *Lab Chip* 15:2688–2699. doi: 10.1039/C5LC00392J
99. Maschmeyer I, Hasenberg T, Jaenicke A, et al (2015) Chip-based human liver-intestine and liver-skin co-cultures - A first step toward systemic repeated dose substance testing in vitro. *Eur J Pharm Biopharm* 95:77–87. doi: 10.1016/j.ejpb.2015.03.002
100. Raasch M, Rennert K, Jahn T, et al (2015) Microfluidically supported biochip design for culture of endothelial cell layers with improved perfusion conditions. *Biofabrication* 7:15013. doi: 10.1088/1758-5090/7/1/015013
101. Rennert K, Steinborn S, Gröger M, et al (2015) A microfluidically perfused three dimensional human liver model. *Biomaterials* 71:119–131. doi: 10.1016/j.biomaterials.2015.08.043
102. Seok J, Warren HS, Cuenca AG, et al (2013) Genomic responses in mouse models poorly mimic human inflammatory diseases. *Proc Natl Acad Sci U S A* 110:3507–12. doi: 10.1073/pnas.1222878110
103. Goral VN, Hsieh Y-C, Petzold ON, et al (2010) Perfusion-based microfluidic device for three-dimensional dynamic primary human hepatocyte cell culture in the absence of biological or synthetic matrices or coagulants. *Lab Chip* 10:3380–6. doi: 10.1039/c0lc00135j
104. Prot JM, Briffaut A-S, Letourneur F, et al (2011) Integrated proteomic and transcriptomic investigation of the acetaminophen toxicity in liver microfluidic biochip. *PLoS One* 6:e21268. doi: 10.1371/journal.pone.0021268
105. Prot JM, Aninat C, Griscom L, et al (2011) Improvement of HepG2/C3a cell functions in a microfluidic biochip. *Biotechnol Bioeng* 108:1704–15. doi: 10.1002/bit.23104
106. Choucha Snouber L, Bunescu A, Naudot M, et al (2013) Metabolomics-on-a-chip of hepatotoxicity induced by anticancer drug flutamide and Its active metabolite hydroxyflutamide using HepG2/C3a microfluidic biochips. *Toxicol Sci* 132:8–20. doi: 10.1093/toxsci/kfs230
107. Gröger M, Rennert K, Giszas B, et al (2016) Monocyte-induced recovery of inflammation-associated hepatocellular dysfunction in a biochip-based human liver model. *Sci Rep* 6:21868. doi: 10.1038/srep21868
108. Verneti LA, Senutovitch N, Boltz R, et al (2016) A human liver microphysiology platform for investigating physiology, drug safety, and disease models. *Exp Biol Med (Maywood)* 241:101–14. doi: 10.1177/1535370215592121
109. McCarty WJ, Usta OB, Yarmush ML (2016) A Microfabricated Platform for Generating Physiologically-Relevant Hepatocyte Zonation. *Sci Rep* 6:26868. doi: 10.1038/srep26868
110. Ebrahimkhani MR, Neiman JAS, Raredon MSB, et al (2014) Bioreactor technologies to support liver function in vitro. *Adv Drug Deliv Rev* 69–70:132–157. doi: 10.1016/j.addr.2014.02.011

111. Schyschka L, Sánchez JJM, Wang Z, et al (2013) Hepatic 3D cultures but not 2D cultures preserve specific transporter activity for acetaminophen-induced hepatotoxicity. *Arch Toxicol* 87:1581–93. doi: 10.1007/s00204-013-1080-y
112. Kinasiewicz A, Kawiak J, Weryński A (2006) 3D Matrigel Culture Improves Differentiated Functions of HepG2 Cells in Vitro. 26:47–54.
113. Baudoin R, Griscom L, Prot JM, et al (2011) Behavior of HepG2/C3A cell cultures in a microfluidic bioreactor. *Biochem Eng J* 53:172–181. doi: 10.1016/j.bej.2010.10.007
114. Kim SS, Sundback CA, Kaihara S, et al (2000) Dynamic Seeding and *in Vitro* Culture of Hepatocytes in a Flow Perfusion System. *Tissue Eng* 6:39–44. doi: 10.1089/107632700320874
115. Tilles AW, Baskaran H, Roy P, et al (2001) Effects of oxygenation and flow on the viability and function of rat hepatocytes cocultured in a microchannel flat-plate bioreactor. *Biotechnol Bioeng* 73:379–389. doi: 10.1002/bit.1071
116. Hegde M, Jindal R, Bhushan A, et al (2014) Dynamic interplay of flow and collagen stabilizes primary hepatocytes culture in a microfluidic platform. *Lab Chip* 14:2033–9. doi: 10.1039/c4lc00071d
117. Trietsch SJ, Israëls GD, Joore J, et al (2013) Microfluidic titer plate for stratified 3D cell culture. *Lab Chip* 13:3548–3554. doi: 10.1039/c3lc50210d
118. Fazili IS, Jiang W, Wang L, et al (2010) Persistent induction of cytochrome P4501A1 in human hepatoma cells by 3-methylcholanthrene: evidence for sustained transcriptional activation of the CYP1A1 promoter. *J Pharmacol Exp Ther* 333:99–109. doi: 10.1124/jpet.109.162222
119. Kinasiewicz J, Kawiak J, Weryński A (2006) 3D matrigel culture improves differentiated functions of HepG2 cells in vitro. *Biocybern Biomed Eng* 47–54.
120. Legendre A, Baudoin R, Alberto G, et al (2013) Metabolic Characterization of Primary Rat Hepatocytes Cultivated in Parallel Microfluidic Biochips. *J Pharm Sci* 102:3264–3276. doi: 10.1002/jps.23466
121. Ma B, Zhang G, Qin J, Lin B (2009) Characterization of drug metabolites and cytotoxicity assay simultaneously using an integrated microfluidic device. *Lab Chip* 9:232–8. doi: 10.1039/b809117j
122. Török E, Pollok JM, Ma PX, et al (2001) Optimization of hepatocyte spheroid formation for hepatic tissue engineering on three-dimensional biodegradable polymer within a flow bioreactor prior to implantation. *Cells Tissues Organs* 169:34–41. doi: 47858
123. Ramaiahgari SC, den Braver MW, Herpers B, et al (2014) A 3D in vitro model of differentiated HepG2 cell spheroids with improved liver-like properties for repeated dose high-throughput toxicity studies. *Arch Toxicol*. doi: 10.1007/s00204-014-1215-9
124. Mueller D, Tascher G, Müller-Vieira U, et al (2011) In-depth physiological characterization of primary human hepatocytes in a 3D hollow-fiber bioreactor. *J Tissue Eng Regen Med* 5:e207–e218. doi: 10.1002/term.418
125. Hsu MN, Tan G-DS, Tania M, et al (2014) Computational fluid model incorporating liver metabolic activities in perfusion bioreactor. *Biotechnol Bioeng* 111:885–895. doi: 10.1002/bit.25157
126. Török E, Lutgehetmann M, Bierwolf J, et al (2011) Primary human hepatocytes on biodegradable poly(L-lactic acid) matrices: A promising model for improving transplantation efficiency with tissue engineering. *Liver Transplant* 17:104–114. doi: 10.1002/lt.22200
127. Dash A, Simmers MB, Deering TG, et al (2013) Hemodynamic flow improves rat hepatocyte morphology, function, and metabolic activity in vitro. *Am J Physiol Cell Physiol* 304:C1053–63. doi: 10.1152/ajpcell.00331.2012
128. Khetani SR, Bhatia SN (2007) Microscale culture of human liver cells for drug development.

129. Bhatia SN, Balis UJ, Yarmush ML, Toner M (1999) Effect of cell-cell interactions in preservation of cellular phenotype: cocultivation of hepatocytes and nonparenchymal cells. *FASEB J* 13:1883–900.
130. Blieden M, Paramore LC, Shah D, Ben-Joseph R (2014) A perspective on the epidemiology of acetaminophen exposure and toxicity in the United States. *Expert Rev Clin Pharmacol* 7:341–348. doi: 10.1586/17512433.2014.904744
131. Ullrich A, Berg C, Hengstler JG, Runge D (2007) Use of a standardised and validated long-term human hepatocyte culture system for repetitive analyses of drugs: repeated administrations of acetaminophen reduces albumin and urea secretion. *ALTEX* 24:35–40.
132. Xia L, Ng S, Han R, et al (2009) Laminar-flow immediate-overlay hepatocyte sandwich perfusion system for drug hepatotoxicity testing. *Biomaterials* 30:5927–5936. doi: 10.1016/j.biomaterials.2009.07.022
133. Norris CA, He M, Kang LI, et al (2014) Synthesis of IL-6 by hepatocytes is a normal response to common hepatic stimuli. *PLoS One* 9:1–14. doi: 10.1371/journal.pone.0096053
134. Wolf J, Rose-John S, Garbers C (2014) Interleukin-6 and its receptors: a highly regulated and dynamic system. *Cytokine* 70:11–20. doi: 10.1016/j.cyto.2014.05.024
135. Ramadori G, Van Damme J, Rieder H, Meyer zum Büschenfelde KH (1988) Interleukin 6, the third mediator of acute-phase reaction, modulates hepatic protein synthesis in human and mouse. Comparison with interleukin 1 beta and tumor necrosis factor-alpha. *Eur J Immunol* 18:1259–64. doi: 10.1002/eji.1830180817
136. Chung J, Shin DY, Zheng M, et al (2011) Carbon monoxide, a reaction product of heme oxygenase-1, suppresses the expression of C-reactive protein by endoplasmic reticulum stress through modulation of the unfolded protein response. *Mol Immunol* 48:1793–1799. doi: 10.1016/j.molimm.2011.05.014
137. Liu Y, Shao M, Wu Y, et al (2015) Role for the endoplasmic reticulum stress sensor IRE1 α in liver regenerative responses. *J Hepatol* 62:590–598. doi: 10.1016/j.jhep.2014.10.022
138. Fardel O, Le Vée M (2009) Regulation of human hepatic drug transporter expression by pro-inflammatory cytokines. *Expert Opin Drug Metab Toxicol* 5:1469–1481. doi: 10.1517/17425250903304056
139. Rubin K, Janefeldt A, Andersson L, et al (2015) Heparg cells as human-relevant in vitro model to study the effects of inflammatory stimuli on cytochrome P450 isoenzymes. *Drug Metab Dispos* 43:119–125. doi: 10.1124/dmd.114.059246
140. Lienenlücke B, Christ B (2007) Impact of interleukin-6 on the glucose metabolic capacity in rat liver. *Histochem Cell Biol* 128:371–377. doi: 10.1007/s00418-007-0327-1
141. Yang R, Lirussi D, Thornton TM, et al (2015) Mitochondrial Ca²⁺ and membrane potential, an alternative pathway for Interleukin 6 to regulate CD4 cell effector function. *Elife* 4:1–22. doi: 10.7554/eLife.06376
142. Wu J-Y, Tsou M-Y, Chen T-H, et al (2008) Therapeutic effects of melatonin on peritonitis-induced septic shock with multiple organ dysfunction syndrome in rats. *J Pineal Res* 45:106–16. doi: 10.1111/j.1600-079X.2008.00567.x
143. Kleber A, Ruf CG, Wolf A, et al (2015) Melatonin or ramelteon therapy differentially affects hepatic gene expression profiles after haemorrhagic shock in rat - A microarray analysis. *Exp Mol Pathol* 99:189–197. doi: 10.1016/j.yexmp.2015.06.019
144. Shin DY, Chung J, Joe Y, et al (2012) Pretreatment with CO-releasing molecules suppresses hepcidin expression during inflammation and endoplasmic reticulum stress through inhibition of the STAT3 and CREBH pathways. *Blood* 119:2523–2532. doi: 10.1182/blood-2011-07-366690

145. Chanda D, Kim DK, Li T, et al (2011) Cannabinoid Receptor Type 1 (CB1R) signaling regulates hepatic gluconeogenesis via induction of endoplasmic reticulum-bound transcription factor cAMP-responsive element-binding protein H (CREBH) in primary hepatocytes. *J Biol Chem* 286:27971–27979. doi: 10.1074/jbc.M111.224352
146. Chaudhari N, Talwar P, Parimisetty A, et al (2014) A molecular web: endoplasmic reticulum stress, inflammation, and oxidative stress. *Front Cell Neurosci* 8:213. doi: 10.3389/fncel.2014.00213
147. Tan D-X, Manchester L, Qin L, Reiter R (2016) Melatonin: A Mitochondrial Targeting Molecule Involving Mitochondrial Protection and Dynamics. *Int J Mol Sci* 17:2124. doi: 10.3390/ijms17122124
148. Akhtar A (2015) The flaws and human harms of animal experimentation. *Camb Q Healthc Ethics* 24:407–19. doi: 10.1017/S0963180115000079
149. Jang M, Neuzil P, Volk T, et al (2015) On-chip three-dimensional cell culture in phaseguides improves hepatocyte functions in vitro. *Biomicrofluidics* 9:34113. doi: 10.1063/1.4922863
150. Shieh JM, Wu HT, Cheng KC, Cheng JT (2009) Melatonin ameliorates high fat diet-induced diabetes and stimulates glycogen synthesis via a PKC β -Akt-GSK3 β pathway in hepatic cells. *J Pineal Res* 47:339–344. doi: 10.1111/j.1600-079X.2009.00720.x
151. Diao L, Li N, Brayman TG, et al (2010) Regulation of MRP2/ABCC2 and BSEP/ABCB1 expression in sandwich cultured human and rat hepatocytes exposed to inflammatory cytokines TNF- α , IL-6, and IL-1 β . *J Biol Chem* 285:31185–92. doi: 10.1074/jbc.M110.107805
152. Anthérieu S, Chesné C, Li R, et al (2010) Stable expression, activity, and inducibility of cytochromes P450 in differentiated HepaRG cells. *Drug Metab Dispos* 38:516–25. doi: 10.1124/dmd.109.030197
153. Arana MR, Tocchetti GN, Rigalli JP, et al (2016) Physiological and pathophysiological factors affecting the expression and activity of the drug transporter MRP2 in intestine. Impact on its function as membrane barrier. *Pharmacol Res* 109:32–44. doi: 10.1016/j.phrs.2016.04.014
154. Donner MG, Topp SA, Cebula P, et al (2013) HbG200-mediated preinduction of heme oxygenase-1 improves bile flow and ameliorates pericentral downregulation of Bsep and Mrp2 following experimental liver ischemia and reperfusion. *Biol Chem* 394:97–112. doi: 10.1515/hsz-2012-0153
155. Geier A, Wagner M, Dietrich CG, Trauner M (2007) Principles of hepatic organic anion transporter regulation during cholestasis, inflammation and liver regeneration. *Biochim Biophys Acta - Mol Cell Res* 1773:283–308. doi: 10.1016/j.bbamcr.2006.04.014
156. Zollner G, Thueringer A, Lackner C, et al (2014) Alterations of canalicular ATP-binding cassette transporter expression in drug-induced liver injury. *Digestion* 90:81–8. doi: 10.1159/000365003
157. Yang Q, Doshi U, Li N, P. Li A (2012) Effects of Culture Duration on Gene Expression of P450 Isoforms, Uptake and Efflux Transporters in Primary Hepatocytes Cultured in the Absence and Presence of Interleukin-6: Implications for Experimental Design for the Evaluation of Downregulatory Effect. *Curr Drug Metab* 13:938–946. doi: 10.2174/138920012802138570
158. Yang J, Hao C, Yang D, et al (2010) Pregnane X receptor is required for interleukin-6-mediated down-regulation of cytochrome P450 3A4 in human hepatocytes. *Toxicol Lett* 197:219–226. doi: 10.1016/j.toxlet.2010.06.003
159. Pascussi JM, Gerbal-Chaloin S, Pichard-Garcia L, et al (2000) Interleukin-6 negatively regulates the expression of pregnane X receptor and constitutively activated receptor in primary human hepatocytes. *Biochem Biophys Res Commun* 274:707–13. doi: 10.1006/bbrc.2000.3219
160. Xu DX, Wei W, Sun MF, et al (2005) Melatonin attenuates lipopolysaccharide-induced down-

- regulation of pregnane X receptor and its target gene CYP3A in mouse liver. *J Pineal Res* 38:27–34. doi: 10.1111/j.1600-079X.2004.00171.x
161. Dickmann LJ, Patel SK, Wienkers LC, Slatter JG (2012) Effects of interleukin 1 β (IL-1 β) and IL-1 β /interleukin 6 (IL-6) combinations on drug metabolizing enzymes in human hepatocyte culture. *Curr Drug Metab* 13:930–7. doi: 10.2174/138920012802138642
 162. Chang TKH, Chen J, Yang G, Yeung EYH (2010) Inhibition of procarcinogen-bioactivating human CYP1A1, CYP1A2 and CYP1B1 enzymes by melatonin. *J Pineal Res* 48:55–64. doi: 10.1111/j.1600-079X.2009.00724.x
 163. Huang C-Y, Chen W-M, Tsay Y-G, et al (2015) Differential regulation of protein expression in response to polyunsaturated fatty acids in the liver of apoE-knockout mice and in HepG2 cells. *J Biomed Sci* 22:12. doi: 10.1186/s12929-015-0118-2
 164. Karlsson JO, Yarmush ML, Toner M (1998) Interaction between heat shock and interleukin 6 stimulation in the acute-phase response of human hepatoma (HepG2) cells. *Hepatology* 28:994–1004. doi: 10.1002/hep.510280414
 165. Zhang H, Kuang S, Wang Y, et al (2015) Bigelovin inhibits STAT3 signaling by inactivating JAK2 and induces apoptosis in human cancer cells. *Acta Pharmacol Sin* 36:507–516. doi: 10.1038/aps.2014.143
 166. Öz E, İlhan MN (2006) Effects of melatonin in reducing the toxic effects of doxorubicin. *Mol Cell Biochem* 286:11–15. doi: 10.1007/s11010-005-9003-8
 167. El-Missiry MA, Fayed TA, El-Sawy MR, El-Sayed AA (2007) Ameliorative effect of melatonin against gamma-irradiation-induced oxidative stress and tissue injury. *Ecotoxicol Environ Saf* 66:278–286. doi: 10.1016/j.ecoenv.2006.03.008
 168. Wang RH, Li C, Xu X, et al (2005) A role of SMAD4 in iron metabolism through the positive regulation of hepcidin expression. *Cell Metab* 2:399–409. doi: 10.1016/j.cmet.2005.10.010
 169. Ritchie DG (1990) Interleukin 6 stimulates hepatic glucose release from prelabeled glycogen pools. *Am J Physiol Endocrinol Metab* 258:E57-64.
 170. Dou L, Zhao T, Wang L, et al (2013) MiR-200s contribute to interleukin-6 (IL-6)-induced insulin resistance in hepatocytes. *J Biol Chem* 288:22596–22606. doi: 10.1074/jbc.M112.423145
 171. Dou L, Wang S, Sui X, et al (2015) MiR-301a mediates the effect of IL-6 on the AKT/GSK pathway and hepatic glycogenesis by regulating PTEN expression. *Cell Physiol Biochem* 35:1413–1424. doi: 10.1159/000373962
 172. Rui L (2014) Energy Metabolism in the Liver. *Compr Physiol* 4:177–197. doi: 10.1002/cphy.c130024.Energy
 173. Hadj Ayed Tka K, Mahfoudh Boussaid A, Zaouali MA, et al (2015) Melatonin modulates endoplasmic reticulum stress and Akt/GSK3-beta signaling pathway in a rat model of renal warm ischemia reperfusion. *Anal Cell Pathol (Amst)* 2015:635172. doi: 10.1155/2015/635172
 174. Kodama S, Koike C, Negishi M, Yamamoto Y (2004) Nuclear receptors CAR and PXR cross talk with FOXO1 to regulate genes that encode drug-metabolizing and gluconeogenic enzymes. *Mol Cell Biol* 24:7931–40. doi: 10.1128/MCB.24.18.7931-7940.2004
 175. Jakubíková J, Sedlák J, Mithen R, Bao Y (2005) Role of PI3K/Akt and MEK/ERK signaling pathways in sulforaphane- and erucin-induced phase II enzymes and MRP2 transcription, G2/M arrest and cell death in Caco-2 cells. *Biochem Pharmacol* 69:1543–1552. doi: 10.1016/j.bcp.2005.03.015
 176. Berthiaume F, MacDonald AD, Kang YH, Yarmush ML (2003) Control analysis of mitochondrial metabolism in intact hepatocytes: Effect of interleukin-1 β and interleukin-6. *Metab Eng* 5:108–123. doi: 10.1016/S1096-7176(03)00010-7
 177. Reyes-Toso CF, Rebagliati IR, Ricci CR, et al (2006) Effect of melatonin treatment on oxygen

- consumption by rat liver mitochondria. *Amino Acids* 31:299–302. doi: 10.1007/s00726-005-0280-z
178. Reyes-Toso CF, Ricci CR, de Mignone IR, et al (2003) In vitro effect of melatonin on oxygen consumption in liver mitochondria of rats. *Neuro Endocrinol Lett* 24:341–4.
179. Martín M, Macías M, Escames G, et al (2000) Melatonin-induced increased activity of the respiratory chain complexes I and IV can prevent mitochondrial damage induced by ruthenium red in vivo. *J Pineal Res* 28:242–8.
180. López A, García JA, Escames G, et al (2009) Melatonin protects the mitochondria from oxidative damage reducing oxygen consumption, membrane potential, and superoxide anion production. *J Pineal Res* 46:188–198. doi: 10.1111/j.1600-079X.2008.00647.x
181. Fabre G, Combalbert J, Berger Y, Cano J-P Human hepatocytes as a key in vitro model to improve preclinical drug development. *Eur J Drug Metab Pharmacokinet* 15:165–171. doi: 10.1007/BF03190200
182. Madan A, Graham RA, Carroll KM, et al (2003) Effects of Prototypical Microsomal Enzyme Inducers on Cytochrome P450 Expression in Cultured Human Hepatocytes. *Drug Metab Dispos* 31:421 LP-431.
183. McGill MR, Yan H-MM, Ramachandran A, et al (2011) HepaRG cells: a human model to study mechanisms of acetaminophen hepatotoxicity. *Hepatology* 53:974–982. doi: 10.1002/hep.24132
184. Anthérieu S, Chesné C, Li R, et al (2012) Optimization of the HepaRG cell model for drug metabolism and toxicity studies. *Toxicol Vitro* 26:1278–1285. doi: 10.1016/j.tiv.2012.05.008
185. Troadec MB, Glaise D, Lamirault G, et al (2006) Hepatocyte iron loading capacity is associated with differentiation and repression of motility in the HepaRG cell line. *Genomics* 87:93–103. doi: 10.1016/j.ygeno.2005.08.016
186. Sumida K, Igarashi Y, Toritsuka N, et al (2011) Effects of DMSO on gene expression in human and rat hepatocytes. *Hum Exp Toxicol* 30:1701–9. doi: 10.1177/09603271111399325
187. Hoekstra R, Nibourg GAA, Van Der Hoeven T V., et al (2011) The HepaRG cell line is suitable for bioartificial liver application. *Int J Biochem Cell Biol* 43:1483–1489. doi: 10.1016/j.biocel.2011.06.011
188. van der Helm MW, van der Meer AD, Eijkel JCT, et al (2016) Microfluidic organ-on-chip technology for blood-brain barrier research. *Tissue barriers* 4:e1142493. doi: 10.1080/21688370.2016.1142493
189. Huh D, Hamilton GA, Ingber DE (2011) From 3D cell culture to organs-on-chips. *Trends Cell Biol* 21:745–754. doi: 10.1016/j.tcb.2011.09.005
190. Materne E-M, Wagner I, Frädriich C, et al (2013) Dynamic culture of human liver equivalents inside a micro-bioreactor for long-term substance testing. *BMC Proc* 7:P72. doi: 10.1186/1753-6561-7-S6-P72
191. Alexandrova A V., Pul'kova N V., Sakharov DA (2016) Complex Approach to Xenobiotics Hepatotoxicity Testing using a Microfluidic System. *Bull Exp Biol Med* 161:50–53. doi: 10.1007/s10517-016-3342-1
192. Schmelzer E, Triolo F, Turner ME, et al (2010) Three-dimensional perfusion bioreactor culture supports differentiation of human fetal liver cells. *Tissue Eng Part A* 16:2007–2016. doi: 10.1089/ten.tea.2009.0569
193. Kalitsky-Szirtes J, Shayeganpour A, Brocks DR, Piquette-Miller M (2004) Suppression of drug-metabolizing enzymes and efflux transporters in the intestine of endotoxin-treated rats. *Drug Metab Dispos* 32:20–27. doi: 10.1124/dmd.32.1.20
194. Schindelin J, Arganda-Carreras I, Frise E, et al (2012) Fiji: an open-source platform for

- biological-image analysis. *Nat Methods* 9:676–682. doi: 10.1038/nmeth.2019
195. Miyajima A, Tanaka M, Itoh T (2014) Stem/progenitor cells in liver development, homeostasis, regeneration, and reprogramming. *Cell Stem Cell* 14:561–574. doi: 10.1016/j.stem.2014.04.010
 196. Kumar A, Sharma P, Sarin SK (2008) Hepatic venous pressure gradient measurement: time to learn! *Indian J Gastroenterol* 27:74–80.
 197. Miki T, Ring A, Gerlach J (2011) Hepatic differentiation of human embryonic stem cells is promoted by three-dimensional dynamic perfusion culture conditions. *Tissue Eng Part C Methods* 17:557–68. doi: 10.1089/ten.TEC.2010.0437
 198. Darnell M, Schreiter T, Zeilinger K, et al (2011) Cytochrome P450 (CYP) dependent metabolism in HepaRG cells cultured in a dynamic three-dimensional (3D) bioreactor. *Drug Metab Dispos* 39:1131–1138. doi: 10.1124/dmd.110.037721
 199. Klein M, Thomas M, Hofmann U, et al (2015) A systematic comparison of the impact of inflammatory signaling on absorption, distribution, metabolism, and excretion gene expression and activity in primary human hepatocytes and HepaRG Cells. *Drug Metab Dispos* 43:273–283. doi: 10.1124/dmd.114.060962
 200. Toivonen S, Malinen MM, Küblbeck J, et al (2016) Regulation of Human Pluripotent Stem Cell-Derived Hepatic Cell Phenotype by Three-Dimensional Hydrogel Models. *Tissue Eng Part A* 22:971–84. doi: 10.1089/ten.TEA.2016.0127
 201. Kim TH, Bowen WC, Stolz DB, et al (1998) Differential expression and distribution of focal adhesion and cell adhesion molecules in rat hepatocyte differentiation. *Exp Cell Res* 244:93–104. doi: 10.1006/excr.1998.4209
 202. Tanimizu N, Saito H, Mostov K, Miyajima A (2004) Long-term culture of hepatic progenitors derived from mouse Dlk+ hepatoblasts. *J Cell Sci* 117:6425–34. doi: 10.1242/jcs.01572
 203. Lee P, Lin R, Moon J, Lee LP (2006) Microfluidic alignment of collagen fibers for in vitro cell culture. *Biomed Microdevices* 8:35–41. doi: 10.1007/s10544-006-6380-z
 204. Niiya T, Murakami M, Aoki T, et al (1999) Immediate increase of portal pressure, reflecting sinusoidal shear stress, induced liver regeneration after partial hepatectomy. *J Hepatobiliary Pancreat Surg* 6:275–280. doi: 90060275.534 [pii]
 205. Rebelo SP, Costa R, Estrada M, et al (2015) HepaRG microencapsulated spheroids in DMSO-free culture: novel culturing approaches for enhanced xenobiotic and biosynthetic metabolism. *Arch Toxicol* 89:1347–1358. doi: 10.1007/s00204-014-1320-9
 206. Malinen MM, Kanninen LK, Corlu A, et al (2014) Differentiation of liver progenitor cell line to functional organotypic cultures in 3D nanofibrillar cellulose and hyaluronan-gelatin hydrogels. *Biomaterials* 35:5110–5121. doi: 10.1016/j.biomaterials.2014.03.020
 207. Matsui H, Takeuchi S, Osada T, et al (2012) Enhanced bile canaliculi formation enabling direct recovery of biliary metabolites of hepatocytes in 3D collagen gel microcavities. *Lab Chip* 12:1857. doi: 10.1039/c2lc40046d
 208. Lin TY, Ki CS, Lin CC (2014) Manipulating hepatocellular carcinoma cell fate in orthogonally cross-linked hydrogels. *Biomaterials* 35:6898–6906. doi: 10.1016/j.biomaterials.2014.04.118
 209. Gunness P, Mueller D, Shevchenko V, et al (2013) 3D organotypic cultures of human heparg cells: A tool for in vitro toxicity studies. *Toxicol Sci* 133:67–78. doi: 10.1093/toxsci/kft021
 210. Leite SB, Wilk-Zasadna I, Zaldivar JM, et al (2012) Three-dimensional HepaRG model as an attractive tool for toxicity testing. *Toxicol Sci* 130:106–16. doi: 10.1093/toxsci/kfs232
 211. Jossé R, Aninat C, Glaise D, et al (2008) Long-term functional stability of human HepaRG hepatocytes and use for chronic toxicity and genotoxicity studies. *Drug Metab Dispos* 36:1111–1118. doi: 10.1124/dmd.107.019901

212. Kotani N, Maeda K, Debori Y, et al (2012) Expression and Transport Function of Drug Uptake Transporters in Differentiated HepaRG Cells.
213. Sakai Y, Yamagami S, Nakazawa K (2010) Comparative analysis of gene expression in rat liver tissue and monolayer- and spheroid-cultured hepatocytes. *Cells Tissues Organs* 191:281–288. doi: 10.1159/000272316
214. Halldorsson S, Lucumi E, Gómez-Sjöberg R, Fleming RMT (2015) Advantages and challenges of microfluidic cell culture in polydimethylsiloxane devices. *Biosens Bioelectron* 63:218–231. doi: 10.1016/j.bios.2014.07.029

Appendix

Supplemental materials

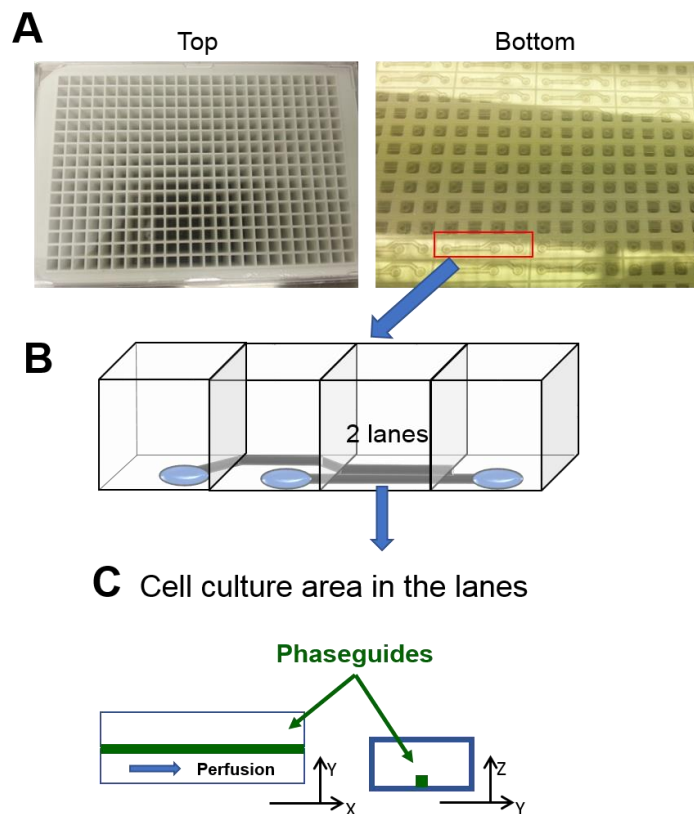


Figure 6.1 (A) Top and bottom views of the 2-lanes biochip, (B) A view of the one culture chamber unit in the 2 lanes-biochip. Cell culture lane possesses only inlet but no outlet. (C) Top and side views of cell culture area in the 2-lanes biochip. One phaseguide is placed between the cell culture lane and the perfusion lane.

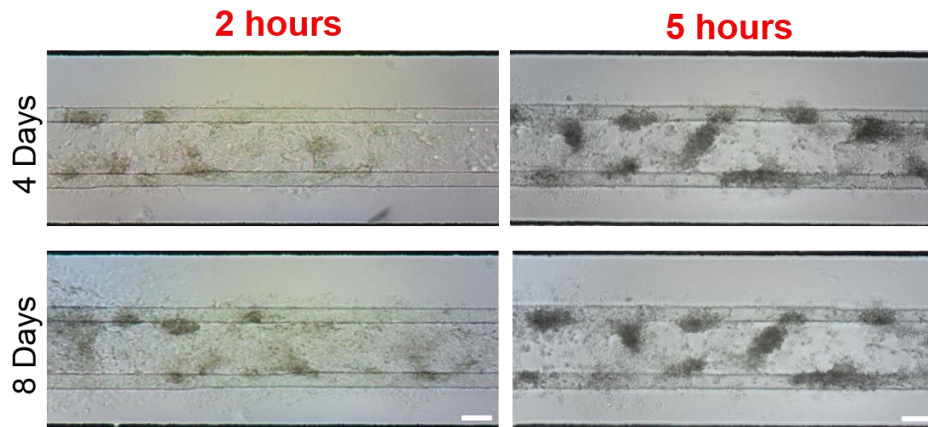


Figure 6.2 Light microscope images of HepG2 cells in comparison to two different second gelation time points (2 hours *versus* 5-6 hours). HepG2 cell clusters showed less flat morphology in culture with a gelation time of 5 hours than 2 hours, and the structure of cell cluster was less collapsed. Scale bars indicate 100 μ m.

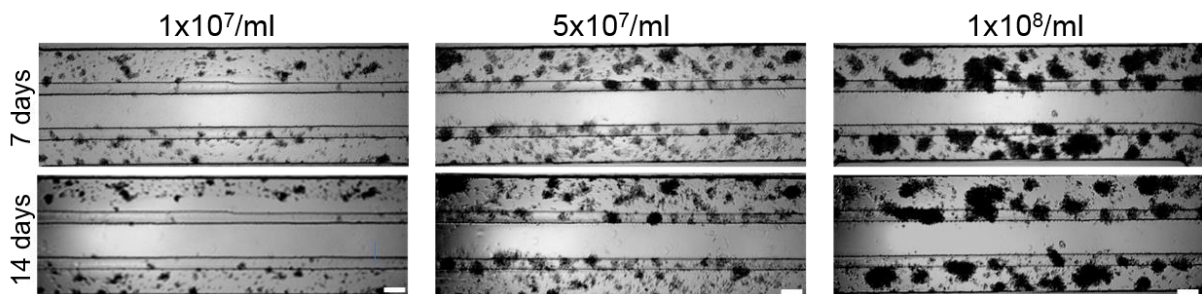


Figure 6.3 Light images of microscope to monitor the formation of cell clusters for 2 weeks of microfluidic cultivation according to different seeding concentration. Scale bars indicate 100 μ m.

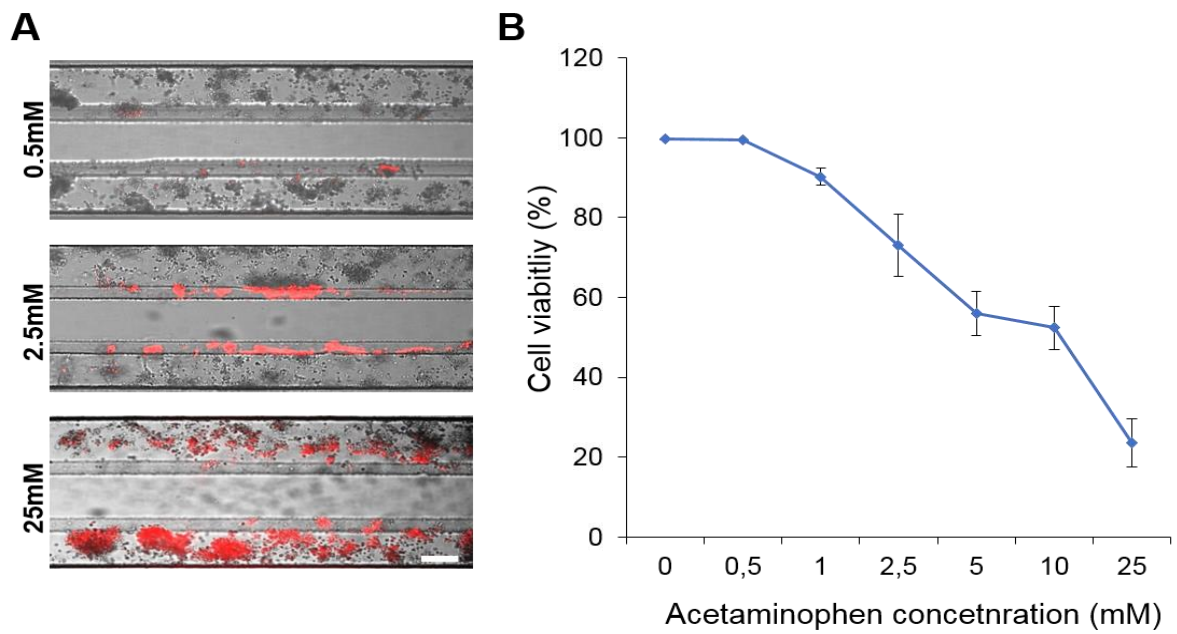


Figure 6.4 Acetaminophen response of HepG2 cells after 5 days of cultivation in microfluidic device. (A) Representative images of HepG2 cells in the perfused chip and exposed to different concentrations of acetaminophen (0.5, 2.5, and 25mM). Dead cells were stained, showing with red color. (B) A dose-response graph of HepG2 cells exposed to different concentration of acetaminophen represents. Scale bar indicates 100 μ m.

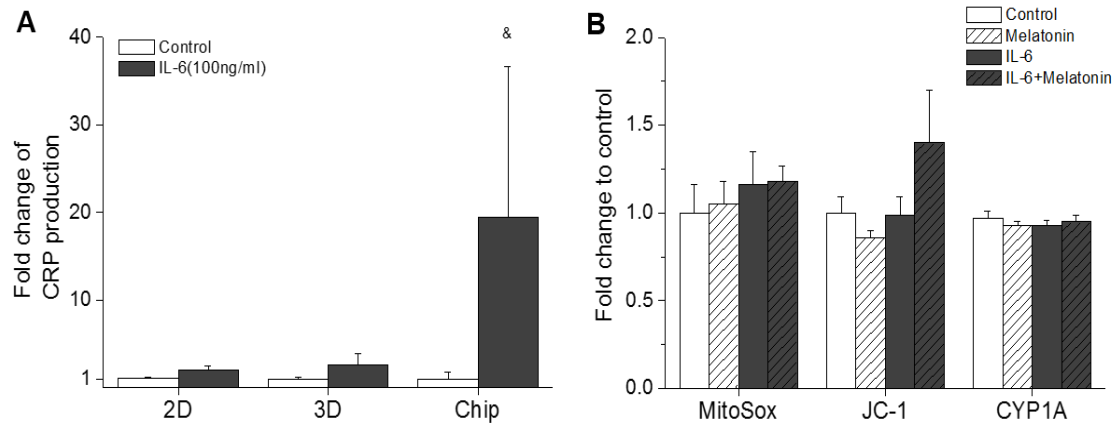


Figure 6.5 (A) CRP production level in each different cultivation model including static 2D, 3D, and biochip culture. & indicates significant difference in comparison to control group. (B) Change of superoxide production in mitochondria, mitochondrial membrane potential, and CYP1A activity in HepG2 monolayer culture model upon treatment with melatonin, IL-6, melatonin + IL-6. All data represented as a fold change to each control group.

Publication list

Part of work in this thesis has been published previously and submitted.

- **M Jang**, A Kleber, T Ruckelshausen, R Betzholz, A manz. Differentiation of human liver progenitor cell line (HepaRG) directly on a biochip. Manuscript submitted to Journal of tissue engineering and regenerative medicine.
- **M Jang**, A Manz, T Volk, A Kleber. New HepG2-on-a-chip platform for study of melatonin effects on various hepatic inflammatory responses stimulated by IL-6. Manuscript submitted to Toxicology in Vitro journal and under revision.
- **M Jang**, P Neuzil, T Volk, A Manz, A Kleber. On chip three-dimensional cell culture in phaseguides improve hepatocyte functions *in vitro*. (2015). *Biomicrofluidics*. 9, 034113.

Past work from my internship has been published during my PhD.

- A Wolf, J I Baumbach, A Kleber, F Maurer, S Maddula, P Favrod, **M Jang**, T Fink, T Volk and S Kreuer. Multi-capillary column-ion mobility spectrometer (MCC-IMS) breath analysis in ventilated rats: a model with the feasibility of long-term measurements. (2014). *Journal of breath research*. 8, 016006

Attendance at conferences

Part of work in this thesis has been presented following international conferences.

- Poster presentation: 20th μ TAS conference in Dublin, Ireland (2016.10.9-2016.10.13) 'Study of melatonin effect on hepatocellular stress response induced by IL-6 using newly developed in vitro liver-on-a-chip'.
- Oral presentation: 20th European congress on Alternatives to animal testing in Linz, Austria (2016.08.24-27) '*In vitro* study of melatonin effect on HepG2 cells treated with IL-6 in newly developed liver on chip device'

- Poster presentation: 19th μ TAS conference in kyung ju, South korea (2015.10.25-2015.10.29 'Human liver cells spheroid culture in perfusion micro reactor for study of drug induced liver injury')
- Poster presentation: 3rd IMTB conference in opatija, Croatia (2015.05.10-2015.05.13) '3D liver cells culture in microfluidic environment to study hepatotoxicity'
This poster was awarded for the best 2nd poster prize at this conference.
- Poster presentation: 9th world congress on alternative and animal use in the life science. Prague, Czech Republic (2014.08.24-2014.08.28) 'A new human liver 3D culture in microfluidic platform as a potential tool for toxicity study'.
- Poster presentation 1st EMBL microfluidics conference, Heidelberg, Germany (2014.07.23-2014.07.25) 'Physiological characterization of human liver 3D culture in microfluidics platform'.

Permission to Reuse AIP Publishing Material

AIP Publishing permits authors to include their published articles in a thesis or dissertation. It is understood that the thesis or dissertation may be published in print and/or electronic form and offered for sale on demand, as well as included in a university's repository. Formal permission from AIP Publishing is not needed.

Reference: <https://publishing.aip.org/authors/copyright-reuse>